

HIGH TEMPERATURE MECHANICAL BEHAVIOR OF
MARYLAND DIABASE

by

YVES DENIS CARISTAN

Thèse de spécialité
Universite de Paris VI
(1975)

SUBMITTED IN PARTIAL FULFILLMENT
OF THE REQUIREMENT FOR THE
DEGREE OF DOCTOR OF PHILOSOPHY

at the

MASSACHUSETTS INSTITUTE OF TECHNOLOGY

December 1980

(i.e. February 1981)

© Massachusetts Institute of Technology 1980

Signature of Author _____
Department of Earth and Planetary Sciences
December 1980

Certified by _____ Thesis Supervisor

Accepted by _____ Chairman, Department Committee

~~Aspirant~~
WITHDRAWN
SEARCHED INDEXED
SERIALIZED FILED
OF TECHNOLOGY
APR 2 1981
MIT LIBRARIES
LIBRARIES

HIGH TEMPERATURE MECHANICAL BEHAVIOR OF MARYLAND DIABASE

by

Yves Caristan

Submitted to the Department of Earth and Planetary Sciences on December 19, 1980, in partial fulfillment of the requirement for the degree of Doctor of Philosophy at the Massachusetts Institute of Technology.

ABSTRACT

The high temperature creep of Maryland diabase has been investigated at a fixed temperature of 1000°C and confining pressures to 450 MPa. Under these conditions, high temperature creep was achieved. For stresses below 300 MPa the strength-strain rate relation can be described by a power law with an activation energy of 276 ± 14 kJ/mol and a stress exponent of 3.0 ± 0.2 . For stresses above 300 MPa the strain rate is stress activated. Electron and optical microscopy indicate that thermal cracking existed even at 450 MPa confining pressure. Bending of the acicular plagioclase and stretching of the pyroxene aggregates and ore minerals commonly occurred. Dislocations were found in both plagioclase and pyroxene. Twinning on a very small scale (500Å) was observed along (100) and (001) planes in pyroxene. Recrystallization of pyroxene and plagioclase occurred after about 12% axial strain. Microprobe analysis and scanning electron microscopy suggested that a minute melt fraction was present during the experiments, but this melt fraction is not thought to have a significant effect on the rock creep strength.

Additionally, the transition from high temperature creep to brittle fracture in Maryland diabase was investigated as a function of confining pressure and strain rate. Experiments were conducted at 1000°C. Confining pressure was varied to 450 MPa and strain rates from $2 \cdot 10^{-3} \text{ s}^{-1}$ to $4 \cdot 10^{-6} \text{ s}^{-1}$. At fixed strain rate, the rock strength first increased with pressure, reached a maximum, and then decreased with increasing pressure. Finally, with high pressures, the strength reached an asymptotic value which was the steady state creep strength at that temperature and strain rate. The positive pressure sensitive domain corresponded to brittle behavior, the negative pressure sensitivity domain to a

transitional behavior, and the pressure insensitive domain to dislocation creep. The boundary between the last two domains occurred where the strength of the rock was about equal to the confining pressure. Similar variations in strength have been reported in the literature for carbonates and silicates, although not associated with a transitional behavior. Frictional strength along the faults decreased with decreasing shearing rate. Microscopic observations indicated that the fault gouge consisted of sintered grains of submicron size with some porosity. Unfaulted specimens deformed in the transitional field showed microcracks and plastically deformed minerals. The boundaries of the transitional domain were extrapolated to geological conditions corresponding to the oceanic lithosphere. The transition depth near ridges is in close agreement with the base of the seismogenic layer (Tapponnier and Francheteau, 1978). However, the old oceanic lithosphere is probably totally brittle over its whole thickness.

The high temperature rheology of polycrystalline aggregates can be described by a power law relating strain rate to stress and temperature. The parameters characterizing this power law are determined from experimental data obtained on cylindrical samples deformed under triaxial loading at high temperature and confining pressure. The effect of stress and temperature distribution along the sample is considered here as a function of axial strain. First the sample shape and the temperature distribution along the sample are fitted with second degree polynomials. The stress distribution in an inhomogeneously deformed sample is analyzed. It is shown that, for axial strains up to 20%, the mean differential stress in an inhomogeneously deformed sample is about the same as the mean differential stress in a homogeneously deformed sample. These results are then used to determine the uncertainties in the experimentally determined power law parameters. Under the conditions investigated the uncertainty in the pre-exponential constant $\dot{\epsilon}_0$ is negligible. For the activation energy an upper bound is given by $\Delta Q/Q < 2\Delta T_0/T_0$ up to $\Delta T_0/T_0 = 10\%$. Uncertainty in the stress exponent is not important as long as the ratio of confining pressure to applied stress is smaller than 0.85 and that the axial strain is below 10%. When that ratio gets close to unity, variations in the stress exponent become important, and above a certain ratio, which depends on the axial strain, the principal stress axes in the sample change. Consequently, special care should be taken in designing and interpreting high confining pressure-low differential stress experiments.

Thesis Supervisor: William F. Brace
Title: Professor of Geology

ACKNOWLEDGMENTS

This work is the result of a research that was started under the guidance of Professor Christopher Goetze. Professor Goetze suddenly died on November 21, 1977, when about one third of the work presented here was completed. His unusual and deep perception of physics has profoundly influenced my work. Therefore I dedicate this thesis to the memory of Professor Christopher Goetze not only for the few points mentioned above, but also because in life and in death he stood as an example that gave me courage to pursue a task that had been undertaken up to its achievement.

This work would not have been possible without the help of Professor W.F. Brace who provided guidance and financial support. Brian Evans provided me with valuable advice and moral support. Numerous discussions with Terry Fong Wong clarified my understanding of brittle behavior, and finally Dr. J. Walsh provided valuable comments on the writing of the last chapter. All of them are gratefully acknowledged.

Derek Hirst, Madge Slavin and Danielle Chouet are all to be thanked for their technical support.

TABLE OF CONTENTS

	Page
TITLE PAGE	i
ABSTRACT	ii
ACKNOWLEDGMENTS	iv
TABLE OF CONTENTS AND TABLES	v
LIST OF FIGURES	viii
INTRODUCTION	1
CHAPTER I. HIGH TEMPERATURE CREEP OF MARYLAND DIABASE	
Introduction	5
Experimental equipment and procedure	6
results	8
Stress dependence	8
Temperature dependence	10
Experimental power law	11
Simultaneous stress relaxation	
measurements	11
Comparison with existing data	12
Microstructural observations	15
Thermal cracking	15
Deformation microstructures	17
Cracks and porosity	17
Transmission optical microscopy	18
Transmission electron microscopy	19
Mineral stability under experimental	
conditions	21
Discussion	23
Conclusion	28
References	30
CHAPTER II. THE TRANSITION FROM HIGH TEMPERATURE CREEP TO FRACTURE IN MARYLAND DIABASE	
Introduction	68
Experimental procedure	70
Mechanical data	71
Effect of strain rate on the mechanical	
behavior at constant pressure	71
Effect of pressure on the mechanical	
behavior at constant strain rate	72
Frictional behavior	74
Microstructure observation	77
Comparison with existing data and discussion	79
Variation of fracture strength with	
temperature	79
The transitional regime and the negative	
pressure effect	80

	Page
The criterion $P = \sigma_D$	83
Application to the earth	85
Conclusions	88
References	90
 CHAPTER III. DETERMINATION OF UNCERTAINTIES IN EXPERIMENTALLY MEASURED FLOW LAW PARAMETERS	
Introduction	115
Stress distribution dependence on axial strain	116
Temperature distribution along the sample	121
Effect of stress and temperature distribution on measured flow law parameters	122
Uncertainty in the first factor $\dot{\epsilon}$	
Dependence on axial strain and temperature variation	125
effect of other parameters	127
Uncertainty in the activation energy	127
Uncertainty in the stress exponent	130
Discussion	134
Stress distribution in the sample	134
Activation energy	135
Stress exponent	136
Conclusion	139
References	140
 BIOGRAPHICAL NOTE	155

TABLE OF TABLES

	Page
CHAPTER I	
Table I: Maryland Diabase creep data	33
Table II: Correlation between silica content and power law parameters	34
CHAPTER II	
Table I: Strength of Maryland Diabase as a function of confining pressure	93
CHAPTER III	
Table I: Flow law parameters for dunite	142
Table II: Flow law parameters for Solnhofen Limestone	143
List of symbols	144

LIST OF FIGURES

	Page
CHAPTER I:	
Figure 1	35
Figure 2	37
Figure 3	39
Figure 4a	41
Figure 4b	43
Figure 5a	45
Figure 5b	47
Figure 6	49
Figure 7	51
Figure 8a	52
Figure 8b	52
Figure 9	55
Figure 10	57
Figure 11	59
Figure 12a	61
Figure 12b	63
Figure 13	65
Figure 14	67
CHAPTER II:	
Figure 1	94
Figure 2	96
Figure 3	98
Figure 4	100
Figure 5	102
Figure 6	104
Figure 7	106
Figure 8a	108
Figure 8b	109
Figure 9	110
Figure 10	111

	Page	
Figure 11	Maryland Diabase behavior as a function of pressure and temperature for a strain rate of $3 \cdot 10^{-6} \text{ s}^{-1}$	112
Figure 12	Transition from creep to fracture in the oceanic crust	114
CHAPTER III		
Figure 1	Homogeneous and inhomogeneous deformation models	146
Figure 2	Sample profiles	148
Figure 3	Mean stress and minimum stress along sample	149
Figure 4	Temperature distribution along profile	150
Figure 5	Preexponential constant dependence on temperature and axial strain	151
Figure 6	Preexponential constant dependence on temperature and activation energy	152
Figure 7	Dependence of stress exponent on the ratio of pressure to axial stress	153
Figure 8	Experimental stress exponent variation as a function of pressure to axial stress ratio	154

INTRODUCTION

High temperature rock mechanics started in the early sixties with an extensive investigation by Griggs et al. (1960) and Heard (1960) of the mechanical properties of crustal rocks under various temperatures and confining pressures. With the plate tectonics revolution the emphasis shifted towards studying ultramafic rocks because their rheology could help in constraining physical conditions in the upper mantle, and interpret continental drift and ocean evolution in terms of mantle rheology. A substantial increase in the knowledge of olivine high temperature rheology resulted from that situation, and research is still very active in this area, although the main results summarized by Goetze (1978) provide a wealth of information. Comparatively little work had been done on the high temperature mechanical behavior of crustal rocks until the work of Tullis and Yund (1977). Despite the fact that the crust is more directly accessible to study by seismologists and structural geologists, there remains a lack of high temperature mechanical data on crustal rocks to help in interpreting seismology and structural geology observations. Because the whole spectrum of mechanical behavior is encountered in the crust, high temperature experiments on crustal rocks must include the transition from dislocation creep to brittle fracture as well as dislocation creep per se, and this is part of the motivation of the presentation.

Stesky et al. (1974) experimentally extended the low temperature fracture mechanics approach to moderately high temperatures (700°C) and crustal rocks such as San Marcos gabbro and Westerly granite, and Tullis and Yund (1977) made extensive observations of the microstructures in the constitutive minerals of Westerly granite. Recently Tullis et al. (1979) studied Hale albite, and Enfield Aplite, and Kronenberg and Selton (1981) studied Maryland diabase at temperatures to 1000°C and pressures to 1.5 GPa. These studies were mainly conducted to determine the microstructures associated with the various types of deformation.

The present study was conducted to determine more specifically the characteristics of the transition from creep to fracture in a polymineralic crustal rock, Maryland diabase. The approach used here is reflected in the structure of the present report. Before studying the transition itself it seemed necessary to determine the creep properties of the rock, and this is the subject of the first chapter. As noted before, very few crustal rocks have been tested at high pressure - only the creep properties of carbonates and quartzite rocks have been precisely determined. It is clear that one may not consider the continental crust as exclusively made of quartzite or limestone, and such minerals probably form only a very small fraction of the oceanic crust. The data presented in Chapter I therefore give an insight into the deformation of pyroxene and plagioclase feldspars, the constitutive minerals of Maryland diabase, which are the

most abundant minerals in the earth's crust, and into the creep processes in Maryland diabase itself. Microstructures were determined using scanning and transmission electron microscopy, and reflection and transmission optical microscopy. Chemical changes in the original phases due to temperature and pressure were detected with an electron microprobe.

The data obtained in the first chapter served as a framework for the work presented in the second chapter, which was designed to investigate the transitional region between creep and fracture. In the first chapter all the experiments were conducted with a confining pressure greater than the strength of the samples. In the second chapter we report on experiments where the confining pressure was varied below that value and where the rock was tested at various strain rates. The results presented there show how the strength is affected at the transition between dislocation creep and brittle fracture. These data are compared with other strength data reported in the literature, and extrapolated to geological conditions. This extrapolation allows the determination of the depth interval in the oceanic crust where the transition from dislocation creep to brittle fracture might occur.

Finally the third chapter deals with a technical aspect of high temperature rock mechanics. During an experiment, stress and temperature are rarely homogeneous in the sample tested, and uncertainties in the measured quantities result from that situation. These measured

quantities, generally stress and strain rate, are used in the determination of the mechanical "equation of state of the material". In the range of pressures and stresses generally encountered in the earth, this equation has the form of a power law. The parameters used in this power law are determined from the measured quantities mentioned above, and therefore any uncertainty in these quantities will lead to uncertainties in the power law parameters. In the third chapter, bounds on these uncertainties are estimated as a function of stress distribution, temperature distribution, and total axial strain. Special attention is given to temperature distributions commonly encountered in solid medium deformation apparatus and the repercussions on the experimentally determined activation energy. The power law stress exponent is very sensitive to the stress distribution in the sample, and this study focuses on the case of experiments done at high confining pressure and low differential stresses, providing some new ideas to interpret results obtained under these conditions.

The various chapters presented in this report are intended to be read separately.

CHAPTER I. HIGH TEMPERATURE CREEP OF MARYLAND DIABASE

INTRODUCTION

High temperature creep of rocks has been extensively studied for more than a decade. Recently data on monomineralic polycrystalline aggregates have been published in the literature. Quartzite has been studied by Christie et al. (1979), peridotite by Post (1977) and Evans and Goetze (1979), websterite by AveLallemant (1978). However most crustal silicate rocks are polymineralic and composed of minerals of intermediate silica content like feldspars and pyroxene. These rocks are therefore intermediate between the silica rich and the highly undersaturated rocks studied up to now. The understanding of the mechanical behavior of the crust is necessarily linked to the determination of the creep properties of these crustal rocks.

The present paper addresses itself to the study of Maryland diabase, a polymineralic assemblage of small grain size (175 μm), vanishing crack porosity, which is elastically isotropic (Brace, 1965). Experiments were conducted at 900°C and 1000°C in order to achieve full plasticity within the pressure range available in the laboratory (450 MPa). Special attention was given to thermal cracking under confining pressure during heating

period and to the stability of the mineral assemblage under the experimental conditions.

EXPERIMENTAL EQUIPMENT AND PROCEDURE

This set of experiments was conducted with the apparatus described by Goetze and Brace (1972). It is a servo-controlled press equipped with a 10 kb pressure vessel, and a molybdenum wound internal furnace (Fig. 1). The load was transmitted to the sample through an alumina column, and measured with an external load cell. Both column and sample were jacketed with copper tubing. Pressure was measured with a Heise gage, and piston displacement with a linear differential transformer ^{N.A.C.} ~~which~~ signal was fed back into the servocontroller. Temperature was measured at the top of the sample with a thermocouple going through the top plug. Consequently the sample was vented. The sample had a smaller diameter than the column in order to gain space for radial deformation of the sample and also to avoid high stresses in the alumina column. The gap between the furnace wall and the furnace assembly was filled with boron nitride to avoid argon convection at high temperature. A buffer mixture of H₂ and CO₂ at a partial pressure of 0.1 MPa was fed into the pressure vessel to prevent furnace oxydation by controlling oxygen fugacity.

For each run the sample was machined into a small cylinder 0.8 inch long and 0.5 inch in diameter, then dried

for a few hours at 80°C under vacuum. It was then mounted with its assembly on the pressure vessel top plug, and 150 MPa were applied to collapse the jacket onto the reduced section sample and tapered alumina mounting pieces. The assembly was then completed outside the pressure vessel by filling the furnace gap with boron nitride. The whole assembly was slid back into the pressure vessel. The desired pressure was first applied and maintained through the heating stage, which generally lasted about 45 minutes. Tests started when the desired temperature was reached. Every 4 or 5 runs a temperature calibration profile was measured through a drilled sample, and sample position adjusted to the hottest spot. During each run a temperature profile was measured from the top of the plug to the top of the sample to check the correctness of the sample position by comparison with the calibration profile. The temperature gradient along the sample never exceeded $40^{\circ}\text{C}\cdot\text{cm}^{-1}$, and was generally smaller than $15^{\circ}\text{C}\cdot\text{cm}^{-1}$.

The sample generally did not deform homogeneously because of the temperature distribution and end constraints. It is shown in Chapter III that for axial strains smaller than 20% the mean stress in an inhomogeneously deformed sample is about the same as the mean homogeneous stress as long as volume is conserved. The data reported here are mean homogeneous differential stresses accurate within 4%. The error

in displacement measurement was due to the alumina column and steel piston elasticity as well as the copper jacket end cap creep strain. It is believed to be within 2%. Pressure was measured within 1MPa, but could vary within 10MPa during some experiments.

Starting material

Maryland diabase comes from a tholeiitic dike swarm extending from Maryland to Nova Scotia. The mineral assemblage is composed of two main constituents: plagioclase (49%), pyroxene (47%), and minor constituents in order of decreasing importance: oxides (3%), biotite (1%). Pyroxene grains exhibit blebs of calcium rich pyroxene exsolved from calcium poor pyroxene (Fig. 10).

RESULTS

Various types of experiments were conducted to determine the stress and temperature dependence of the creep rate. All experiments were conducted at 1000°C, except when specifically mentioned, and confining pressures greater than the applied differential stress. There was no noticeable pressure sensitivity in the range of pressure investigated and within the experimental scatter.

Stress dependence

Stress dependence of creep strain rate was determined by differential stress testing. Load was manually applied and maintained at a fixed value while the sample was creeping.

Load and displacement were recorded as a function of time. Strain rate was obtained by measuring the slope of the displacement-time curves after the sample deformed at least 1%. Goetze and Brace (1972) showed that in Maryland diabase steady state was reached after 1% axial strain. Figure 2 shows the actual experimental record. Load was set at three different values, then brought back to its initial value. At each value the slope of the displacement-time record decreased slowly with time. This effect was due to the decrease in applied stress at constant load resulting from radial strain. Between each new loading the piston was moved up and down without touching the sample in order to determine the O ring frictional force on the piston. The wiggly line on the load record corresponds to twice the friction. Thus the load could be friction corrected. Strain rates measured on Figure 2 are plotted as a function of applied differential stress on Figure 3. The strain rate values corresponding to the first and last load setting (point C and F) are in reasonably good agreement. Thus after 4% axial strain no major structural change occurred in the sample. The stress exponent corresponding to the equation $\dot{\epsilon} = A \sigma^n \exp(-Q/RT)$ and measured from data points on Figure 3 is 2.91.

Constant displacement rate experiments were conducted to obtain suitable samples for observation of microstructures. These samples were strained at least 10%. Data from these experiments as well as the differential tests are listed on Table I, and represented on Figure 4. They span almost 4 orders of magnitude in strain rate, and can be divided into a power law region for strain rates lower than about 300 MPa and a region where strain rates are stress activated. A stress exponent of 3.05 was obtained by least square fitting for the power law region.

A few experiments were conducted at 900°C. A stress exponent of 2.92 was obtained for these experiments. This value is in good agreement with the values obtained above.

Temperature dependence

The creep thermal activation energy was determined by differential temperature testing between 900°C and 1000°C. A value of 276 kJ/mol was obtained. Figure 4a shows some data points at 900°C corresponding to differential stress testing. The activation energy obtained by comparing these points to the 1000°C data points leads to an activation energy of 230 kJ/mol. However the value of 276 kJ/mol obtained by specific differential temperature testing was adopted for all the reduction necessary to express data at 1000°C.

Experimental power law

The stress and temperature dependence determined above for the low stress region can be expressed by the following empirical power law parameters:

$$A = 6.12 \times 10^{-2} \text{ MPa}^{-n} \quad n = 3.05 \quad Q = 276 \text{ kJ.mol}^{-1}.$$

The maximum uncertainty on n and Q is 5% (Chapter III).

Simultaneous stress relaxation measurements

Constant load experiments were conducted by compensating for load relaxation by manually giving small incremental displacements to the piston. These small load relaxation events were recorded separately as a function of time. They correspond to the creep of the sample under the load, and could be related to the creep strain in the sample through the following relation:

$$\dot{\epsilon} = (dF/dt)/kL_0$$

where dF/dt is the slope of the load time record, k the stiffness of the system between the two loading platens, and L_0 the sample initial length. Figure 5a represents the original load record, and Figure 5b the corresponding strain rates computed with the measured stiffness of $5.4 \times 10^7 \text{ N.m}^{-1}$

for the loading column. After a short initial transient state a quasi steady state is reached where strain rates decrease slowly with time and radial strain in the sample. These strain rate values, measured from stress relaxation data, can be directly compared to the strain rate values obtained from the piston displacement record of the same experiment. These last values are represented by solid dots on Figure 5b. There is a remarkably good agreement between both independent data sets. This observation comes in support of using stress relaxation data for determining flow law parameters in rocks (Rutter et al., 1978).

COMPARISON WITH EXISTING DATA

Few data on the strength of basaltic rocks at high temperature and high pressure can be found in the literature. In the steady state regime Griggs et al. (1960) deformed a basalt at temperatures ranging from 25°C to 800°C. Although these temperatures were lower than the temperatures used in our study, the strength they report was substantially lower than the values measured here. However, as no description of the rock texture was given, it is difficult to determine if any correlation between Griggs et al. data and the data reported here is justified.

Recently Tullis and Yund (1980) reported an activation of 263 kJ/mol for the creep activation energy of Maryland

diabase at pressures up to 1.5GPa. This value confirms the value found here.

Goetze and Brace (1972) studied Maryland Diabase in the transient creep regime, and for small strains. They found a stress exponent of 1.8. This low value compared to the one reported here could be due to the transient state but also to the ratio of confining pressure to applied differential stress ($P/\sigma_0 = 0.994$). When P/σ_0 is close to unity the apparent stress exponent can be substantially lower than the intrinsic stress exponent, even with small axial strains (Chapter III). In the same study an activation energy of 334 to 376 kJ/mol was found. This value, which is 20% higher than the value found in this study could be specific of the transient state.

Brace (1961) measured the hardness of Maryland Diabase from room temperature to 1000°C. Evans (1978) transformed these hardness data into equivalent yield strength. By comparing these values with that obtained in the present set of data he concluded that the indentation experiments were carried at an equivalent strain rate of $5 \cdot 10^{-6} \text{ s}^{-1}$. At that strain rate a plot of yield strength versus \sqrt{T} , where T is the temperature, shows a linear correlation (Fig. 4b) indicating that a Dorn law of the following form could be fitted to the data (Goetze, 1978):

$$\dot{\epsilon} = \dot{\epsilon}_0 \exp\left[(-Q/RT) \left(1 - \frac{\sigma_D}{\sigma_P}\right)^2\right]$$

where $\dot{\epsilon}$ is the strain rate, Q the activation energy, R the gas constant, T the temperature, σ_D the differential stress and σ_p the characteristic strength. This characteristic strength is the polycrystalline equivalent of dislocation glide in a single crystal, and can be determined on Figure 4b from the intercept of the straight line with the ordinate axis. A value of 4.6 GPa is obtained. In the creep data reported here (Fig. 4a) strain rates are stress activated for stresses higher than 300 MPa. The hardness data suggest that a Dorn law be used to represent this stress activated range. To do so the same activation energy as in the power law range was chosen (Goetze, 1978). With $Q = 276$ kJ/mol the characteristic strength is then $\sigma_p = 2.0$ GPa as compared to the hardness value of $\sigma_p = 4.6$ GPa. This discrepancy could be explained by the small amount of partial melting observed (see mineral stability).

AveLallemant (1978) deformed a clinopyroxene at 500 MPa confining pressure and 1000°C. The reported activation energy was 284 kJ/mol and the stress exponent 4.3. However, the data trend (AveLallemant, Fig. 10) is similar to the trend observed in this report: a power law with a stress exponent of about 3 could be fitted to the data points for stresses below 300 MPa, and for stresses above that value the power law stress exponent starts to increase, suggesting a Dorn law. Therefore, there are great similarities between the diopside

and diabase creep properties, in thermal activation energy as well as in stress exponent. This suggests that pyroxene creep is an essential component of diabase deformation.

MICROSTRUCTURAL OBSERVATIONS

Deformed samples were sectioned and observed by reflection and transmission optical microscopy (ROM and TOM) as well as reflection and transmission electron microscopy (SEM and TEM). SEM and TEM samples were ion thinned with an ion milling machine. Because plagioclase had a much higher milling rate than pyroxene, small copper washers were used with a 50 μm hole in the center to select the mineral to be thinned for TEM observation.

Although macroscopic stress-strain curves indicated that a quasi steady state had been reached in the constant displacement rate experiments, microcracking could have occurred simultaneously with plastic creep. In order to differentiate between thermal cracking and cracking due to loading it was necessary to study thermal cracking independently.

Thermal cracking

Samples were heated to 800°C and 1000°C at 400 MPa confining pressure without any load. No microcracking was observed at 800°C (Fig. 6). Abundant microcracking was observed at 1000°C (Fig. 7) with the following characteristics:

Plagioclase grains are almost free of intragranular cracks, but their boundaries are outlined by intergranular cracks. These cracks are due to thermal expansion anisotropy. The crack width is generally below 0.1 μm .

On the contrary pyroxene grains do not show much intergranular cracking, but transgranular cracks are abundant. They are generally generated at places where the boundary between pyroxenes and plagioclase is concave and angular. Thus they are caused by a combination of thermal expansion mismatch and boundary geometrical conditions. The crack width can be as much as 1 μm .

Wong and Brace (1979) observed that thermal cracking in their experiments was suppressed if at the same time as temperature a confining pressure was applied that was higher than the room temperature crack closure pressure. For Maryland Diabase, Johnston and Toksöz' data (1980) indicate that for 800°C the crack closure pressure is about 250 MPa. Therefore the absence of microcracking observed at 800°C is in accord with Wong and Brace's data.

Pores were observed together with acicular crystallites (Fig. 8a). In TOM these crystallites had a high birefringence (Fig. 8b) and could also be observed in minute proportions in the starting material. The background on Figure 8a is grainy, suggesting a fine grained material. In TOM it was impossible to resolve individual grains. This background

was brown in natural light and opaque in polarized light. It could possibly correspond to iron oxides resulting from biotite decomposition during heating stage, the crystallites representing remaining biotite flakes.

Deformation microstructures

Microstructures were observed with the same techniques in experimentally deformed samples. Strain was not homogeneous because of end constraints and temperature distribution. Radial strain was greater in the center than at the ends. No brittle or ductile strain localization was observed in thin section. In samples strained at least 12% axially a foliation developed perpendicularly to the loading direction through recrystallization.

Cracks and porosity

Deformed samples were observed with SEM. They generally showed the following features:

Transgranular cracks in plagioclase, which were almost absent in the thermally cracked samples, were well developed, subperpendicularly to the 100 direction, with a width below 0.1 μm . Intergranular cracks were still present. Most cracks were not directly related to the loading direction. These cracks were either parallel or perpendicular to the plagioclase long direction.

Pyroxene aggregates showed some new cracks generally of very small width, but these aggregates were mostly

characterized by the opening of the preexisting thermal cracks that were parallel to the loading direction. Figure 9 shows these cracks opening perpendicularly to the loading direction, with a width of a few microns and filled with a material containing pores.

Decomposed biotite had a flaky, grainy and porous appearance similar to that observed under hydrostatic conditions. For samples deformed to small strains the decomposed biotite was found at the location where the parent biotite had crystallized during magma cooling. The boundary between biotite and pyroxene was often sinuous, suggesting partial melting. For samples deformed to more than about 12% axial strain the decomposed biotite was smeared in the flow direction, which was radial.

Transmission optical microscopy

Observations of thin sectioned samples by optical microscopy confirmed the strain gradient in the samples. Near the ends strain was small, and plagioclase grains were randomly oriented. Deformation increased toward the center of the specimen. For specimens strained to 10% this increase in strain was reflected by a pronounced plastic bending in the plagioclase grains (Fig. 10). This bending could be accompanied by secondary transgranular cracking similar to that observed by SEM. In samples deformed above 10% the plagioclase grains recrystallized into neoblasts of about

50 μm grain size, and formed a foliation perpendicularly to the loading direction. This foliation was also marked by the elongation of pyroxene aggregates and ore minerals. In the pyroxene aggregates cracks parallel to the loading direction observed by SEM were visible and marked by ore minerals.

The density of albite twins in the plagioclase was observed to be not noticeably different from the original twin density. Pyroxene grains often showed (100) twins.

Transmission electron microscopy

Plagioclase and pyroxene were observed by transmission electron microscopy. Because of the difficulty in preparing samples of small grain size, most grains observed were non recrystallized large grains.

Plagioclase grains generally showed a high dislocation density (10^{10}cm^{-2}), these dislocations being arranged in deformation bands parallel to (010). In one area (Fig. 11) dislocations were in full contrast for the diffraction vector $g = [002]$, and in quasi extinction for several vectors subperpendicular to $[001]$, among which $g = [500]$. This suggests a Burgers vector $b = [001]$. Such a Burgers vector has been reported by Sacerdoti et al. (1980) in potassic feldspars.

Pyroxene grains had extensive twinning on a fine scale. (100) twins were as thin as 500 \AA (Fig. 12a). It was not

always possible to distinguish twins from exsolution lamellae. Twins generally had a high dislocation density, but these dislocations were not easy to individualize. They ran straight across the twin from one boundary to the other in the [100] direction, and disappeared into the boundaries, indicating that most twin boundaries acted as dislocation sources. At some places dislocations could be pictured (Fig. 12b) and followed across several twin bands, cross slipping into the boundary from band to the other. In non-twinned areas

(Fig. 13), jogged dislocations tended to give dislocation dipoles. These observations indicate that dislocation motion was mostly conservative, or in other words that glide was the predominant mechanism.

The highest dislocation density measured was 10^9 lines per cm^2 for pyroxene and 10^{10} lines per cm^2 for plagioclase. These values are within the values measured by Kronenberg and Shelton (1981) in Maryland Diabase deformed above 800°C at 1.5 GPa confining pressure.

All these microscopic observations suggest that no extensive microcracking occurred during the experiments. In pyroxene preexisting thermal cracks parallel to the loading direction tended to open. They were filled with a material containing subspherical pores. The sample deformation was achieved through plastic deformation of

pyroxene and plagioclase grains. Both minerals contained high dislocation densities, but twinning and gliding was more characteristic of pyroxene grains.

MINERAL STABILITY UNDER EXPERIMENTAL CONDITIONS

Any polymineralic assemblage held under pressure and temperature conditions far from its equilibrium conditions can undergo metamorphic reactions or partial melting. SEM and TOM observations already showed that biotite was not stable. In order to detect changes in the other phases the chemical composition of pyroxene and plagioclase in the starting material was compared to the composition of the same phases in a deformed sample, and in a sample that simply underwent temperature and pressure without being deformed. Sample sections were polished and analyzed by electron microprobing. For pyroxene grains the beam was fully focussed and its size was of the order of 3 μm . For plagioclase the beam was defocussed to a larger diameter. The composition thus obtained was representing a composition averaged over a wider area.

Pyroxene in the starting material was mostly pigeonite coexisting with smaller proportions of augite (Fig. 14). In samples heated to 1000°C under 400 MPa confining pressure pyroxene composition showed some depletion with respect to iron content. The reverse trend is known to occur during

magma crystallization (Hess and Poldervaart, 1963). This suggests that the samples analyzed had undergone some partial melting.

Plagioclase did not show any significant changes in composition, at least on the scale of the microprobe beam diameter. This does not preclude any local rearrangement on a finer scale. The absence of chemical change indicates that plagioclase, which is more refractory than pyroxenes, has not started to participate in the melting process. Therefore the temperature was much closer from the solidus than from the liquidus during the experiment.

These chemical changes, together with the observation of pores of subspherical shape in the pyroxene thermal cracks suggest the presence of some melt in the rock during deformation. The pores could be interpreted as follows:

The increase in crack porosity due to the axial cracks opening was larger than the melt available; the residual porosity was therefore expressed through subspherical pores in the melt. The amount of melting was certainly less than 1% as attested by the difficulty in detecting partial melting, even in very thin sections (less than 10 μm). Applying some interstitial water pressure under these conditions would not have prevented but on the contrary enhanced partial melting, although biotite might not have decomposed. Brown and Fyfe (1970) showed that the partial melting of dry crustal rocks is generally triggered by

the decomposition of hydrous phases present in the rocks. From their data on granite and diorite it can be inferred that diabase partial melting, if triggered by biotite decomposition, can be expected to start at about 800°C for pressure conditions similar to that of this investigation.

DISCUSSION

Maryland diabase, within the range of temperatures and pressures investigated, was deformed quasi-steady state creep up to 20% axial strain. It has been shown that a melt fraction smaller than 1% was present during the experiments. Arzi (1978a) and van der Molen and Paterson (1979) showed that the strength of rocks is not significantly affected by melt when the melt percentage is under the critical melt fraction. They estimate this critical melt fraction to be 20 to 30%. When the melt fraction is smaller the rock deformation is due to the deformation of the constitutive mineral framework. This is indeed what was observed in the experiments reported here.

Kronenberg and Shelton (1981) concluded from their electron microscopic observations that deformation was more important in plagioclase than in pyroxene because dislocation density was higher in the first phase than in the second. They inferred from that conclusion that plagioclase was weaker than pyroxene, and that it was the stress supporting mineral. It is however difficult to determine exactly how

much deformation is taking place in individual minerals from dislocation densities only, and in fact the present study shows that (1) twinning was occurring at the same time as dislocation motion, but that mechanism is not accounted for in the dislocation density measurements. (2) Pyroxene aggregates did deform in a plastic way; their shape changed from about equant to lenticular, with the long axis in the flow direction. (3) The diabase strength expressed in terms of power law is very similar to that of the clinopyroxene deformed by AveLallemant (1978). Therefore it seems more justified to conclude that, at 1000°C, both principal phases participated in the deformation in a similar way.

Certain tectonic problems require that tectonic stress bounds be estimated by extrapolation of experimentally determined flow law. Before extrapolating the diabase flow law to natural geological conditions, the following remarks should be considered.

At temperatures lower than about 800°C a different mechanical behavior could occur because of the absence of melt and its effect on dislocation sources along grain boundaries. However, it was noted above that, in granite, such changes have not been observed for low melt fractions. Therefore it seems reasonable to extrapolate the diabase flow law at temperatures below 800°C, as long as deformation mechanisms are similar to those observed in the laboratory.

Dislocations and twinning have been observed in feldspars naturally deformed under crustal conditions (White, 1975, Sacerdoti et al, 1980) or in clinopyroxenes deformed at about 800°C (Caristan, 1975) suggesting that mechanisms observed in the laboratory are operative under geological conditions. These observations argue for the extrapolation of the creep law to low temperature.

SEM revealed the presence of subspherical pores in the deformed samples. Therefore the diabase strength can be expected to show some pressure sensitivity at higher pressure than the present range of investigation. However this pressure sensitivity should not be important considering that the porosity observed was negligible, or at least not detectable by any optical means.

There have been few data published on creep of rocks of mafic composition, although these are an important part of the oceanic and, at some places, continental crust. In their study of oceanic ridges Tapponnier and Francheteau (1978) had to estimate the creep properties of Maryland diabase from scarce data. They did come quite close to the power law determined here although they overestimated the activation energy by a factor of 1.5. They used Maryland diabase as an equivalent for the oceanic crust. The oceanic crust is a complex entity, and, although it has a chemical composition similar to that of a diabase, it must be emphasized that a

variety of textures can be found in the rocks constituting the crust, textures ranging from gabbros to diabase to basalts. The use of the flow law determined above is legitimate as long as, under geological conditions, the grain size sensitivity of the creep strength is negligible. It is known that grain size sensitivity comes in at low differential stresses (Schmidt et al., 1977). Stresses in the crust are presumably much higher than stress at which grain size sensitive mechanisms are predominant. Maryland diabase strength is therefore a reasonable estimate of the oceanic crust strength in the creep regime.

In general, creep properties of acid and ultramafic rocks have been studied ^{for} ~~since~~ more than a decade. As long as stresses do not exceed a certain limit these creep properties can be represented by a power law. Above that stress limit a Dorn law can be used, as in the present study. Recent data on the flow laws of these dry polycrystalline rocks are summarized on Table II. For quartzite the stress limit of 1000 MPa was determined from Evans and Goetze's data (1979). Table I shows that the stress limit increases with increasing SiO₂ content, whereas the first factor A and the activation energy Q decrease monotonically with increasing SiO₂ content. The stress exponent is about constant over the entire composition range. Data on dry websterite by AveLallemant (1978) are not included in

Table II. His experiments were conducted at stresses higher than the stress limit of 300 MPa suggested by his clinopyroxene and wet websterite data. Consequently they reflect a stress activated behavior and cannot be fitted with a power law, as indicated by the high and not well-defined stress exponent (4.3). The correlation between SiO₂ content and power law parameters is certainly interesting in the sense that it allows the estimation of creep properties of untested dry polycrystalline aggregates by interpolation from their SiO₂ content only. However more experimental data are needed to fill up the gaps between the various compositions presented in Table II. Spry (1969) noticed that in naturally deformed rocks quartz deformation is generally more intense than feldspars deformation. The experimentally determined flow laws represented on Table II do show that, when extrapolated to natural crustal conditions, quartzite is weaker than diabase, although under experimental conditions the reverse is true (10^{-5}s^{-1} , 1000°C).

The study of the mechanical behavior of ultramafic rocks has been highly concentrated on the determination of creep properties. For crustal rocks, because of the relatively low pressures and temperatures prevailing in the crust, fracture and frictional sliding along preexisting faults are important mechanisms (Brace and Kohlstedt, 1980)

as well. Few studies have been conducted on the transition from creep to brittle mechanisms. Tullis and Yund (1977) studied that transition in Westerly granite, but without fully investigating the creep properties. There is still a broad field of investigation opened in the creep and in the transitional regime of crustal rocks (Chapter II).

CONCLUSION

Maryland diabase was experimentally deformed at confining pressures to 50 MPa. The strength-strain rate relation obtained can be described by a power law for stresses lower than 300 MPa and a Dorn Law for stresses higher than 300 MPa. The power law activation energy was 276 ± 14 kJ/mol and the stress exponent 3.0 ± 0.2 . The same activation energy was used for the Dorn Law, with a characteristic strength σ_p of 2.0 GPa. Microstructural observations show that thermal microcracking was important even at 450 MPa confining pressure. However, additional cracking during deformation, when it occurred, was minor. Constitutive minerals deformed plastically. Acicular plagioclase grains were progressively bent with strain, and dislocations in bands were observed. Pyroxene grains, mostly pigeonite, exhibited twinning on a very fine scale (500 \AA). Both minerals participated in the rock deformation to the same extent. The small amount of partial melt found (less than 1%) is not thought to have any significant effect

on the measured strength. The flow law determined above can be extrapolated to geological conditions provided the pressure conditions do not substantially exceed the experimental range of confining pressure under which the flow law was determined.

References

- Arzi, A.A., 1978a. Critical phenomena in the rheology of partially melted rocks, *Tectonophysics*, 44, 173-184.
- AveLallemant, H.G., 1978. Experimental deformation of diopside and websterite, *Tectonophysics*, 48, 1-27.
- Brace, W.F., 1961. Experimental study of the indentation of rocks and minerals, Final Report, NSF Grant G-4647, National Acad. Sci., Washington, D.C., Oct. 1.
- Brace, W.F., 1965. Some new measurements of linear compressibility of rocks, *J. Geophys. Res.*, 70, 391-398.
- Brace, W.F., and D.L. Kohlstedt, 1980. Limits on lithospheric stress imposed by laboratory experiments, *J. Geophys. Res.*, 85, in press.
- Brown, C.G., and W.S. Fyfe, 1970. Production of granitic melts during ultrametamorphism, *Contr. Mineral. Petrol.*, 28, 310-318.
- Caristan, Y., 1975. Les lherzolites de l'Etang de Lers - Microstructures et nanostructures, These de 3e cycle, Université de Paris VI.
- Christie, J.H., P.S. Koch, and R.P. George, 1979. Flow law of quartzite in the alpha quartz field, *EoS*, 60, 948.
- Evans, B., 1978. Indentation hardness and its relation to mechanical yield in quartz and olivine, Ph.D. Thesis, M.I.T., Cambridge, Mass.

- Evans, B., and C. Goetze, 1979. The temperature variation of hardness of olivine and its implication for polycrystalline yield stress, *J. Geophys. Res.*, 84, 5505-5524.
- Goetze, C., 1978. Mechanisms of creep in olivine, *Phil. Trans. Roy. Soc. Lond. A*, 288, 99-119.
- Goetze, C., and W.F. Brace, 1972. Laboratory observations of high temperature rheology of rocks, *Tectonophysics*, 13, 583-600.
- Griggs, D.T., F.J. Turner, and H.C. Heard, 1960. Deformation of rocks at 500°C to 800°C, *G.S.A. Memoir* 79.
- Hess, H.H., and A. Poldervaart, 1968. Basalts (2 volumes), Wiley and Sons.
- Johnston, D.H., and M.N. Toksöz, 1980. Thermal cracking and amplitude dependent attenuation, *J. Geophys. Res.*, 85, 937-942.
- Kronenberg, A., and G.L. Shelton, 1981. Deformation microstructures in experimentally deformed Maryland diabase, *J. Struct. Geol.*, in press.
- Paterson, M.S., 1978. Experimental rock deformation - The brittle field, Springer-Verlag, 254 pp.
- Post, R.L., 1977. High temperature creep of Mt. Burnet dunite, *Tectonophysics*, 42, 75-110.
- Rutter, E.H., B.K. Atkinson, and D.H. Mainprice, 1978. On the use of the stress relaxation testing method in studies

- of the mechanical behavior of geological materials, *Geophys. J.R. astr. Soc.*, 55(1), 155-170.
- Sacerdoti, M., H. Labernardiere, and M. Gandais, 1980. Transmission electron microscope study of geologically deformed potassic feldspars, *Bull. Mineral.*, 103, 148-155.
- Schmid, S.M., J.N. Boland, and M.S. Paterson, 1977. Superplastic flow in fine-grained limestone, *Tectonophysics*, 43, 257-291.
- Spry, A., 1969. *Metamorphic textures*, Pergamon Press, 350 pp.
- Tapponnier, P., and J. Francheteau, 1978. Necking of the lithosphere and the mechanics of slowly accreting plate boundaries, *J. Geophys. Res.*, 83, 3955-3970.
- Tullis, J., and R.A. Yund, 1977. Experimental deformation of dry Westerly granite, *J. Geophys. Res.*, 82, 5705-5718.
- Tullis, J., and R.A. Yund, 1980. An experimental study of the rheology of crustal rocks, USGS Open File Report 80-6.
- van der Molen, I., and M.S. Paterson, 1979. Experimental deformation of partially melted granite, *Contrib. Mineral. Petrol.*, 70, 299-318.
- White, S., 1975. Tectonic deformation and recrystallization of oligoclase, *Contrib. Mineral. Petrol.*, 50, 287-304.
- Wong, T.-F., and W.F. Brace, 1979. Thermal expansion of rocks: Some new measurements at high pressure, *Tectonophysics*, 57, 95-117.

TABLE I

T°C	P (MPa)	σ_o (MPa)	$\dot{\epsilon}$ (S ⁻¹)
1000	*600	90	1.7 10 ⁻⁷
	425	296	1.1 10 ⁻⁵
	425	291	9.9 10 ⁻⁶
	425	284	8.1 10 ⁻⁶
	425	204	3.4 10 ⁻⁶
	425	152	1.4 10 ⁻⁶
	425	275	7.9 10 ⁻⁶
	400	296	8.8 10 ⁻⁶
	450	343	9.2 10 ⁻⁶
	450	336	9.5 10 ⁻⁶
	450	386	1.8 10 ⁻⁵
	450	255	4.8 10 ⁻⁶
	425	244	6.0 10 ⁻⁶
	425	424	1.9 10 ⁻⁴
	425	433	3.2 10 ⁻⁴
	425	427	2.7 10 ⁻⁴
	450	357	8.7 10 ⁻⁵
	450	287	1.5 10 ⁻⁵
	450	213	5.5 10 ⁻⁶
	350	271	2.3 10 ⁻⁵
400	367	4.1 10 ⁻⁵	
400	429	1.6 10 ⁻⁴	
350	215	4.6 10 ⁻⁶	
900	400	290	8.5 10 ⁻⁷
	400	269	1.5 10 ⁻⁶
	400	348	2.7 10 ⁻⁶
	400	402	5.0 10 ⁻⁶
	400	345	2.5 10 ⁻⁶

Creep data for Maryland diabase

* Goetze, unpublished data.

TABLE II

Dry poly- crystalline silicates	SiO ₂ content %	Q kJ/mol	n	A MPa ⁻ⁿ	Stress limit MPa	Source
Olivine	30-40	520	3.0	7×10^4	200	Goetze, 1978
Diabase	50-55	276	3.1	6×10^{-2}	300	This study
Quartzite	100	150	2.9	10^{-7}	1000	Christie et al. 1979

Correlation between silica content and power law parameters.

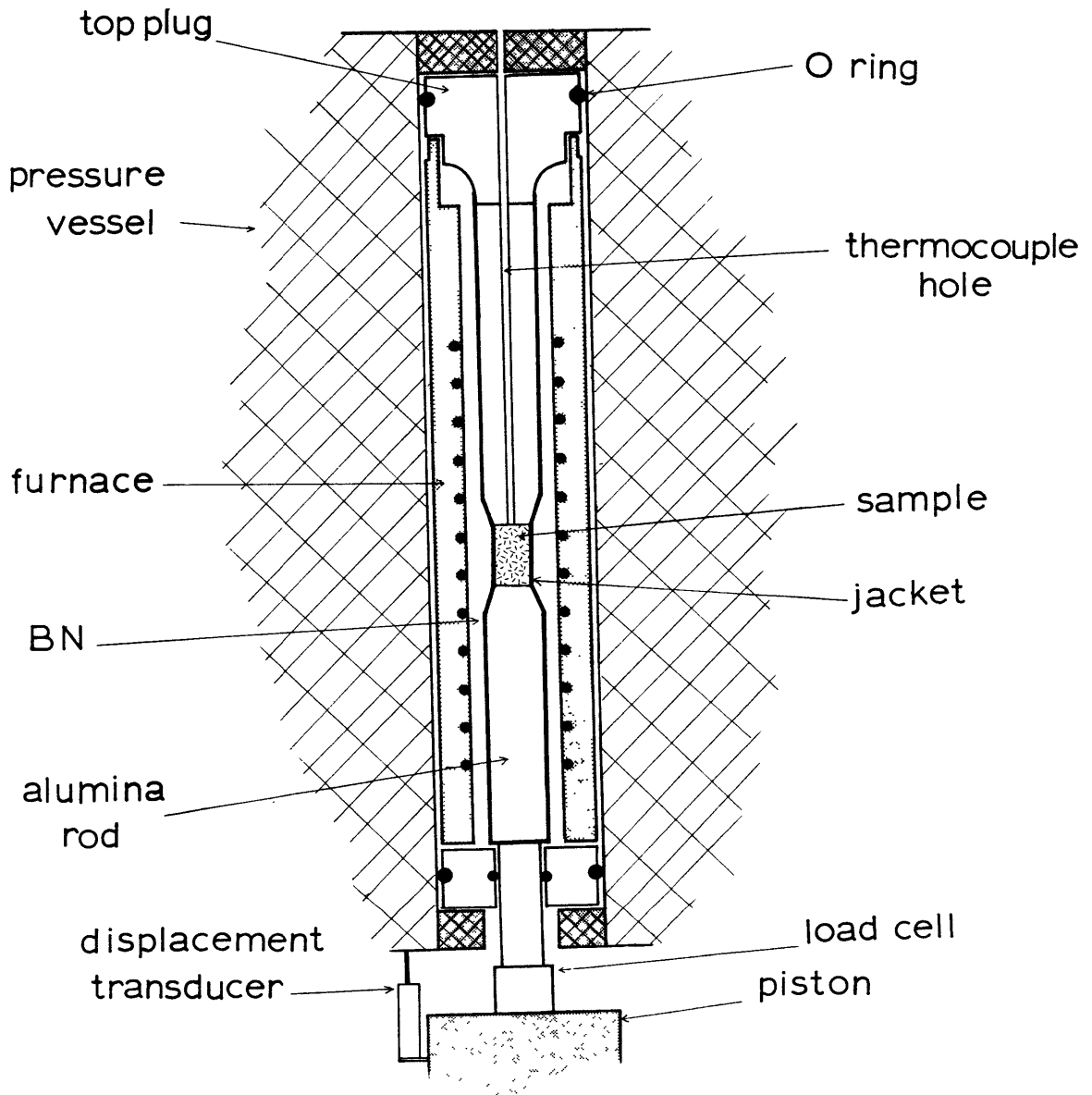


Fig. 1. Experimental assembly inside pressure vessel.

Fig. 2. Experimental record of differential stress testing.
f is the applied differential load and ϵ the axial
displacement.

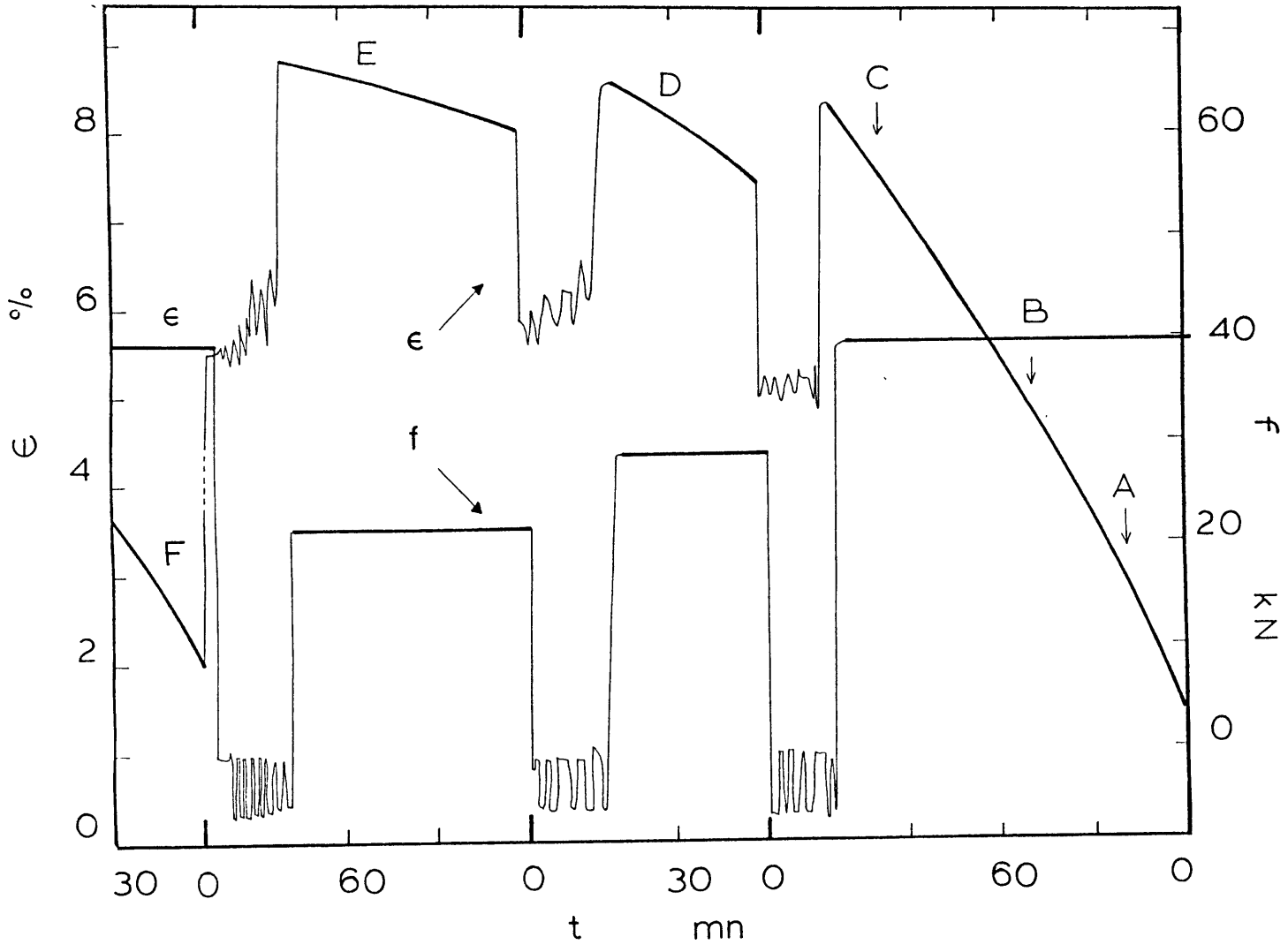


Fig. 3. Same experimental data as Figure 2 with differential stress plotted versus strain rate. Lettering refers to Figure 2.

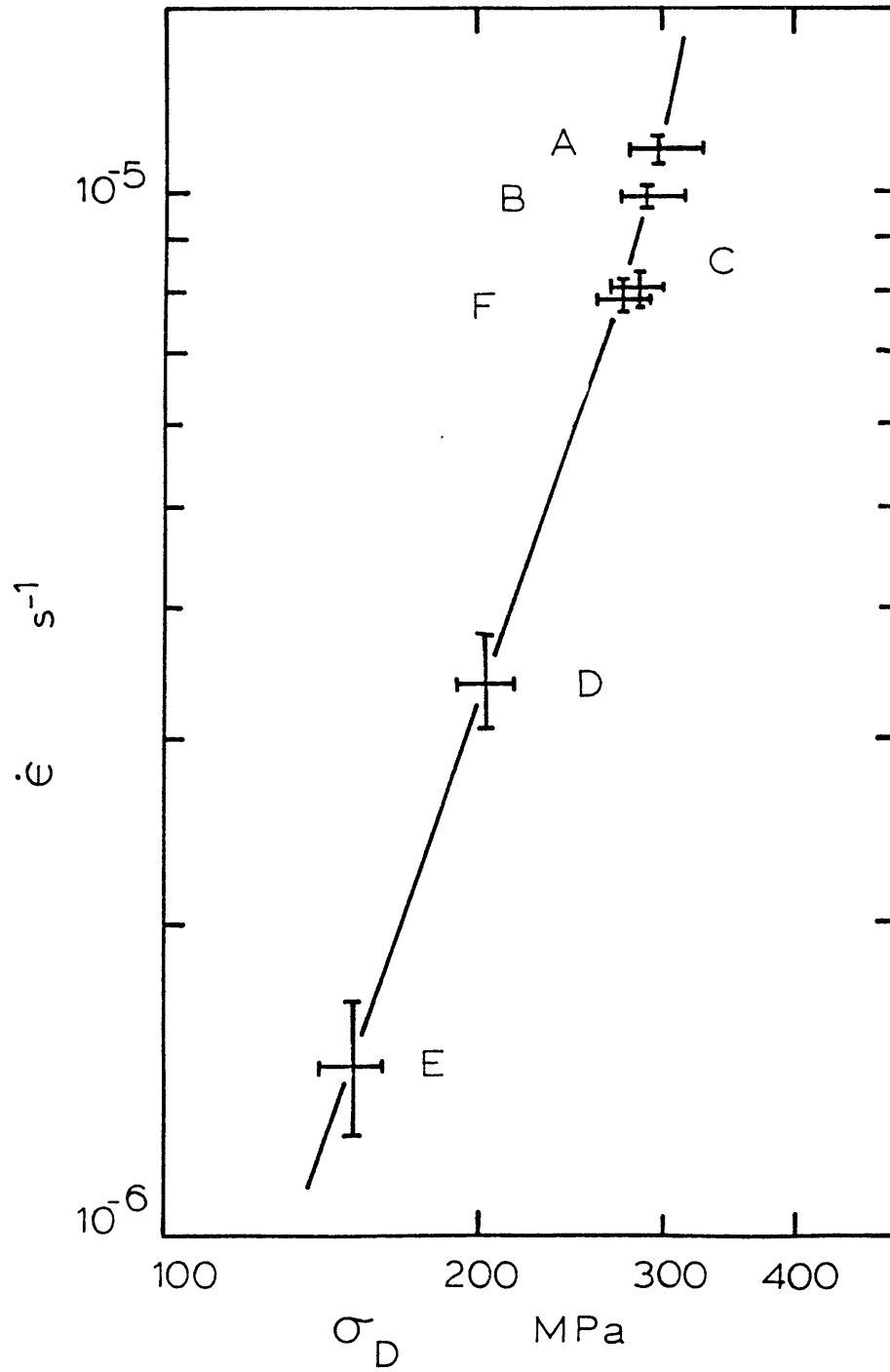
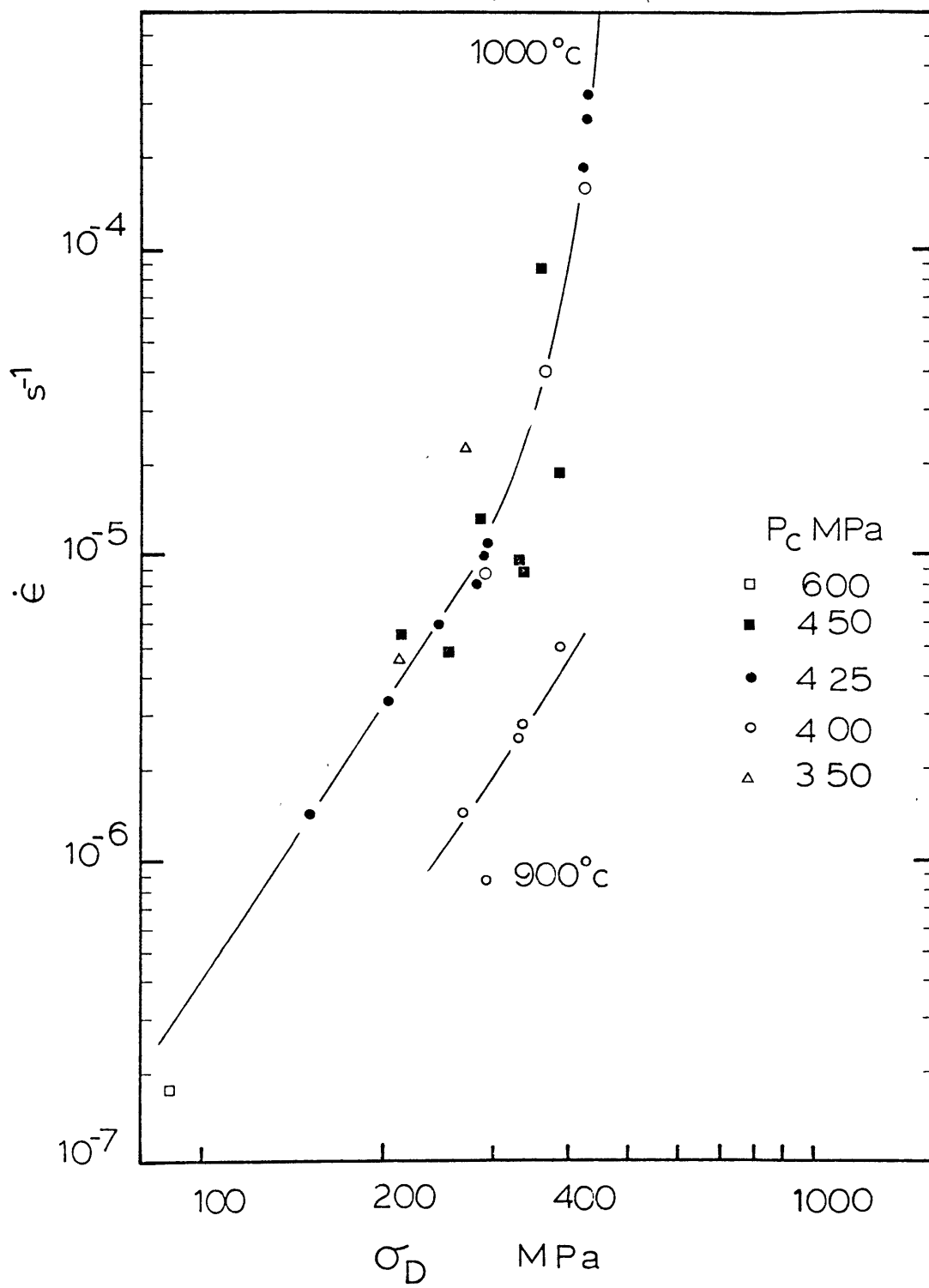


Fig. 4a. Experimentally determined flow law for Maryland diabase. For stresses lower than 300 MPa a power law can be fitted with a stress exponent of 3.0 and an activation energy of 276 kJ/mol. For stresses higher than 300 MPa data can be fitted with a Dorn Law of characteristic strength 2.0 GPa and same activation energy as the power law.



4b. Yield strength of Maryland diabase versus square root of the temperature. Data come from indentation hardness measurements (Brace 1961, Evans and Goetze, 1979). The equivalent strain rate is $5 \times 10^{-6} \text{ s}^{-1}$. Open circles are power law data from this report.

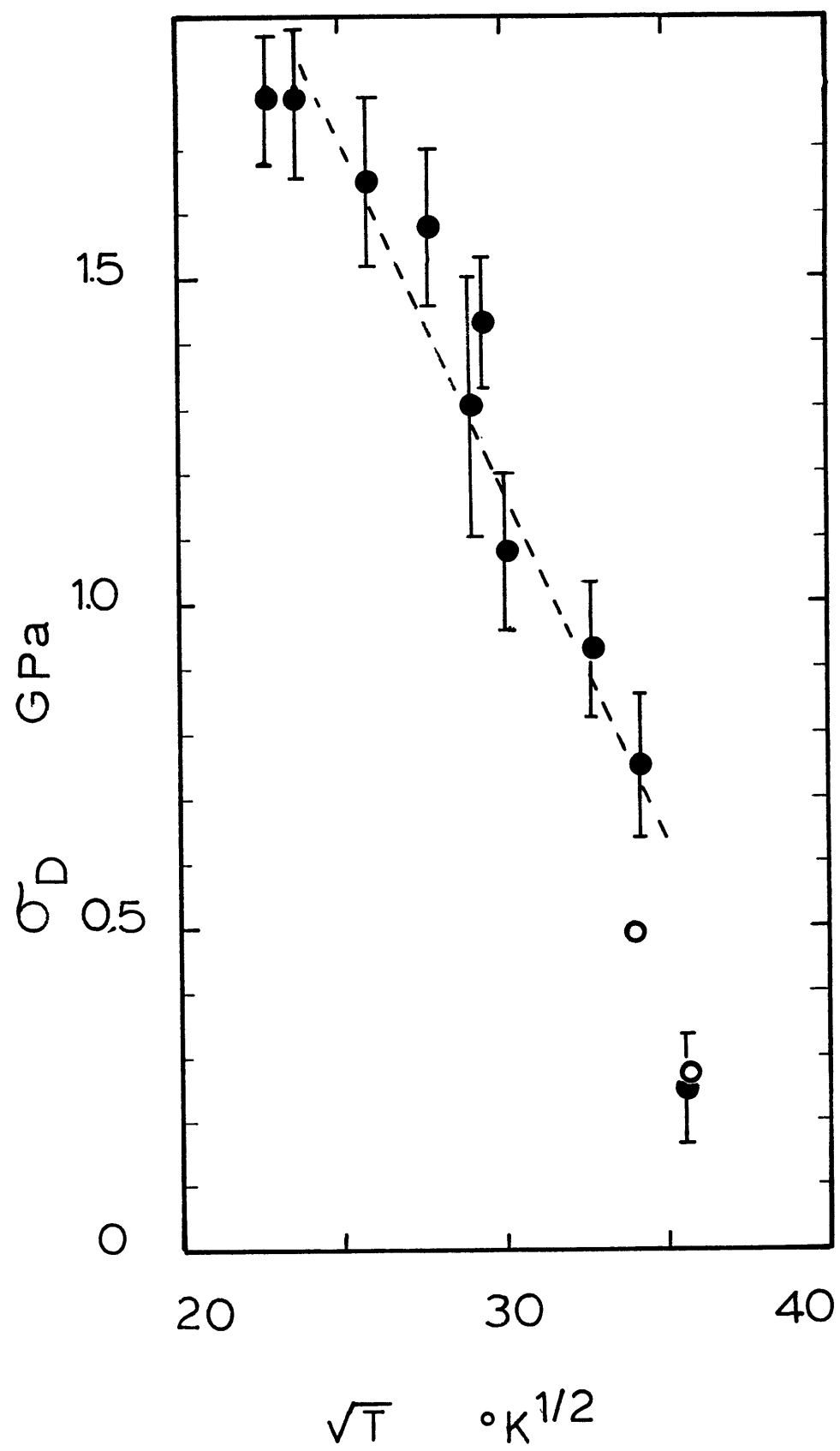


Fig. 5a. Pressure and load record of constant load experiment: the small oblique segments correspond to load relaxation. These segments are modulated by the small variations in confining pressure.

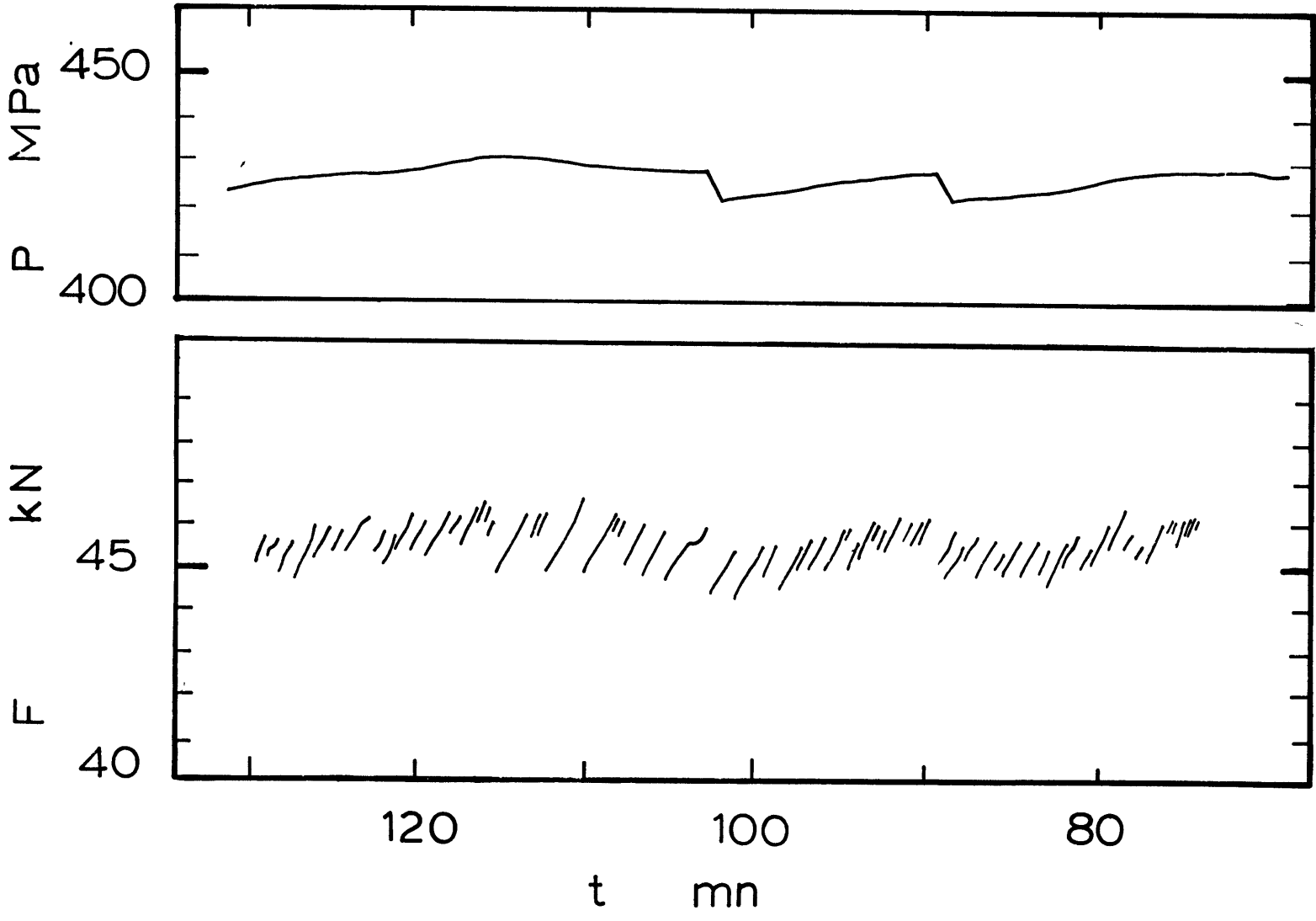


Fig. 5b. Equivalent strain rates computed from load relaxation data (open circles), and strain rates as measured from the time-displacement record (solid circles) simultaneously.

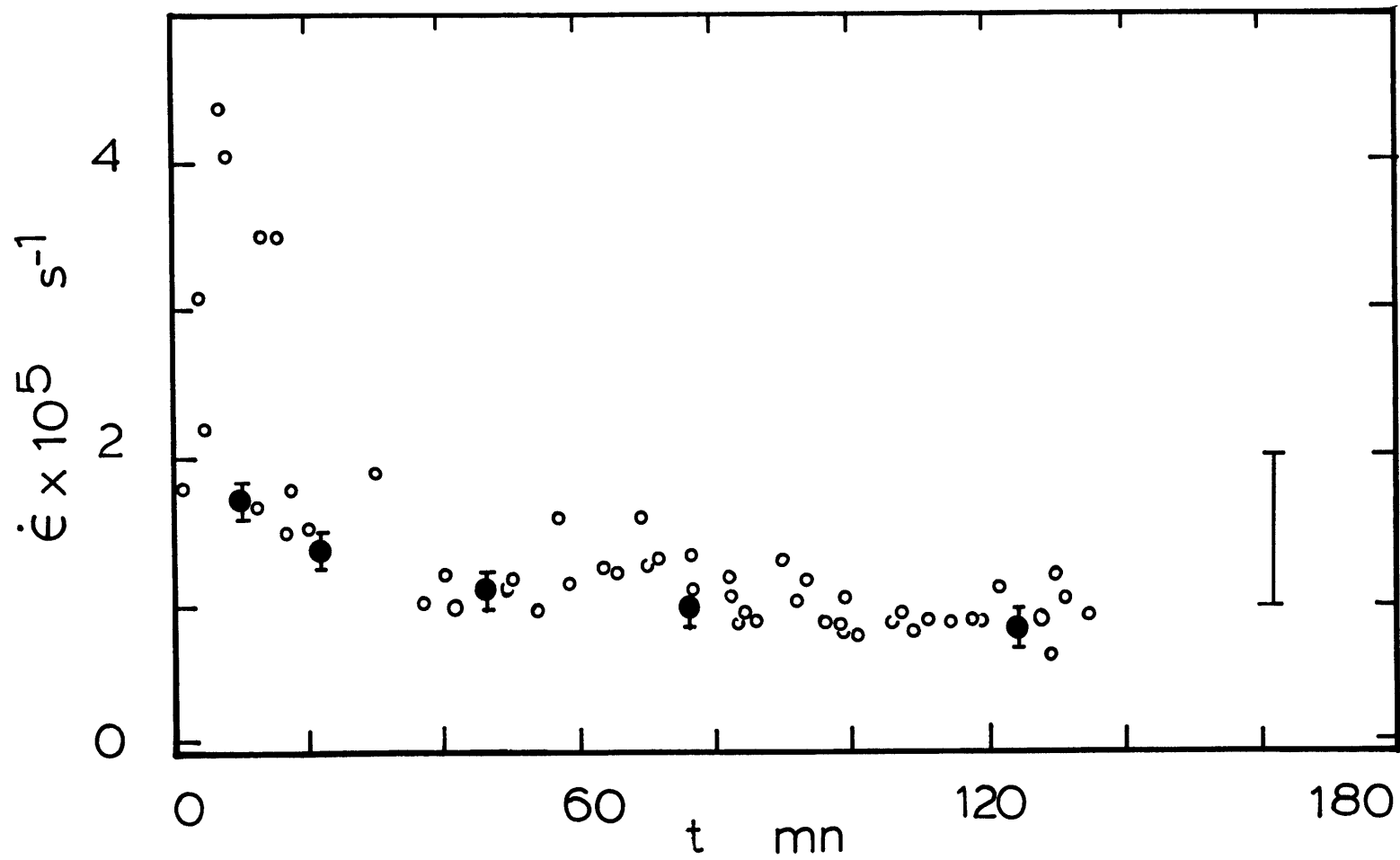


Fig. 6. SEM picture of diabase sample heated to 800°C. This sample is virtually crack free. Pyroxene (Py), Plagioclase (PL).

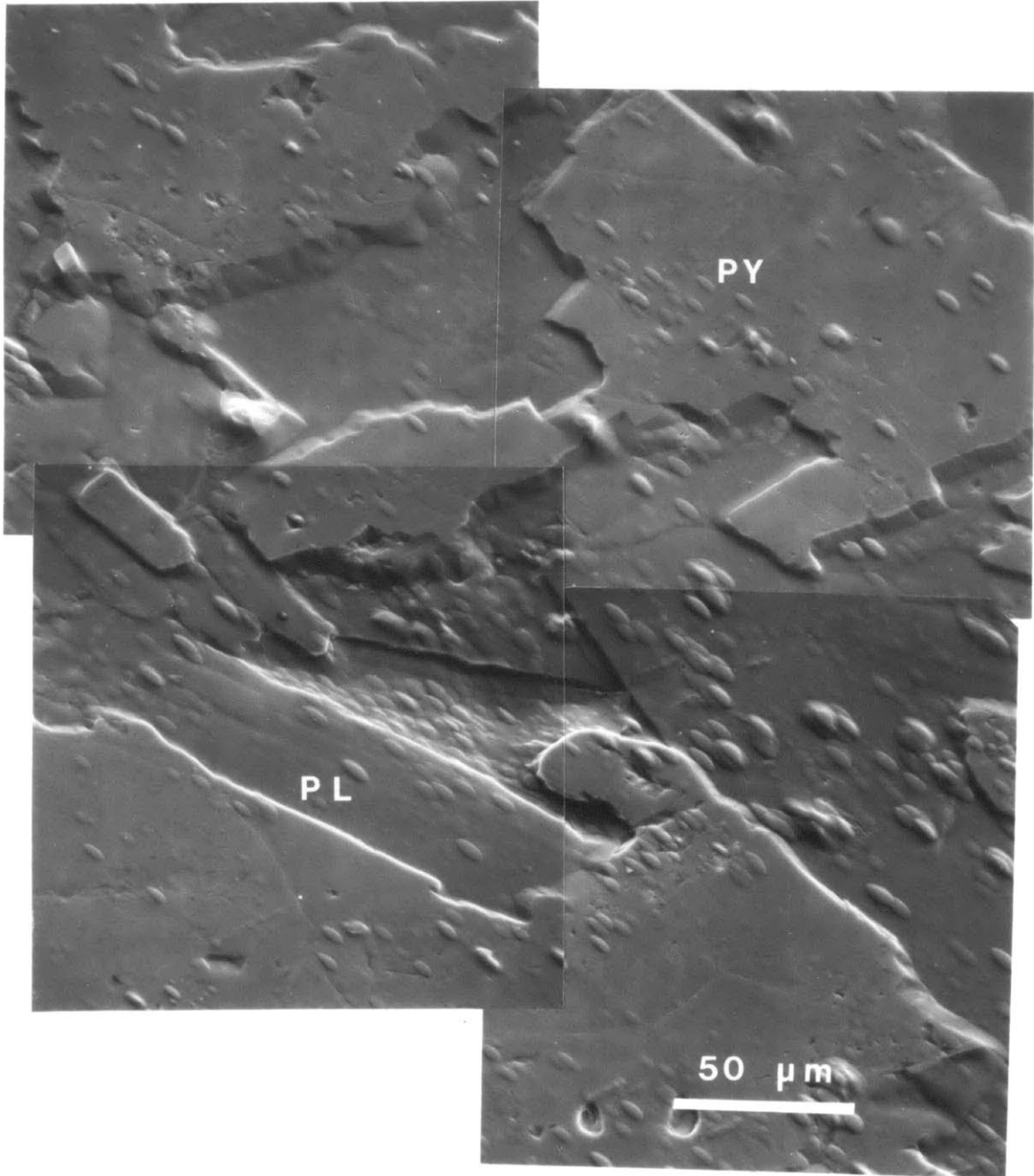


Fig. 7. SEM picture of sample heated to 1000°C. Transgranular thermal cracking is particularly visible in pyroxene (lighter minerals), and intergranular cracking in plagioclases (darker minerals).

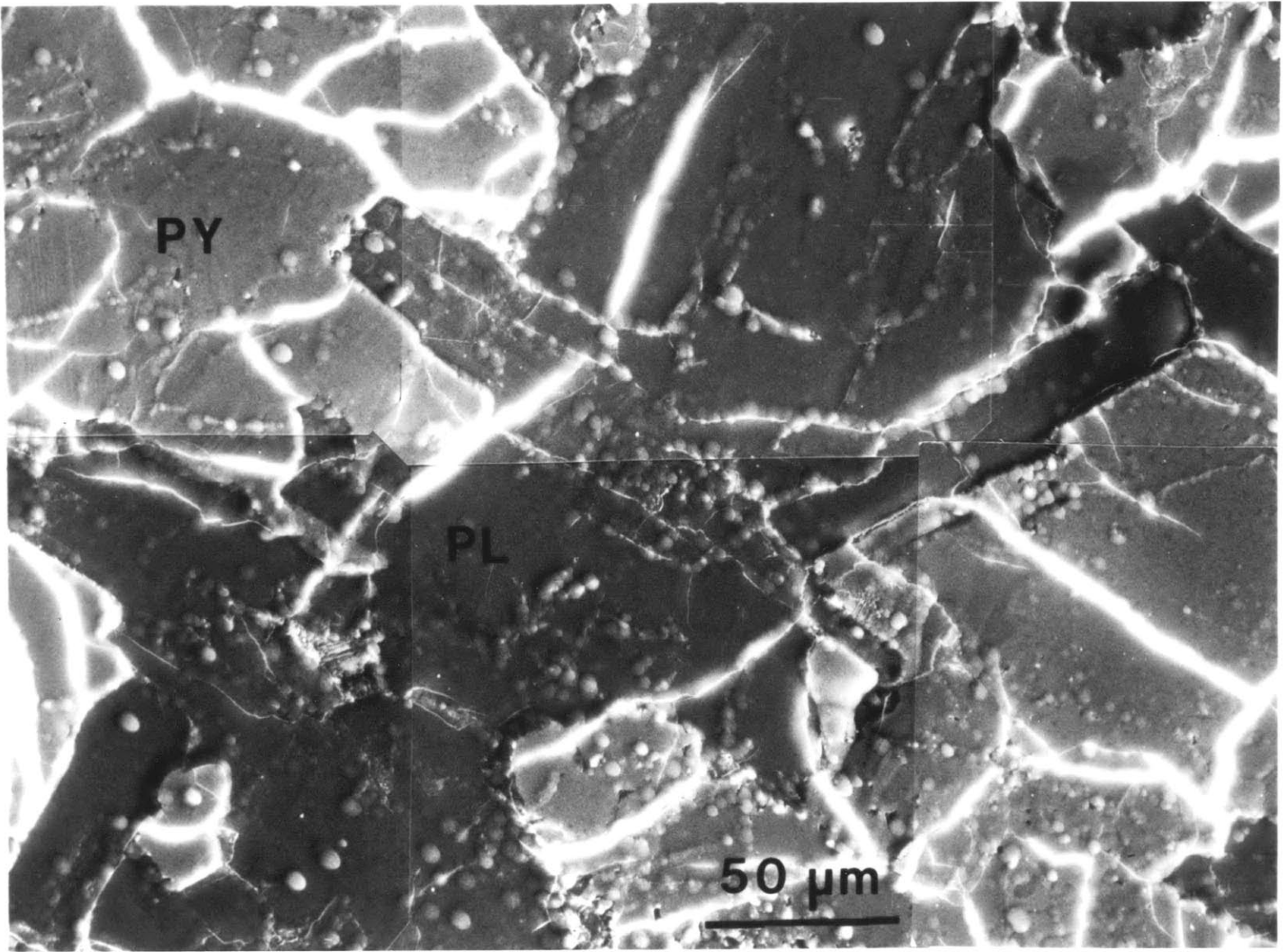
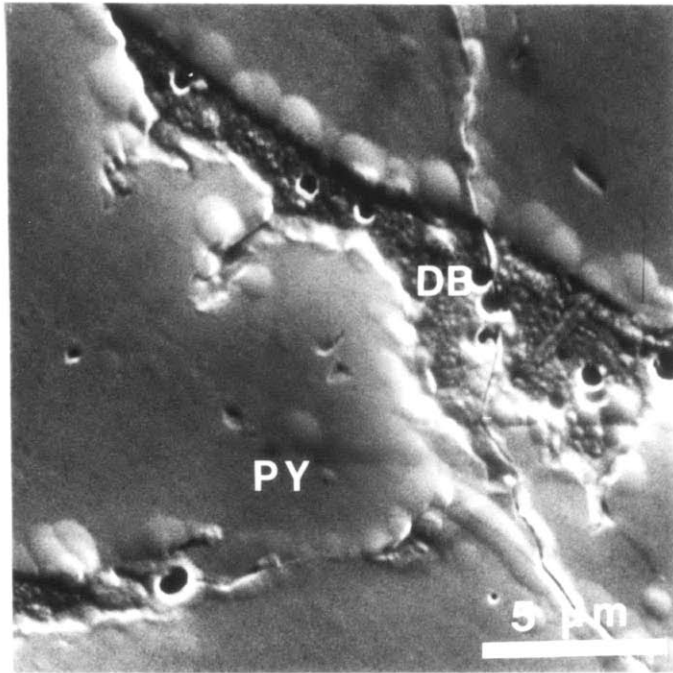
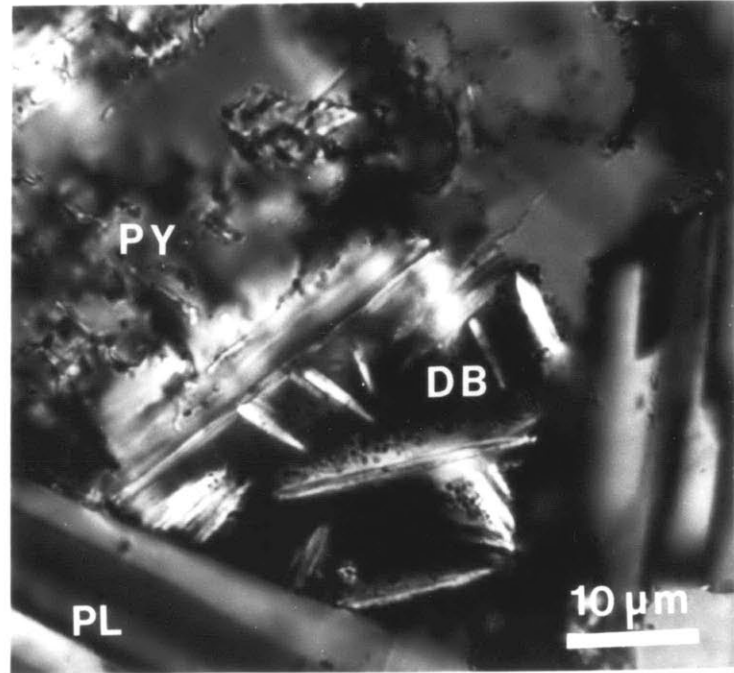


Fig. 8a. SEM picture of decomposed biotite showing acicular crystallites and grainy background, and spherical or circular pores. Post loading crack can be seen running across the picture. Lobate pyroxene boundaries and spherical pores suggest partial melting.

8b. Decomposed biotite observed with TOM. High birefringence biotite crystallites are visible on a dark and grainy background of ore minerals.



a



b

Fig. 9. Pyroxene grains with open thermal cracks parallel to the stress axis (stress axis is vertical). Small spherical pores can be seen in the material filling the open cracks (upper right hand picture).

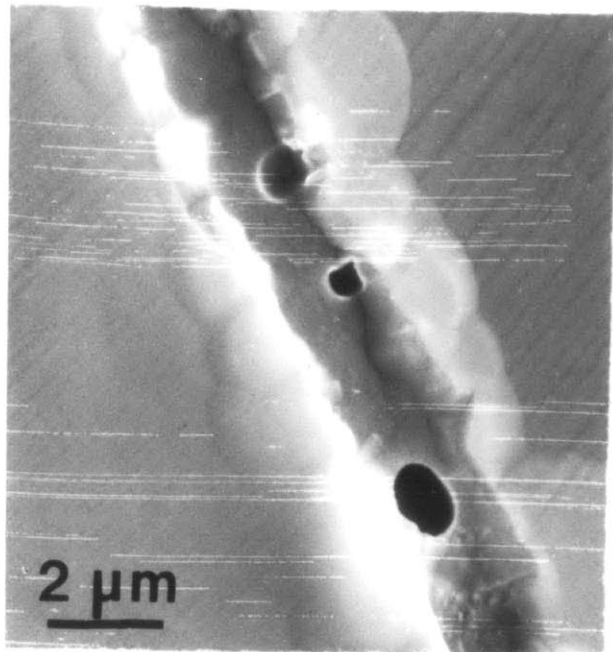
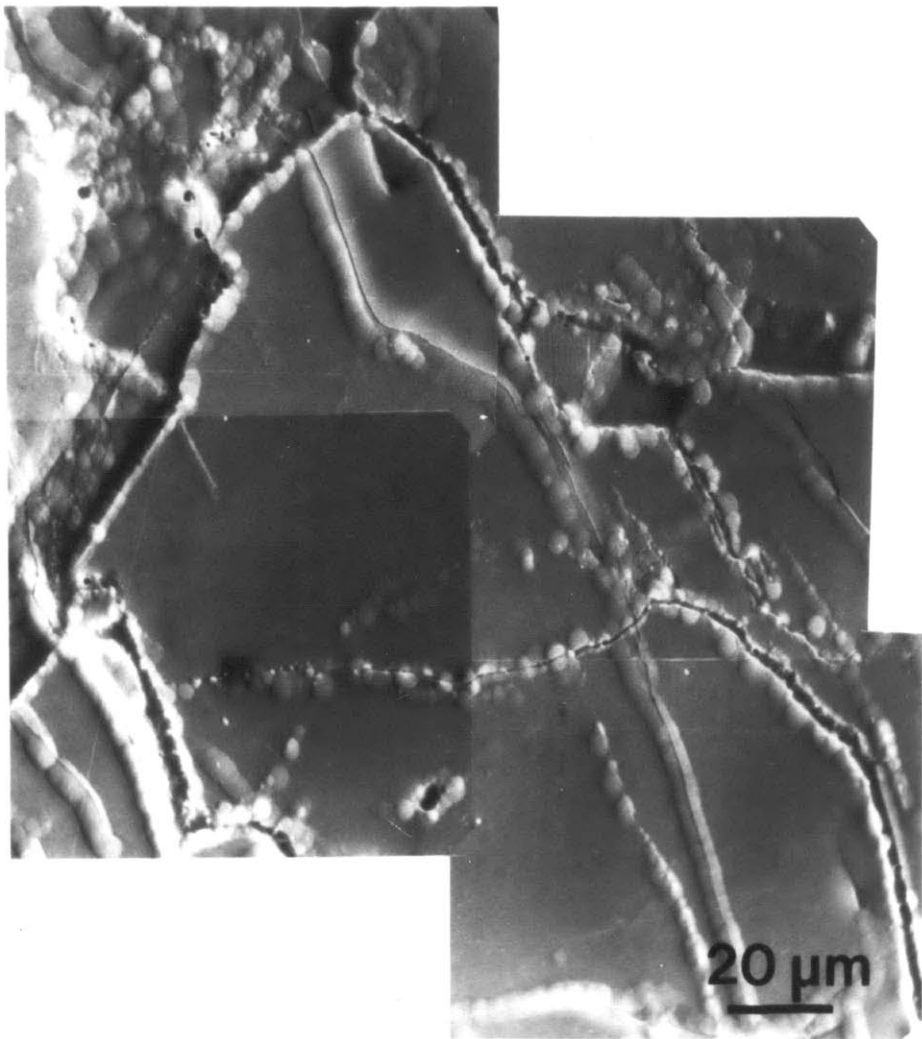


Fig. 10. Plastically bent plagioclase grains. White patches are pyroxene aggregates. Arrow points to pigeonite crystal exhibiting blobs of exsolved augite.

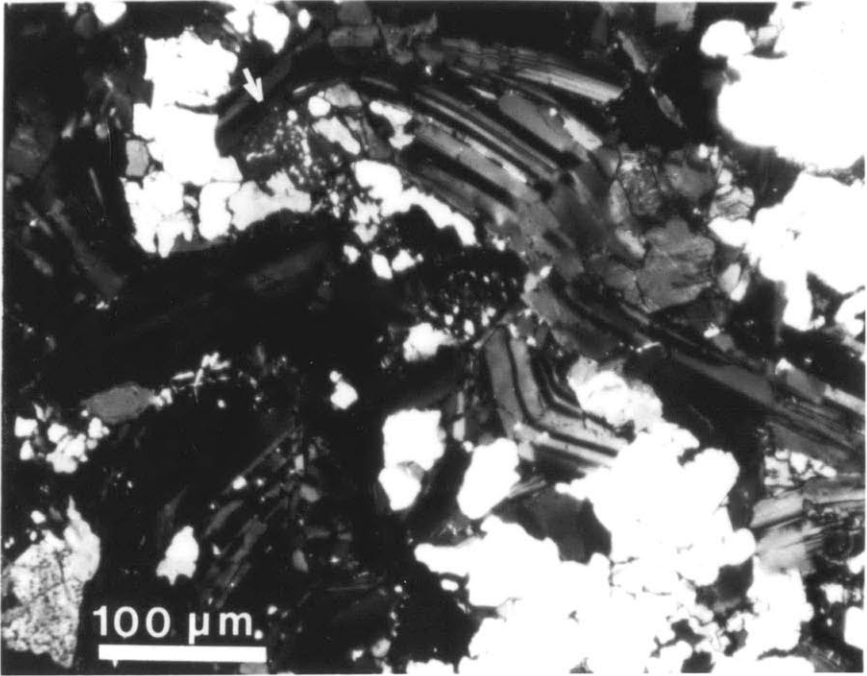
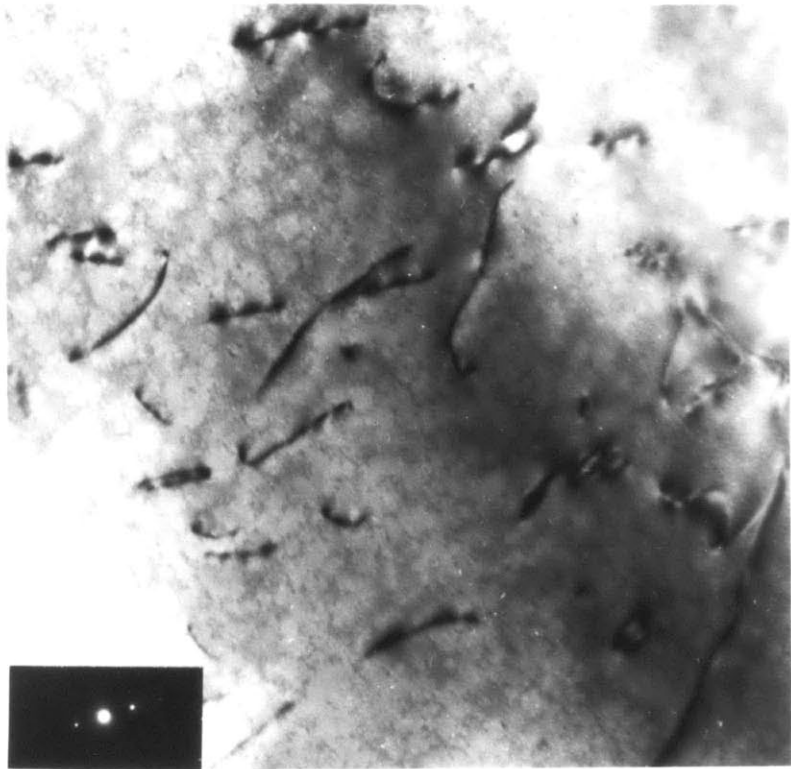


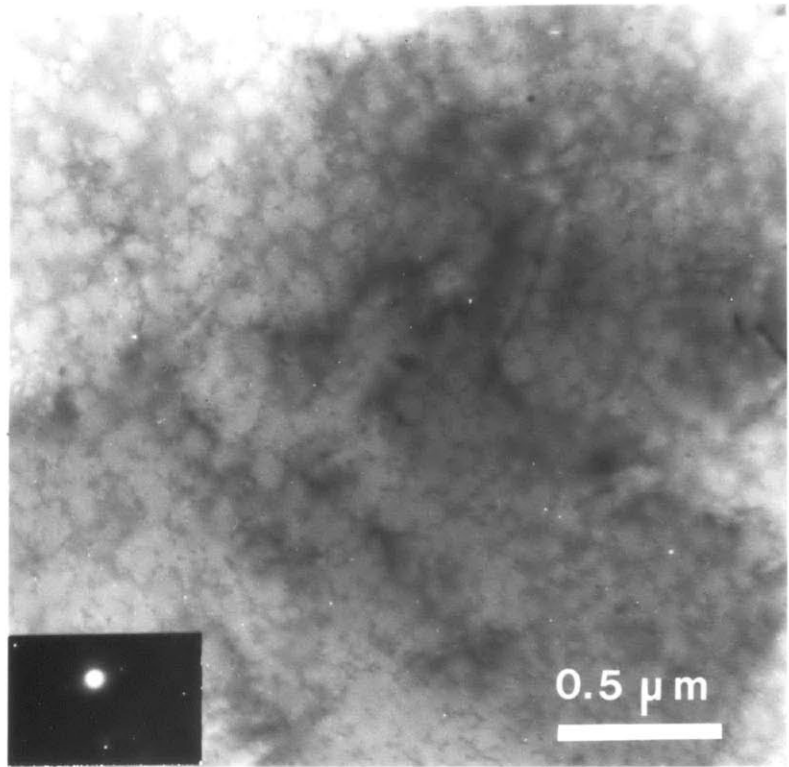
Fig. 11. Dislocations in plagioclase.

11a. Dislocations in contrast for $g = [002]$.

11b. Dislocations out of contrast for $g = [500]$.



a



b

Fig. 12a. Very fine double twinning along (100) and (001) in pyroxene. The change in lattice direction can be seen in both sets of twins.

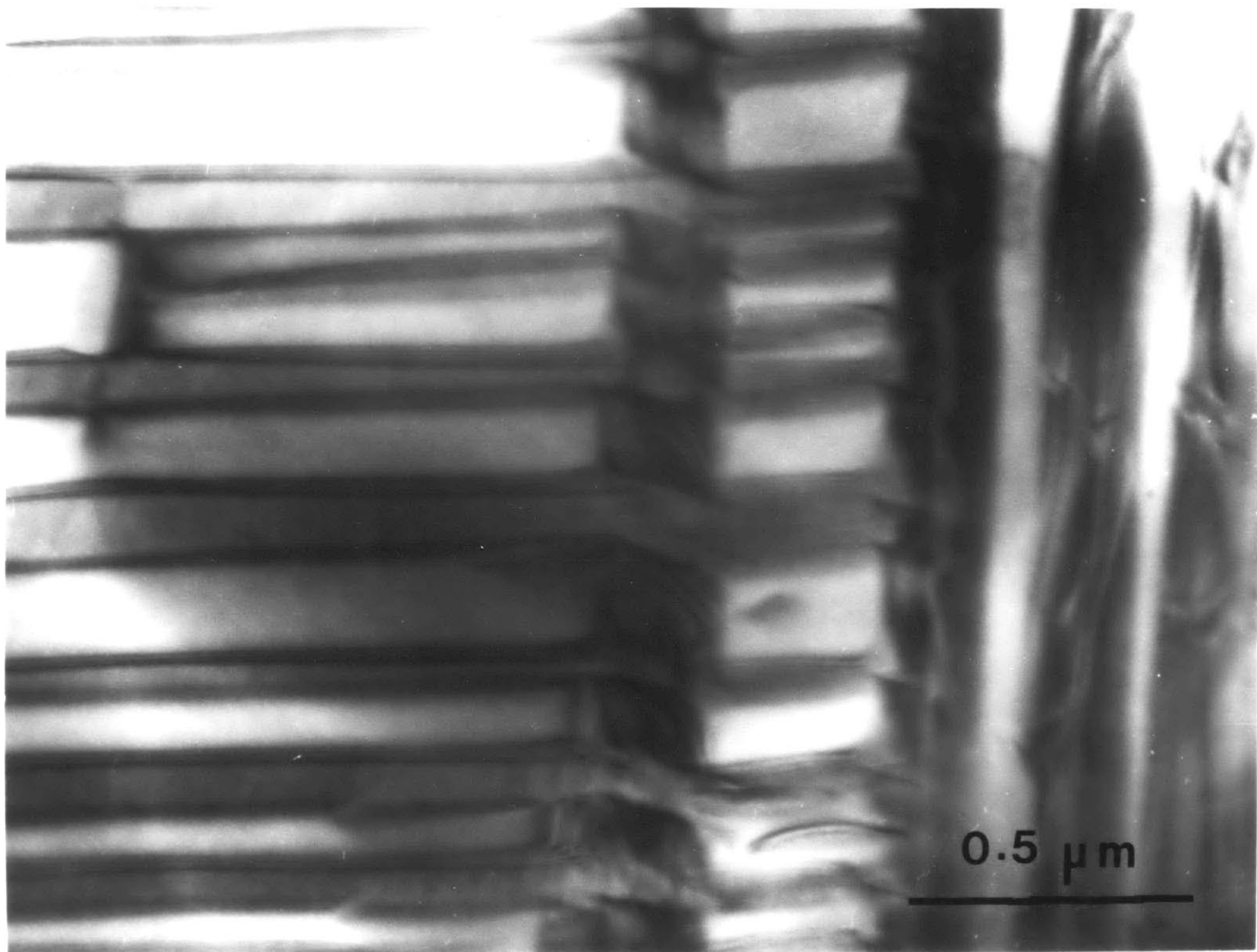


Fig. 12b. Dislocations in twinned pyroxene. Some dislocations move from one twin to the next by cross slipping into the twin boundary plane.

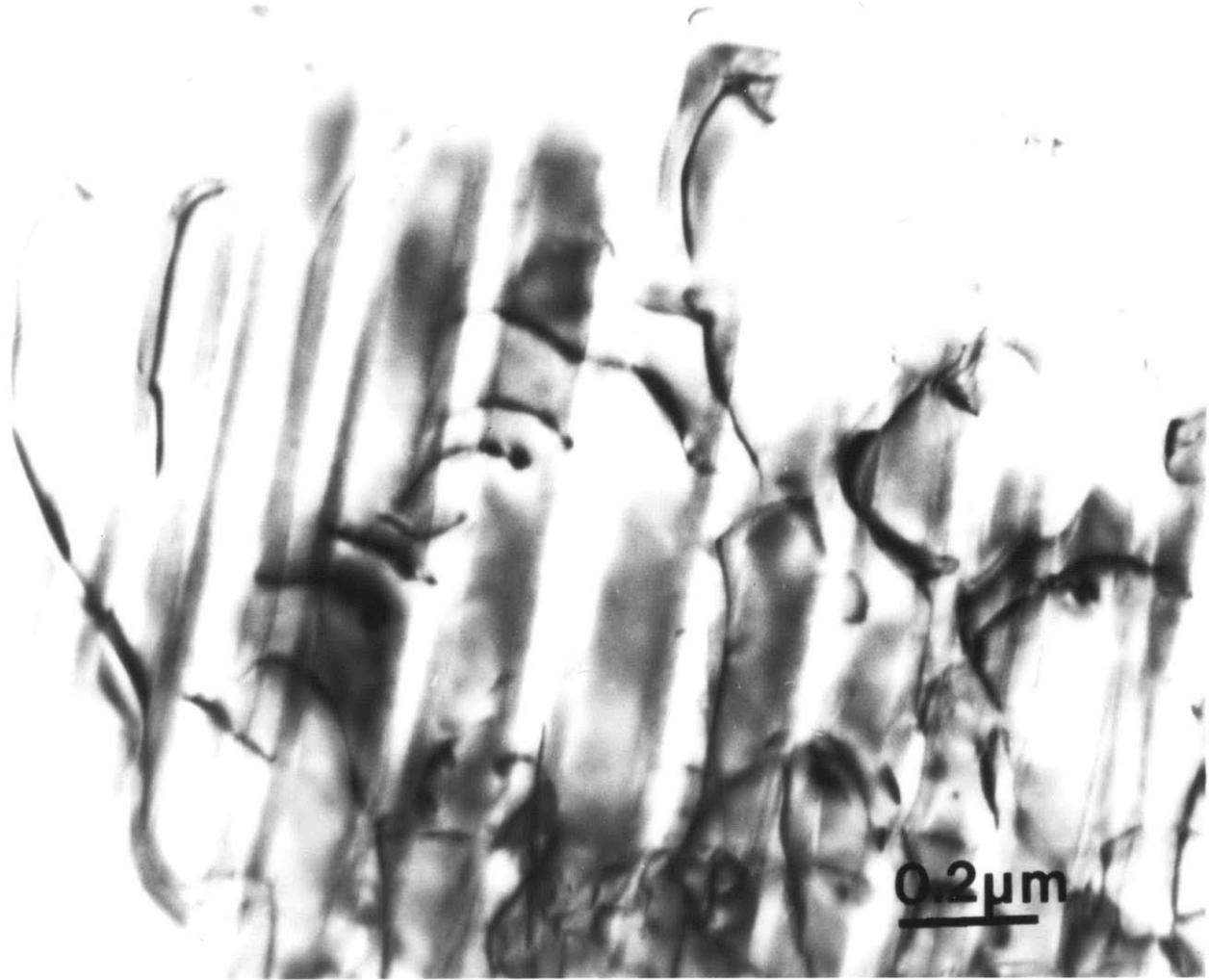


Fig. 13. Dislocations in pyroxene.

Dislocation network (dn), small dislocation dipole (d) with symmetrical contrast on dislocation line, and jogged dislocations are suggestive of glide mechanism (273 MPa, $2 \times 10^{-5} \text{s}^{-1}$).

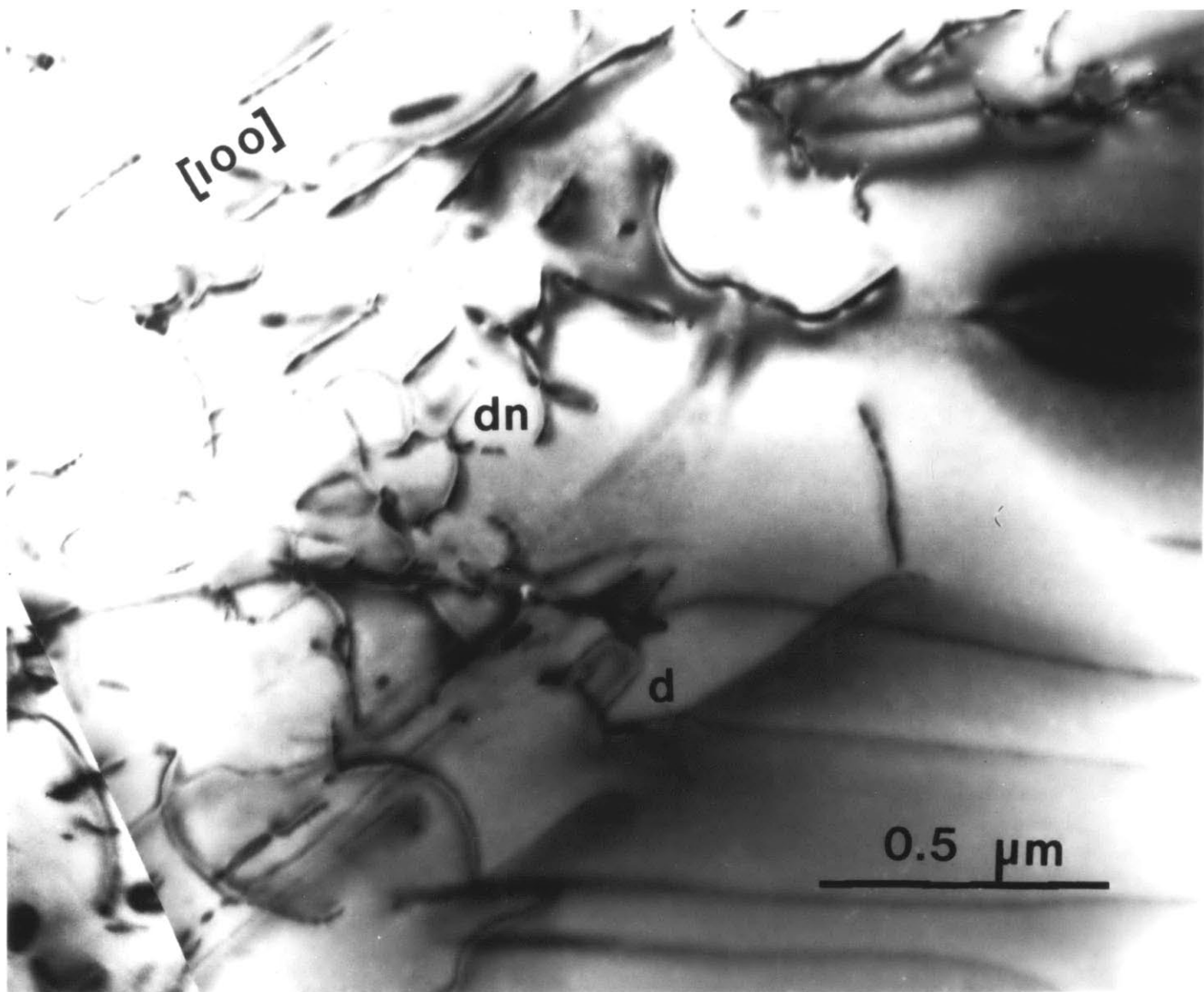
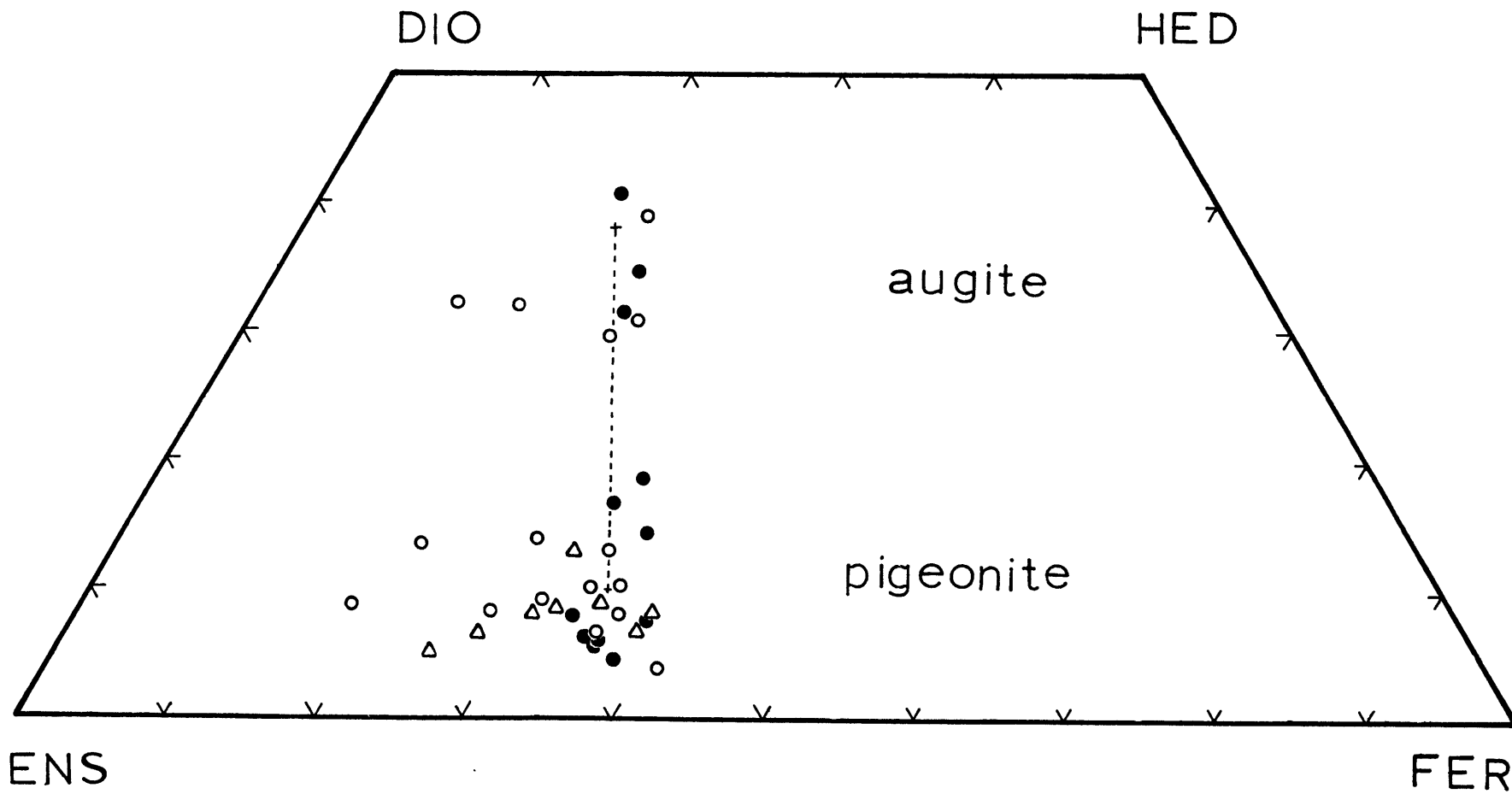


Fig. 14. Chemical composition of Maryland diabase pyroxenes. Solid dots represent original compositions corresponding to augite and pigeonite. Open circles correspond to sample deformed at 1000°C and triangles to sample just heated to 1000°C. Open symbols show a trend with respect to the original composition just reverse of a crystallization trend, suggesting partial melting.



CHAPTER II
THE TRANSITION FROM HIGH TEMPERATURE CREEP
TO FRACTURE IN MARYLAND DIABASE

INTRODUCTION

Under conditions prevailing in the mantle, most ultramafic rocks are believed to deform plastically. In the crust the conditions for rock deformation are such that the whole spectrum of possible mechanical behavior is spanned, from elasticity and brittle fracture to high temperature plasticity. Before the first determination of a reasonable strength profile for the lithosphere by Goetze and Evans (1978), the crust was considered mainly as an elastic body (Caldwell et al., 1976) or an elastic perfectly plastic body (Turcotte et al., 1978). However, stress magnitudes are substantially modified when the strength of crustal rocks and their mechanical behavior are taken into consideration, and the understanding of specific problems like the state of stress near trenches, volcanic islands or oceanic ridges (Tapponnier and Francheteau, 1978) requires knowledge of the rock strength under crustal pressures and temperatures.

Since the work of Heard (1960) on Solnhofen limestone, there has been no experimental study of the influence of various parameters such as temperature, pressure and strain rate on the transition from brittle fracture to dislocation creep in crustal rocks. This gap has been partially filled

by recent experimental studies of crustal rocks (Tullis and Yund, 1977, Kronenberg and Shelton, 1981). Additional data are presented here for Maryland diabase, a basaltic crystalline rock of fine grain size (175 μm). Experiments were conducted in order to study the transition from brittle fracture to dislocation creep at high temperature.

In order to achieve steady state creep within the pressure range available in the laboratory all experiments were conducted at 1000°. All experiments were conducted at constant displacement rate. Strain rate was varied over three orders of magnitude, at constant pressure to investigate strain rate effects on the sample behavior, and pressure was varied up to 450 MPa at constant strain rate to investigate the pressure effect. In a few cases frictional properties were studied through sliding and stress relaxation experiments. The microstructures produced were observed with a scanning electron microscope and an optical reflection microscope.

The mechanical behavior of Maryland diabase thus determined is compared to that of other silicate rocks at high temperature and pressure and to the behavior of sedimentary rocks. A criterion is proposed for the conditions under which dislocation creep can be achieved, and its application to geological conditions is considered.

EXPERIMENTAL PROCEDURE

All experiments were conducted in a high pressure servocontrolled deformation apparatus, at 1000°, and at pressures up to 450 MPa. The experimental set-up and starting material have been described in detail in the first chapter. The apparatus was internally heated and the pressurizing medium was argon. Temperatures were measured at the top of the sample, and temperature variations along the sample were of the order of 15°. Load was measured by an external load cell, and homogeneous mean stress data reported here are accurate within 4%. Error in displacement is believed to be within 2%, and pressure, measured within 1 MPa, could vary within 10 MPa during some experiments.

The sample assembly used (Fig. 1) consisted of the sample itself, 0.5 inch in diameter by 0.8 inch in length, and an alumina column, about 5 inches long that could transmit the applied load to the sample at 1000° without deforming plastically. Because its geometrical dimensions were larger than that of the sample, the alumina column stiffness was about one order of magnitude smaller than that of the sample. However, the stress strain curve pattern was not affected by this low stiffness. A stress strain curve indicating a strain softening behavior would still indicate a strain softening behavior after correction for the column stiffness, and the stress strain curve of a

creeping sample would not be modified by such a correction. Therefore, as we were concerned mainly with the stress strain curve pattern and strength of the rock, all stress strain curves presented here have not been corrected for column stiffness.

MECHANICAL DATA

Effect of strain rate on the mechanical behavior at constant pressure

A series of 5 experiments was conducted at 150 MPa confining pressure, 1000°, and at strain rates varying from $2 \times 10^{-3} \text{s}^{-1}$ to $8 \times 10^{-6} \text{s}^{-1}$ in order to investigate the effect of strain rate on the mechanical behavior and the strength of Maryland diabase. The corresponding stress strain curves are presented on Figure 2. They show that the peak stress was almost constant for strain rates higher than about 10^{-5}s^{-1} , but permanent strain at fracture increased with decreasing strain rates, and was distributed throughout the sample (Fig. 3). For strain rates below 10^{-5}s^{-1} the peak stress decreased with decreasing strain rates.

Sample 1 and 2 fractured with a sudden release of energy, and a stress drop generally associated with brittle fracture at low temperatures. The process was loud. Samples 3 and 4 were also fractured but the process was not acoustically loud, and was only revealed by the stress drop. Finally sample 5 was not acoustically noticeable, and no strain localization

was observed, as can be seen on Figure 3. There was no sharp stress drop but a gradual strain softening. This gradual change in loudness indicates that either the stress drop was smaller at low strain rates or that the instability occurring during the stress drop was slower from runs 1 to 5. Because the instability during runs 1 and 2 was too fast to be graphically recorded (Fig. 2), but was actually recorded during runs 3 to 5, it is probable that the instability was slower during these runs.

Effect of pressure on the mechanical behavior at constant strain rate

A series of constant strain rate experiments was conducted from room pressure to 450 MPa. Peak stresses are listed on Table I, and grouped by strain rates on Figure 4. Data were divided into three groups according to the behavior: brittle behavior when the sample fractured with a fault going through, and stress strain curves showed a sudden and sharp stress drop; transitional when no stress drop was noticed, but the sample had a fault going through, or when stress strain curves showed strain softening, even without a throughgoing fault; and finally creep when the sample reached a quasi-steady state regime, without strain softening or localization of deformation. Creep refers here to high temperature dislocation creep, and data come from Chapter I. Some of these points represent differential stress tests.

The most striking features on Figure 4 is the shape of the constant strain rate curves well exemplified by the $2 \times 10^{-5} \text{s}^{-1}$ curve. At $2 \times 10^{-5} \text{s}^{-1}$ peak stress increased with increasing confining pressure. The corresponding behavior was brittle. Then, above about 150 MPa confining pressure, peak stress started to decrease, showing therefore a negative pressure sensitivity. The sample behavior was transitional. At 350 MPa samples were creeping and the peak stress did not vary with pressure any more. The same pattern was observed at strain rates of $2 \times 10^{-3} \text{s}^{-1}$ and $8 \times 10^{-6} \text{s}^{-1}$.

Brace (1964) measured the fracture strength of Maryland diabase at room temperature (Fig. 4). For the whole pressure range the fracture strength was substantially higher than the 1000° fracture strength. At 150 MPa and room temperature the strength was 1.50 GPa, but 0.80 GPa at 810°, and only 0.55 GPa at 1000°. These data indicate that, in the brittle regime, the fracture strength of Maryland diabase was temperature sensitive.

In the transitional regime strength was also temperature sensitive: at 300 MPa confining pressure and $4.1 \times 10^{-5} \text{s}^{-1}$ a 30° change in temperature caused a decrease of 130 MPa in strength. But unlike strength in the brittle regime, the strength of sample deformed in the transitional regime was decreasing with decreasing strain rate, as indicated by

data on Figure 4.

In summary, in the brittle regime the strength of Maryland diabase increased with increasing pressure or decreasing temperature, but did not change with strain rate. In the transitional regime strength decreased with increasing pressure and temperature, but also decreased with decreasing strain rate. Finally in the creep regime strength decreased with increasing temperature or decreasing strain rate (Chap. I) but did not change with pressure.

It was suggested by Goetze (personnel communication) that in order to achieve full creep a confining pressure P in excess of the differential stress was necessary. The criterion $P = \sigma_D$ is represented by a thin straight line on Figure 4. On that Figure all samples deformed under conditions such that $P < \sigma_D$ did show a transitional or brittle behavior. Samples deformed with $P > \sigma_D$ achieved full creep. It seems therefore that the criterion proposed by Goetze holds for Maryland diabase.

FRICITIONAL BEHAVIOR

The goal of the present study was not to study in detail the frictional behavior of Maryland diabase. However, data are presented here that have been gathered from three different experiments: F1, F2, and F3, all of them conducted

in the transitional regime. Structural observations revealed that, in these experiments, the fault width was about 25 μm . Displacements rates were therefore transformed into equivalent shear strain rates, taking account of the angle α of the fault with the loading direction:

$$\dot{\gamma} = \dot{\delta}/t\cos(\alpha) \quad \text{and} \quad \gamma = \delta/t\cos(\alpha)$$

where $\dot{\gamma}$ is the shear strain rate, γ the shear strain, δ the recorded displacement, $\dot{\delta}$ the recorded displacement rate, and t the thickness of the fault. F3 was a stress relaxation experiment. The corresponding data were reduced using the following formula:

$$\dot{\delta} = \Delta F/k\Delta t$$

where k is the stiffness of the loading system, ΔF the load decrement, Δt the time interval for the load decrement. Data are presented on Figure 5.

Sample F1 was loaded under 250 MPa, and $4 \times 10^{-5} \text{s}^{-1}$. A fault developed, and a leak occurred through the copper jacket. However, friction strength was recorded as a function of strain rate. Although that strength is much lower than the strength of F2 and F3, it is not zero, suggesting that either the effective pressure was different from zero, or the fault

had some cohesion.

Sample F2 was deformed under 150 MPa confining pressure by differential testing. Sample F3 was loaded under 400 MPa confining pressure until the yield point was reached, then unloaded. At the second loading strength had dropped from 790 MPa to 320 MPa, and subsequent observation revealed that a fault had developed making an angle of 30° with the loading direction. Stress relaxation data were then recorded in order to determine the strain rate dependency of the frictional strength. These data together with data from F2 showed that frictional strength decreased with decreasing strain rate. This behavior was very different from room temperature dynamic friction reported by Dietrich (1973b): the dynamic frictional strength decreases with increasing slip velocity. Furthermore, frictional strength reported on Figure 5 was not pressure dependent: frictional strength at 150 MPa and 400 MPa confining pressure were similar. Thus it seems that Byerlee's law did not apply (Byerlee, 1978). The frictional characteristics represented on Figure 5 are therefore closer to high temperature creep than to low temperature friction. Stesky (1978) measured the rate sensitivity of friction sliding strength as a function of temperature from 300° to 700° . The rate sensitivity increased with temperature. The rate sensitivity of the data on Figure 5 would be higher than that reported by Stesky at 700° , therefore following

the trend he noticed from 300° to 700° which indicate that the change from low temperature friction to high temperature friction is a gradual one.

MICROSTRUCTURAL OBSERVATIONS

Two samples deformed in the transitional regime were sectioned, polished, ion milled for a few hours (Sprunt and Brace, 1974), then sputter coated with a 500 Å thick gold palladium coating. They were then observed under scanning electron microscope.

Sample F2 had a throughgoing fault making an angle of about 35° with the loading direction. That fault is represented on Figure 6. It is characterized by the absence of dilatant cracks typically associated with low temperature faults (Tapponnier and Brace, 1976, Wong, 1981). A closer look at the fault itself revealed that the strained zone was composed of grains a few microns in size (Fig. 7) with pores dispersed in the fine grained matrix. Pores had concave boundaries and sharp corners suggesting that they were formed through boundary sliding (Evans and Rana, 1979). The difference in the fault microstructures observed at low temperature (Wong, 1981) where microcracks and non-sintered fault gauge are present, and the microstructures presented here might account for the differences noted above between the low-temperature frictional behavior and the high-

temperature frictional behavior reported here, the high-temperature friction process being controlled by the creep of the porous fine grained matrix represented in Figure 7.

The second sample chosen for observation under SEM was also deformed in the transitional regime, under 300 MPa, at a strain rate of $4 \times 10^{-5} \text{s}^{-1}$. After reaching a peak stress of 470 MPa the sample did not fracture, but showed a stable strain softening without any faulting. The general sample appearance is shown on Fig. 8a, and can be compared with the undeformed material as it appeared also under SEM (Fig. 8b). Most pyroxene aggregates were thermally cracked during the heating stage of the experiment and among the thermal cracks, those oriented parallel to the loading direction tended to be wider (about $1 \mu\text{m}$). This characteristic feature was also observed in samples deformed in the creep regime (Chap. I, Fig. 9). The number of pores and cavities of irregular shape that could be observed was slightly higher than in the creep samples. It is difficult to assess an exact number to that porosity, but the porosity difference between creep and transitional samples is certainly not more than a factor of 2. Therefore no dramatic difference was found between the microstructures in strain softening sample of the transitional regime, and samples that were deformed in the creep regime, except the slightly higher porosity noticed above.

COMPARISON WITH EXISTING DATA AND DISCUSSION

The brittle-ductile transition in Solnhofen limestone has been studied previously by Heard (1960), and more recently Tullis and Yund (1977), Kronenberg and Shelton (1981), and Shelton et al. (1981) studied the mechanical behavior of silicates as a function of temperature and pressure. It is of interest to compare these data with the data reported here. Before looking at the transition and the negative pressure sensitivity associated with it, we will look at the brittle regime and the variation of fracture strength with temperature.

Variation of fracture strength with temperature

The present study showed that the fracture strength of Maryland diabase decreased with increasing temperature, for confining pressure up to 450 MPa. A similar conclusion was reached by Friedman et al. (1979) on Cuerbio basalt under 50 MPa confining pressure. The strength decreased about linearly up to about 900°, and then much more rapidly until about 1050°, where the basalt melted and the strength dropped to nearly zero. In Dresser basalt (Lindholm et al., 1974) the fracture strength at room pressure showed the same pattern. Stesky et al. (1974) studied the fracture strength of San Marcos gabbro and Westerly granite. Under 400 and 500 MPa confining pressure and experimental strain rates similar to those used in the present study, both rocks exhibited a

decrease of fracture strength with temperature. That decrease was almost linear from room temperature to 700°. Therefore the decrease of strength observed here for Maryland diabase between room temperature (Brace, 1964) and 1000° is not specific of that rock but seems to occur in all the silicates mentioned above. For Maryland diabase the fracture strength at 150 MPa and 1000° did not vary when strain rate was varied between 10^{-3} and 10^{-5}s^{-1} . It seems therefore difficult to attribute the decrease of fracture strength with temperature to rate dependent plasticity. Other processes might lead to the decrease in strength such as thermal microcracking, although recent studies seem to indicate that thermal cracks do not significantly lower the fracture strength of granite and basalt (Wong, 1981, Friedman, 1979). The question is therefore still open.

The transitional regime and the negative pressure effect

The strength of Maryland diabase was observed to decrease with increasing pressure in the transitional regime. This drop in strength has also been observed for carbonates and silicates, although not associated with a transitional regime.

Heard (1960) studied the behavior of Solnhofen limestone at a strain rate of $2 \times 10^{-4}\text{s}^{-1}$ and confining pressures to 500 MPa. In the low temperature range (up to about 350°-400°),

and within the strain rate and pressure range of his investigation the ductile regime certainly involved cataclastic flow (Paterson, 1978). Above that temperature range creep mechanisms similar to those involved in the creep of diabase under high pressure and temperature (see Chap. I) were presumably the prevalent mechanisms (Schmid et al., 1977). The high-temperature range is, therefore, the range of interest in order to make a useful comparison with the results of this study. Heard noted that in that range of temperature the strength of Solnhofen limestone decreased with pressure, in other words, a negative pressure effect similar to that reported here in the transitional regime was observed in Solnhofen limestone. Griggs (1951) reported the same effect on Yule marble at lower temperature (150°), but higher confining pressures (0.5 to 1.0 GPa).

The fracture strength of Westerly granite has been studied up to 800° at 500 MPa confining pressure by Griggs et al. (1960), and recently by Wong (1981) up to 700° at 400 MPa. Wong noticed that up to about 400° the strength of Westerly granite was greater at 500 MPa than at 400 MPa, but above 400° the trend was reversed; the strength at 500 MPa was actually getting smaller than the strength at 400 MPa. The same negative pressure sensitivity was noticed by Tullis et al. (1979) in Hale albite and Enfield aplite. These

authors interpreted this result as caused by hydrolytic weakening, although their experiments were nominally "dry experiments", hydrolytic weakening being enhanced by high pressure. However, it seems that the effect observed is general, and not limited to silicates. We therefore propose an alternative explanation.

The decrease of strength with pressure in Maryland diabase has been linked here with a mechanical behavior that we called transitional. Up to now the transition from fracture to crystal plasticity had been presented in the following way (Paterson, 1978). A sample under load could yield under two possible mechanisms (1) brittle fracture: in that case strength was on the fracture curve of a strength versus pressure diagram, and its behavior was governed by the development of microcracks (2) crystal plasticity: in that case its strength was essentially pressure insensitive, and its behavior was governed by dislocation slip and glide. Of the two possible mechanisms the one by which the sample actually yielded was, under the conditions prevailing, the mechanism which corresponded to the least strength, both mechanisms being considered as non-interacting. The strength versus pressure diagram resulting from such an approach is represented on Figure 9 by curve OACD. The transition is limited to point A. The experiments on Maryland diabase presented above suggest however that the transition is not

so sharp, but extended over a pressure domain which on Figure 9 would extend from P_B to P_C . The strength curve in that domain, curve BC, is intermediate between the fracture curve OF and the creep curve AD. This suggests that, when pressure is such that fracture and creep strength are getting close to one another, both mechanisms interact, and the resulting strength is intermediate between creep and fracture strength. This is a tentative explanation and further investigation of the interaction between cracks, pores and creep under compression is needed before definite conclusion can be drawn.

The $P = \sigma_D$ criterion

We mentioned above that, on Figure 4, at 1000° , the boundary between the creep regime and the transitional regime seemed to be well approximated by the line $P = \sigma_D$. This seems also to be the case for the behavior of Hale albite. Shelton et al. (1981) studied the deformation of Hale albite, a polycrystalline rock, under confining pressures to 1.5 GPa, temperatures to 1125° , and at a strain rate of 10^{-6}s^{-1} . Figure 10 shows the strength of the rock as a function of pressure and temperature. The 900° and 800° data show the negative pressure sensitivity already noticed by Tullis et al. (1979). The behaviors reported on this diagram labelled brittle, transitional and ductile were added to the original

diagram (Shelton, personal communication). Within the precision of the data the boundary between ductile and transitional regime seems to be adequately approximated by the line $P = \sigma_D$.

If true, such a criterion would allow one to predict, for a given temperature T and strain rate $\dot{\epsilon}$, the pressure P at which the transition from creep to transitional behavior should occur:

$$P = \sigma_D(T, \dot{\epsilon})$$

σ_D being given by the flow law of the rock. Therefore, from these data alone the boundary between creep and transitional behavior could be located on a P - T diagram. Kronenberg and Shelton (1981) studied the behavior of Maryland diabase over a range of confining pressure and temperature different from this study, and at a strain rate of $3 \times 10^{-6} \text{ s}^{-1}$, and experimentally determined the boundary between brittle and ductile behavior as function of pressure and temperature (Fig. 11). It is believed that samples located in the ductile regime deformed by creep, that samples located on the boundary were transitional, and that samples located in the brittle regime were faulted and showed stress drops. The experimental boundary given by these authors would therefore be located somewhere in our transitional regime.

We also plotted on Figure 11 the boundary between transitional and creep field determined by the criterion mentioned above and the flow law for Maryland diabase presented in the first Chapter: $\dot{\epsilon} = A\sigma_D^n \exp(-Q/RT)$, with

$$A = 6.12 \cdot 10^{-2} \text{MPa}^{-n}, \quad n = 3.05, \quad \text{and} \quad Q = 276 \text{ kJ/mol} .$$

The boundary is represented by a curved solid line where the use of the flow law is appropriate, and by a dashed line where a stress activated law should in fact be used. The use of a stress activated law would slightly move the boundary towards lower temperatures. On Figure 11 there is a fairly good agreement between the boundary experimentally determined by Kronenberg and Shelton (thin straight line) and the boundary corresponding to the criterion $P = \sigma_D$, this last boundary being slightly to the right of the experimental boundary, as should be expected from their slightly different meaning. This agreement is certainly arguing for the extrapolation of the equation $P = \sigma_D$ to pressure, temperatures and strain rates representative of geological conditions.

Application to the earth

Tectonic problems such as the determination of the state of stress in the oceanic crust require that the strength of the lithosphere be estimated as a function of depth.

Strength profiles have been proposed for the oceanic lithosphere near ridges (Tapponnier and Francheteau, 1978), near trenches (Goetze and Evans, 1979), or in the old oceanic crust (Brace and Kohlstedt, 1980). In all cases the transition between creep on one hand, and fracture or frictional behavior on the other hand was determined by assuming that the mechanisms were not interacting. Therefore the transition would correspond on Figure 9 to point A, curve OF representing either fracture or frictional strength.

The data presented here suggest that the transition might actually happen over a range of pressures such as P_B - P_C (Fig. 9) which in the earth would correspond to a certain depth range. P_C corresponds to the criterion $P = \sigma_D$, and can be extrapolated to geological conditions using the flow law determined in Chapter I. However the exact location of point B along the curve OF depends on strain rate as well as temperature (see Fig. 4), and there is not enough data on that rate and temperature dependency to extrapolate the strength at point B to geological conditions. But the pressure range where the transition should occur can be approximated by P_A - P_C instead of P_B - P_C , remembering that P_A is a low bound for P_B .

The two curves corresponding to P_A and P_C have been represented on Figure 12 for a strain rate of 10^{-14}s^{-1} . In the determination of P_A the temperature dependence of fracture strength (curve OF on Fig. 9) has been taken into

account by interpolation from data on Figure 4. Dashed portion of P_A and P_C lines correspond to domain where a stress activated creep law should be used instead of a power law. The correction is believed to be a 20° to 30° shift down in temperature for the two curves. The geotherms, figured as thin straight lines are from Miyashiro (1972), and are in good agreement with the intraplate oceanic geotherm used by Goetze and Evans (1979), and geotherms near ridges (Tapponnier and Francheteau, 1978). On this diagram the transition ranges are represented by thick line segments.

Near ridges the transition temperature obtained from Figure 12 is about 425° . This value is lower than that found by Tapponnier and Francheteau, their value being about 600° . This discrepancy comes mainly from the high activation energy they used for their extrapolated flow law. According to their geotherms the 425° isotherm is very close to the base of the seismogenic layer, and in better agreement with that boundary than the 600° isotherm. From Figure 12 the transitional region would be about 15. km thick.

For intraplate geotherms the extrapolated part of curve P_A and P_C give a transition temperature of about 350° . This corresponds to a depth of about 20 km. Such a depth is intermediate between the transition depth of 15 km and 25 km for respectively dry quartz and olivine determined by Brace and Kohlstedt (1980). To the extent that Maryland diabase

is a good representative of the oceanic crust, and because the crust thickness is much shallower than the 20 km found, it is possible that the old oceanic crust is mainly brittle.

CONCLUSION

The transition from fracture to creep in Maryland diabase has been investigated experimentally at a temperature of 1000°C, confining pressures to 450 MPa, and strain rates from 2×10^{-3} to $7 \times 10^{-6} \text{ s}^{-1}$. Microstructures were observed by scanning electron microscopy. In a pressure versus strength diagram three regimes were identified:

(1) A brittle regime where the fracture strength was pressure and temperature sensitive, but strain rate insensitive. In this regime stress strain curves showed sharp stress drops and the strength had a positive pressure sensitivity. Sample had throughgoing faults.

(2) A transitional regime where the rock strength was pressure, temperature and strain rate sensitive. Stress strain curves showed strain softening without any faulting, or creep along a fault. The strength had a negative pressure sensitivity.

(3) A creep regime, where the rock strength was temperature and pressure sensitive, but pressure insensitive. The deformation in this field proceeded through dislocation creep of constitutive mineral (Chap. I), and was distributed throughout the sample.

Frictional strength in the transitional regime was strain rate sensitive, but did not show any significant pressure sensitivity, therefore differing from low temperature friction. Microstructural observations revealed that the fault zone consisted of a fine-grained porous matrix suggestive of grain boundary sliding.

The boundary between the creep and the transitional regime corresponded to conditions where the peak differential stress was equal to the confining pressure. That criterion seems to apply equally to Hale albite (Shelton et al., 1981).

Data presented above have been extrapolated to geological conditions prevailing in the oceanic crust. Ridges seem to be the only place where a diabasic oceanic crust might deform by dislocation creep. The depth corresponding to the transition corresponds to the 425° geotherm and is in very good agreement with the base of the seismogenic layer proposed by Tapponnier and Francheteau (1978).

References

- Brace, W.F., Brittle fracture of rocks, in State of Stress in the Earth's Crust, W.R. Judd Ed., pp. 110-178, (American Elsevier), 1964.
- Brace, W.F., D. L. Kohlstedt, Limits on lithospheric stress imposed by laboratory experiments, J. Geophys. Res., 85, 6248-6252, 1980,
- Byerlee, J., Friction of rocks, Pure and Applied Geophys., 116, 116, 615-626, 1978.
- Caldwell, J.G., W.F. Haxby, D.E. Karig, and D.L. Turcotte, On the applicability of a universal elastic trench profile, Earth Planet. Sci. Lett., 31, 239-246, 1976.
- Dietrich, J.H., Time dependent friction and the mechanics of stick-slip, Pure Appl. Geophys. 116, 790-806, 1978b.
- Evans, A.G. and A. Rana, High temperature failure mechanisms in ceramics, Acta Met., 28, 129-141, 1980
- Friedman, M., J. Handin, N.G. Higgs, and J.R. Lantz, Strength and ductility of four dry igneous rocks at low pressures and temperatures to partial melting, Proceedings of the 20th Symposium on Rock Mechanics, Austin, Texas, 1979.
- Goetze, C. and B. Evans, Stress and temperature in the bending lithosphere as constrained by experimental rock mechanics, Geophys. J.R. Astr. Soc., 59, 463-478, 1979.
- Griggs, D.T., and W.B. Miller, Deformation of Yule marble, Part I, Geol. Soc. America Bull., 62, 853-862, 1951.

- Griggs, D.T., F.J. Turner and H.C. Heard, Deformation of rocks at 500° to 800°C in G.S.A. Memoir, 79, 39-104, 1960.
- Heard, H.C., Transition from brittle fracture to ductile flow in Solnhofen Limestone as a function of temperature, confining pressure, and interstitial fluid pressure, in Rock Deformation, Griggs, D., J. Handin (eds), G.S.A. Memoir, 79, 193-226, 1960.
- Kronenberg, A.K., and G.L. Shelton, Deformation microstructures in experimentally deformed Maryland Diabase, J. of Struct. Geol., in press.
- Lindholm, U.S., L.M. Yeakley, and A. Nagy, The dynamic strength and fracture properties of Dresser Basalt, Int. J. Rock Mech. Min. Sci., 11, 181-191, 1974.
- Miyashiro, A., Pressure and temperature conditions and tectonic significance of regional and ocean floor metamorphism, Tectonophysics, 13, 141-159, 1972.
- Paterson, M.S., Experimental rock deformation - The brittle field, 254 pp., Springer Verlag, 1978.
- Schmid, S.M., J.N. Boland, and M.S. Paterson, Superplastic flow in fine grained limestone, Tectonophysics, 43, 257-291, 1977.
- Shelton, G.L., J. Tullis and T. Tullis, Experimental high temperature and high pressure faults, in Press Geophys. Research Letters, 1981.

Sprunt, E.S., and W.F. Brace, Direct observation of microcavities in crystalline rocks, *Int. J. Rock Mech. Min. Sci.*, 11, 139-150, 1974a.

Stesky, R.M., Mechanism of high temperature sliding in Westerly Granite, *Can. J. Earth Sci.*, 15, 361-375, 1978.

Stesky, R.M., W.F. Brace, D.K. Riley, and P.Y. Robin, Friction in faulted rock at high temperature and pressure, *Tectonophysics*, 23, 177-203, 1974.

Tapponnier, P., and W.F. Brace, Development of stress-induced microcracks in Westerly Granite, *Int. J. Rock Mech. Min. Sci.*, 13, 103-112, 1976.

Tapponnier, P. and J. Francheteau, Necking of the lithosphere and the mechanics of slowly accreting plate boundaries, *J. Geophys. Res.*, 83, 3955-3970, 1978.

Tullis, J., G. Shelton, and R.A. Yund, Pressure dependence of rock strength: implications for hydraulic weakening, *Bull. Minéral*, 102, 110-114, 1979.

Tullis, J., and R.A. Yund, Experimental deformation of dry Westerly Granite, *J. Geophys. Res.*, 82, 5705-5718, 1977.

Turcotte, D.L., D.C. McAdoo, and J.G. Caldwell, An elastic perfectly plastic analysis of the bending of lithosphere at a trench, *Tectonophysics*, 47, 155-160, 1978.

Wong, T.F., Post failure behavior of Westerly Granite at elevated temperatures, Ph.D. Thesis, M.I.T., 1981.

TABLE I

T (°C)	P (MPa)	$\dot{\epsilon}$ (s ⁻¹)	σ_D (MPa)	
810	150	5.3 10 ⁻⁶	780	F
970	150	4.6 10 ⁻⁶	385	F
1005	400	1.1 10 ⁻³	790	T
1005	450	1.4 10 ⁻³	710	T
970	0	1.0 10 ⁻⁵	223	F
1010	300	2.8 10 ⁻⁵	380-440	T
995	0	2.1 10 ⁻³	193	F
1030	305	4.1 10 ⁻⁵	347	T
1000	300	4.1 10 ⁻⁵	470	T
1030	250	8.4 10 ⁻⁶	291	T
1000	200	1.4 10 ⁻⁵	474	T
1007	150	7.5 10 ⁻⁶	376	T
950	0	1.7 10 ⁻³	199	F
1000	50	1.1 10 ⁻³	440	F
1000	30	1.1 10 ⁻³	370	F
994	150	2.0 10 ⁻³	535	F
1000	150	2.0 10 ⁻⁴	566	F
1000	150	8.0 10 ⁻⁵	561	F
1000	150	2.7 10 ⁻⁵	573	F
1000	425	7.9 10 ⁻⁶	275	C
1000	350	2.3 10 ⁻⁵	271	C
1000	425	1.1 10 ⁻⁵	296	C
1000	450	1.5 10 ⁻⁵	287	C
1000	400	1.6 10 ⁻⁴	429	C
1000	425	1.9 10 ⁻⁴	424	C

High temperature mechanical data for Maryland diabase.

T is the temperature, P is the confining pressure,

$\dot{\epsilon}$ the strain rate, and σ_D the peak differential stress.

F stands for fracture, T for transitional, C for creep.

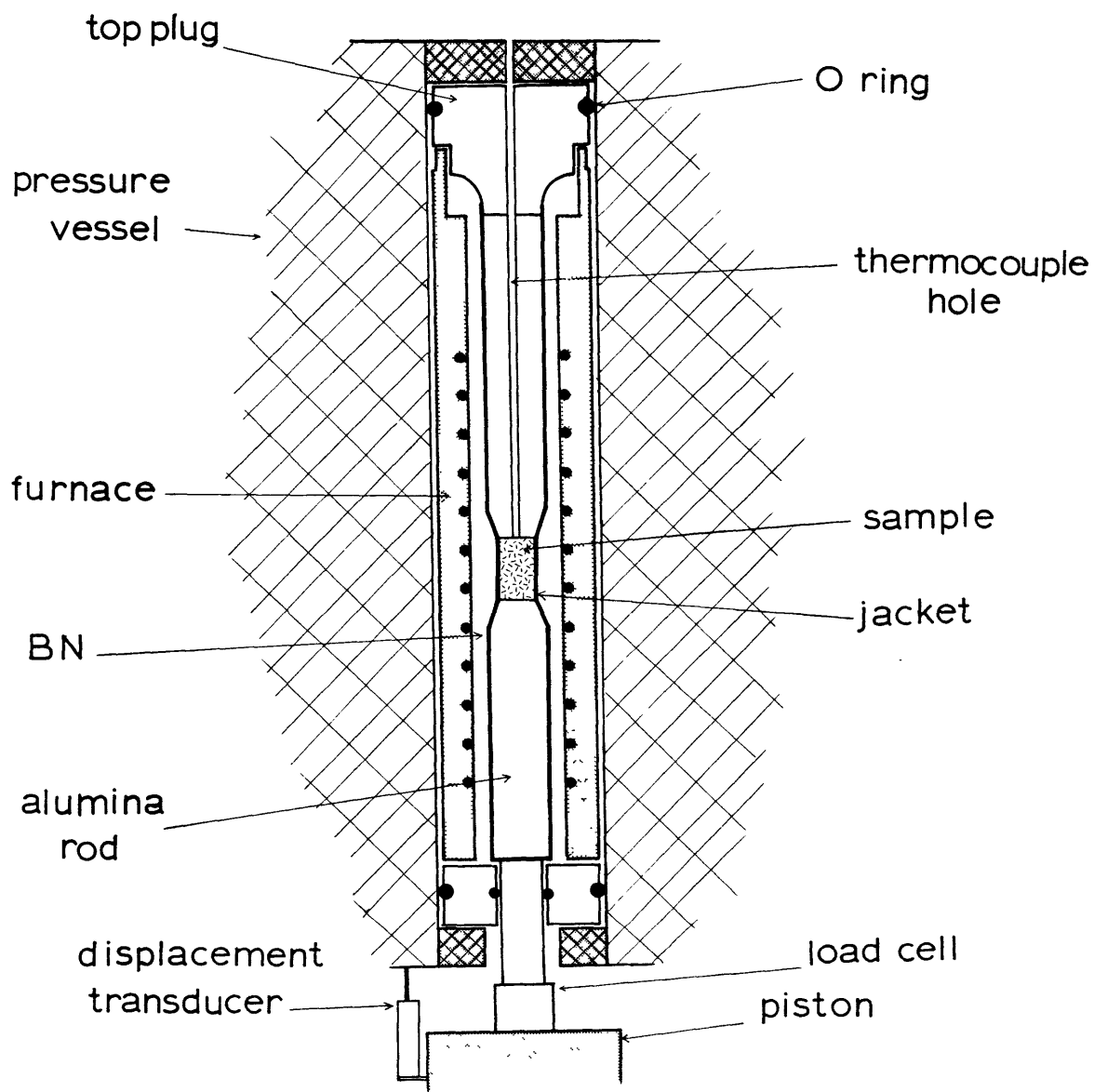


Fig. 1. Experimental assembly inside pressure vessel.

Fig. 2. Stress-strain curves of samples deformed at 1000°C, 150 MPa confining pressure. Strain rate decreases from sample 1 to sample 5.

1. $2 \times 10^{-3} \text{ s}^{-1}$

2. $2 \times 10^{-4} \text{ s}^{-1}$

3. $8 \times 10^{-5} \text{ s}^{-1}$

4. $2 \times 10^{-5} \text{ s}^{-1}$

5. $8 \times 10^{-6} \text{ s}^{-1}$

F is the differential load and ϵ the axial strain.

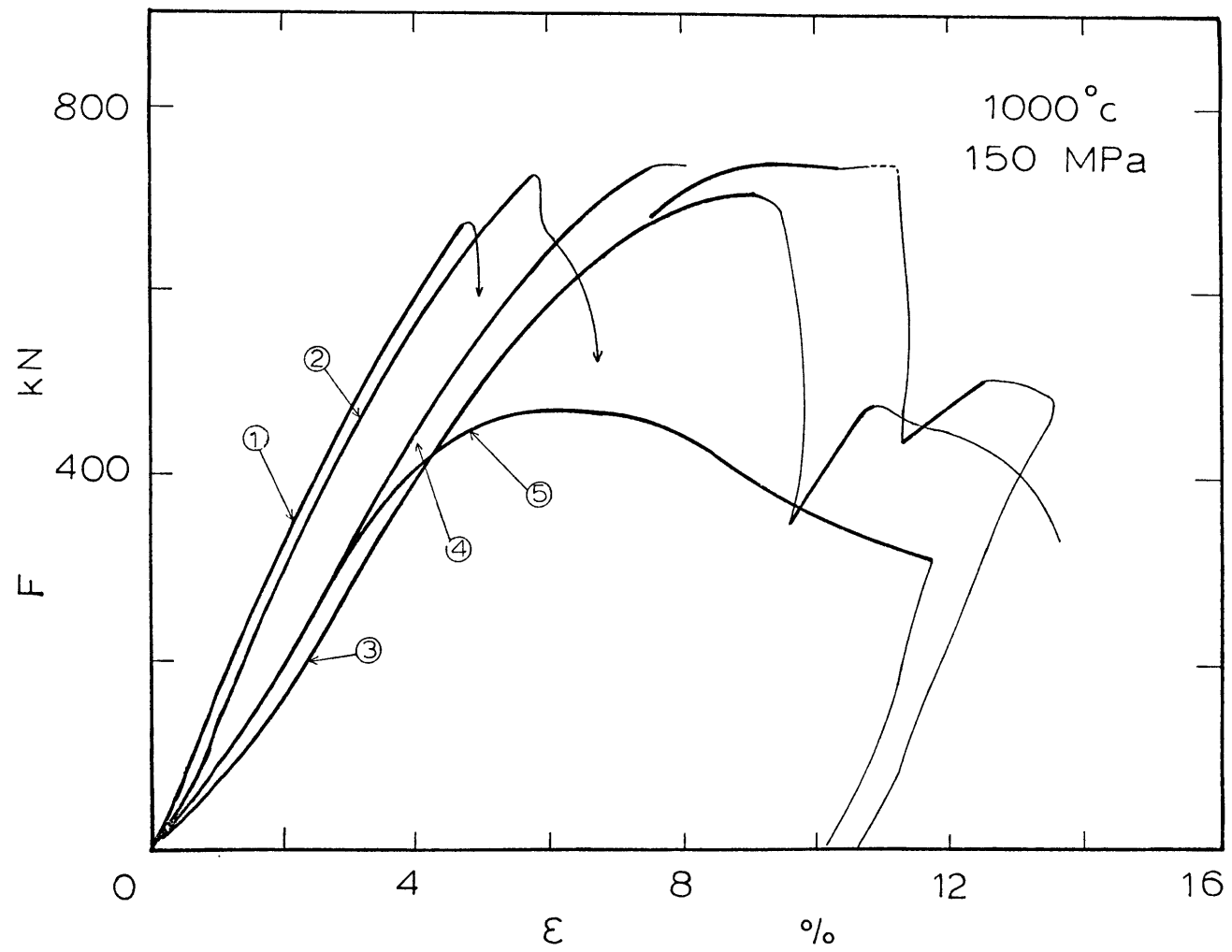
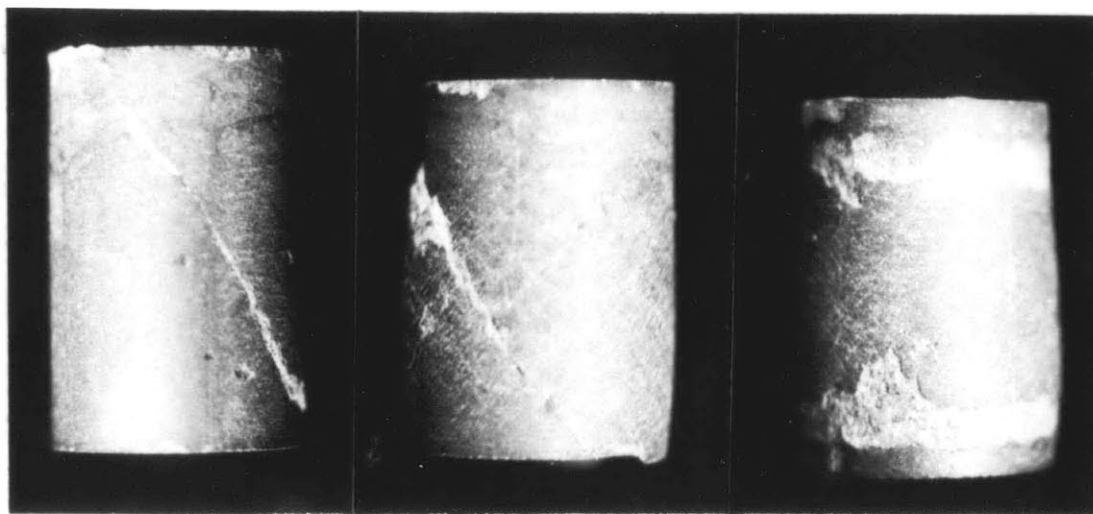


Fig. 3. Samples corresponding to stress strain curves of Fig. 2. Numbers refer to that Figure. Samples were deformed at 1000°C, 150 MPa and following strain rates:

1. $2 \times 10^{-3} \text{ s}^{-1}$
4. $2 \times 10^{-5} \text{ s}^{-1}$
5. $8 \times 10^{-6} \text{ s}^{-1}$

Sample 5 was held in place with a graphite ring instead of a copper ring. This is the cause of the two dark marks at both ends of the sample. The peeling of the copper jacket after the run is responsible for the white areas on the same sample.



1

4

5

Fig. 4. Strength of Maryland diabase versus confining pressure. All data are 1000°C data except Brace's points at room temperature and one point at 800°C. Open symbols are for fracture, solid symbols for creep, and intermediate symbols for transitional behavior (see text). The boundary between transitional behavior and creep is approximated by the thin straightline on the diagram, and corresponds to conditions such that pressure is equal to differential stress. Curves in the transitional regime are constant strain rate curves.

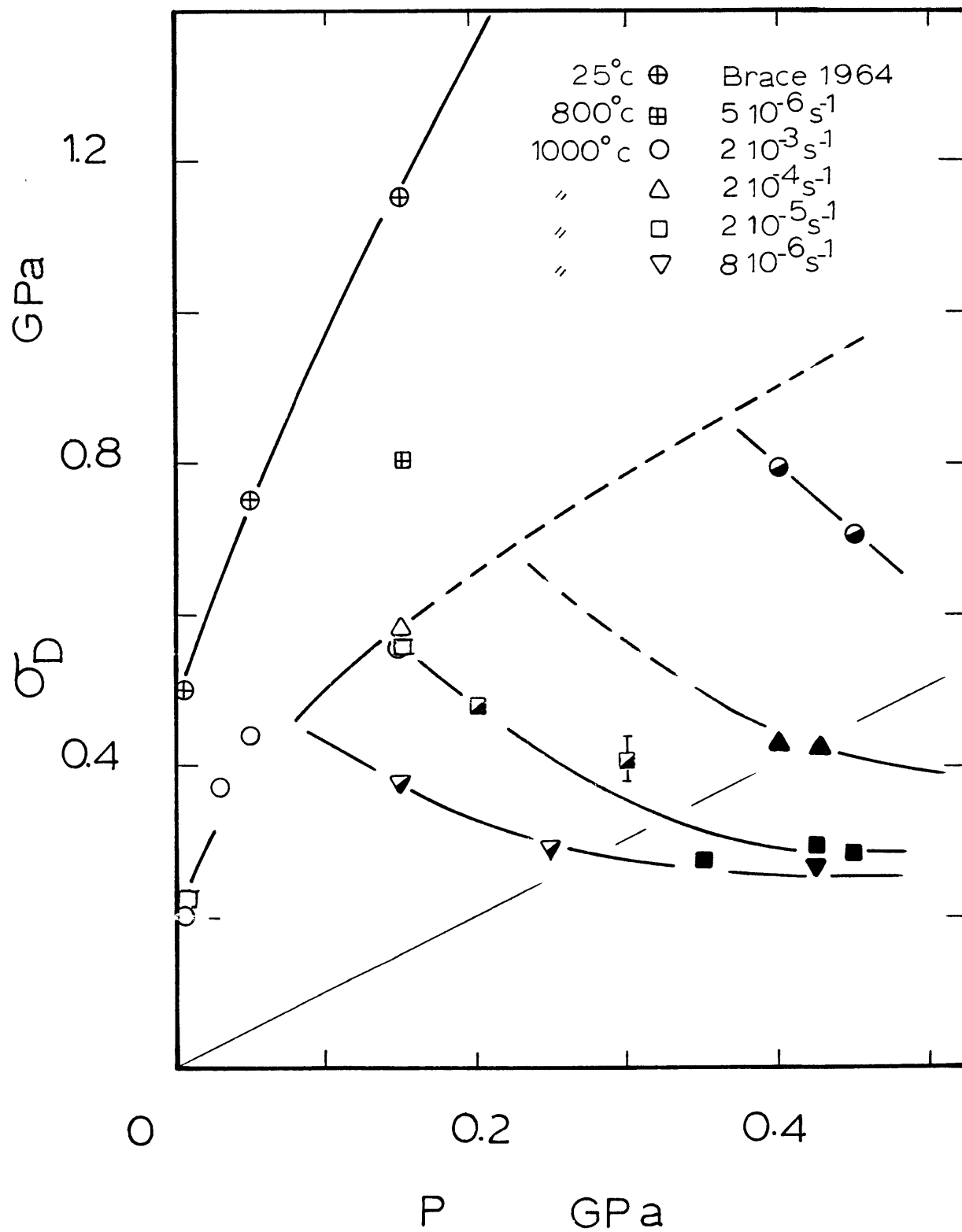


Fig. 5. Shear rate along a fault of 25 μm width versus differential stress along the principal axis for various confining pressures. F1 corresponds to zero effective pressure.

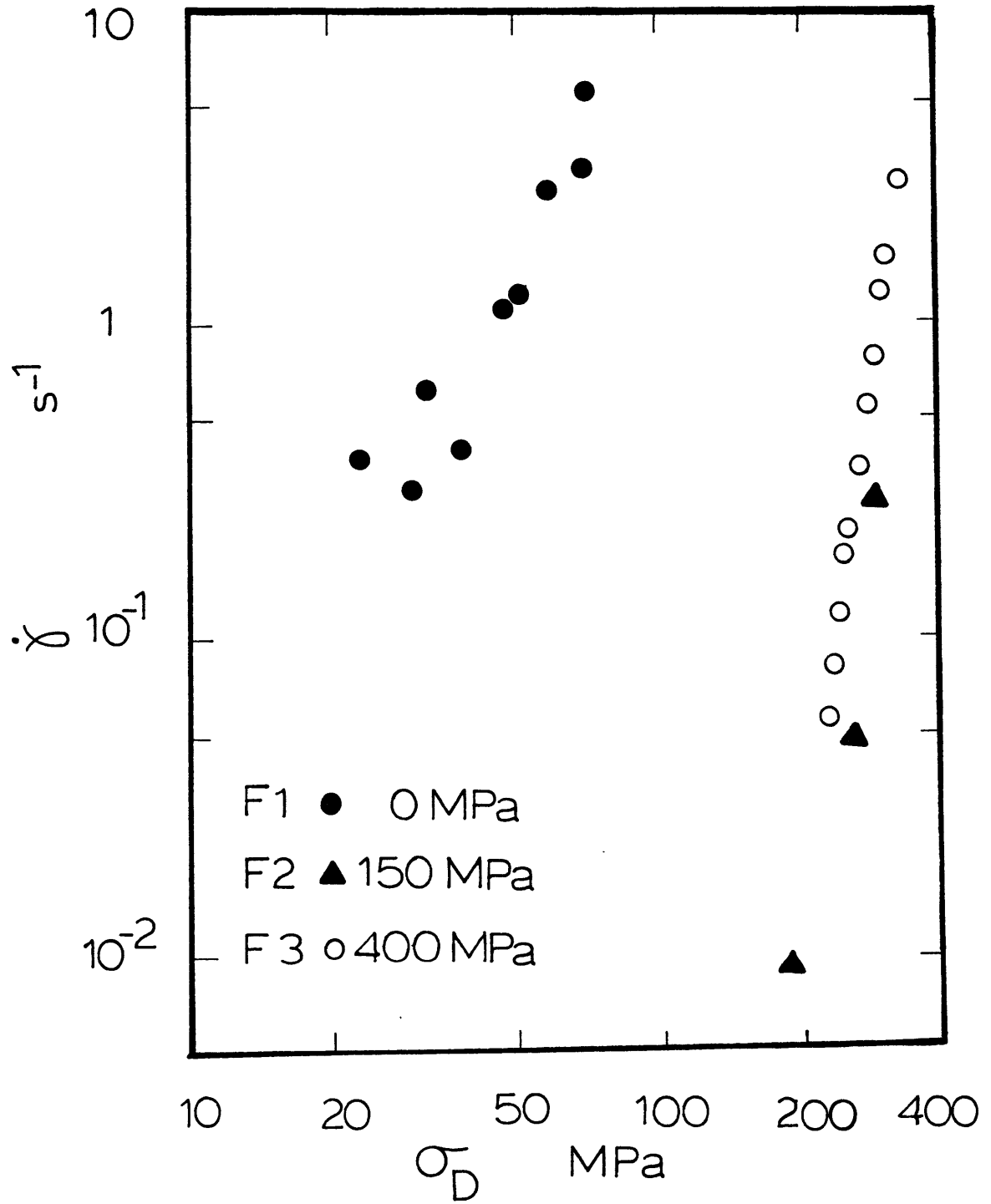


Fig. 6. Fault developed in the transitional regime in sample F2 (Fig.). PL: Plagioclase, PY: Pyroxene, O: Ore minerals. Few cracks are visible and fault is clear cut.

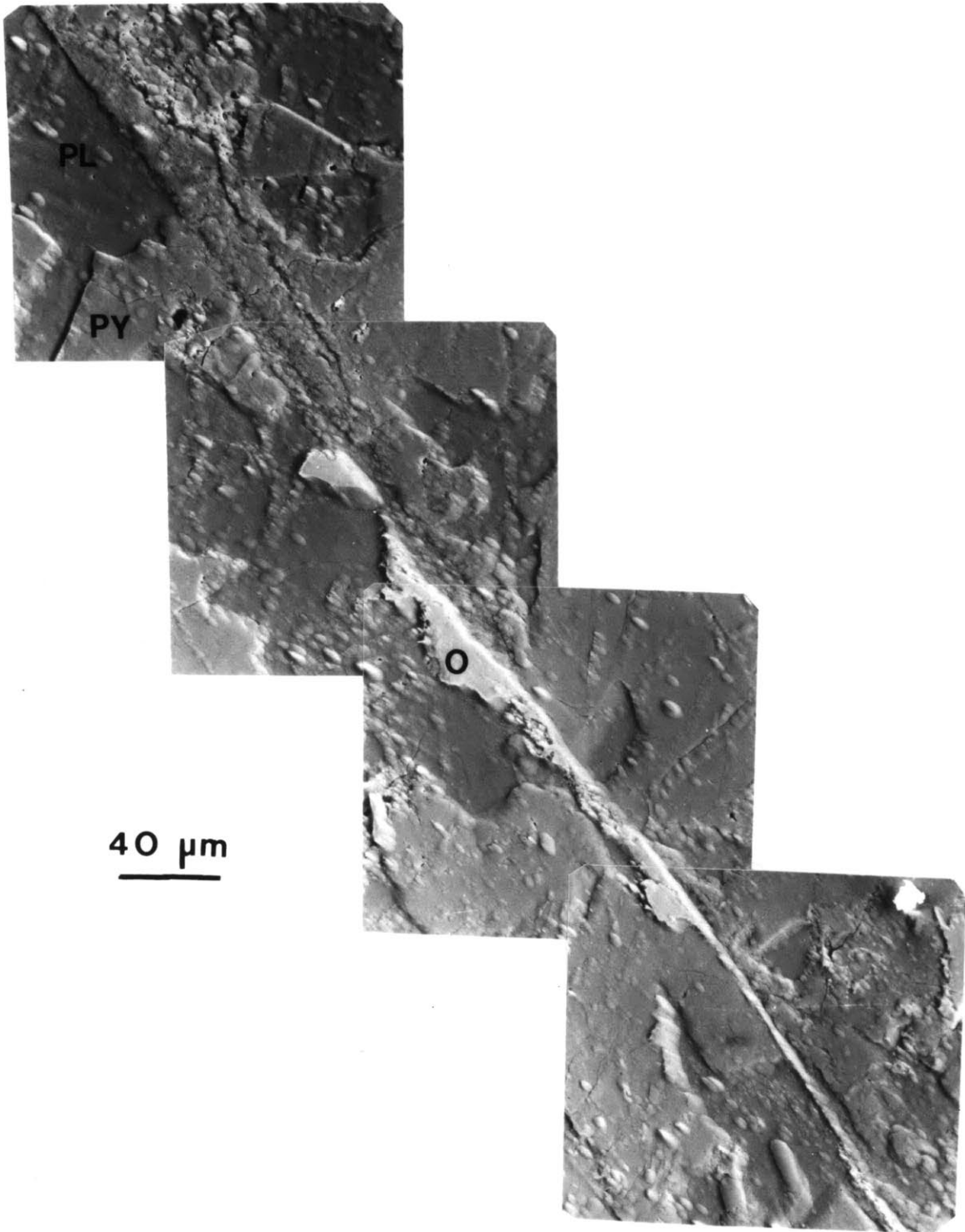


Fig. 7. Sample F2. Close up of the fault zone showing pores with concave boundaries and sharp corners.

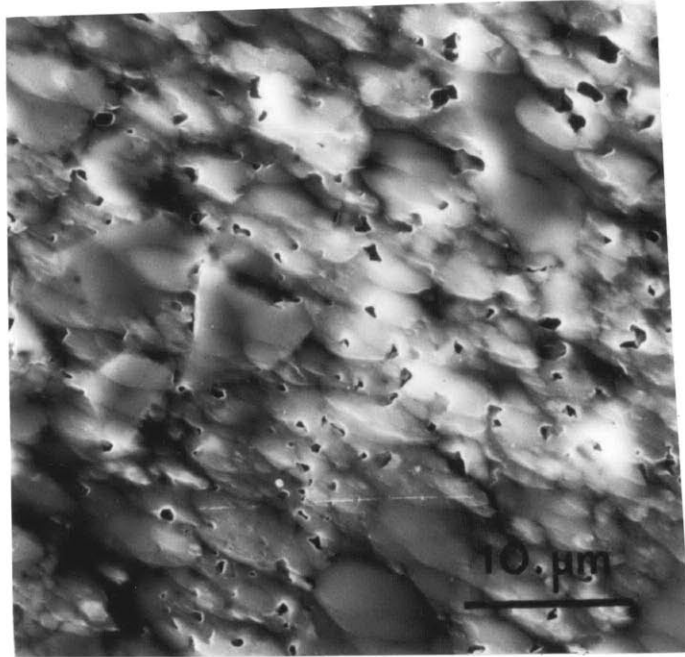


Fig. 8a. This sample deformed in the transitional regime at $4 \times 10^{-5} \text{s}^{-1}$, under 300 MPa confining pressure, did not show any fault but a stable strain softening after reaching a peak stress of 470 MPa.

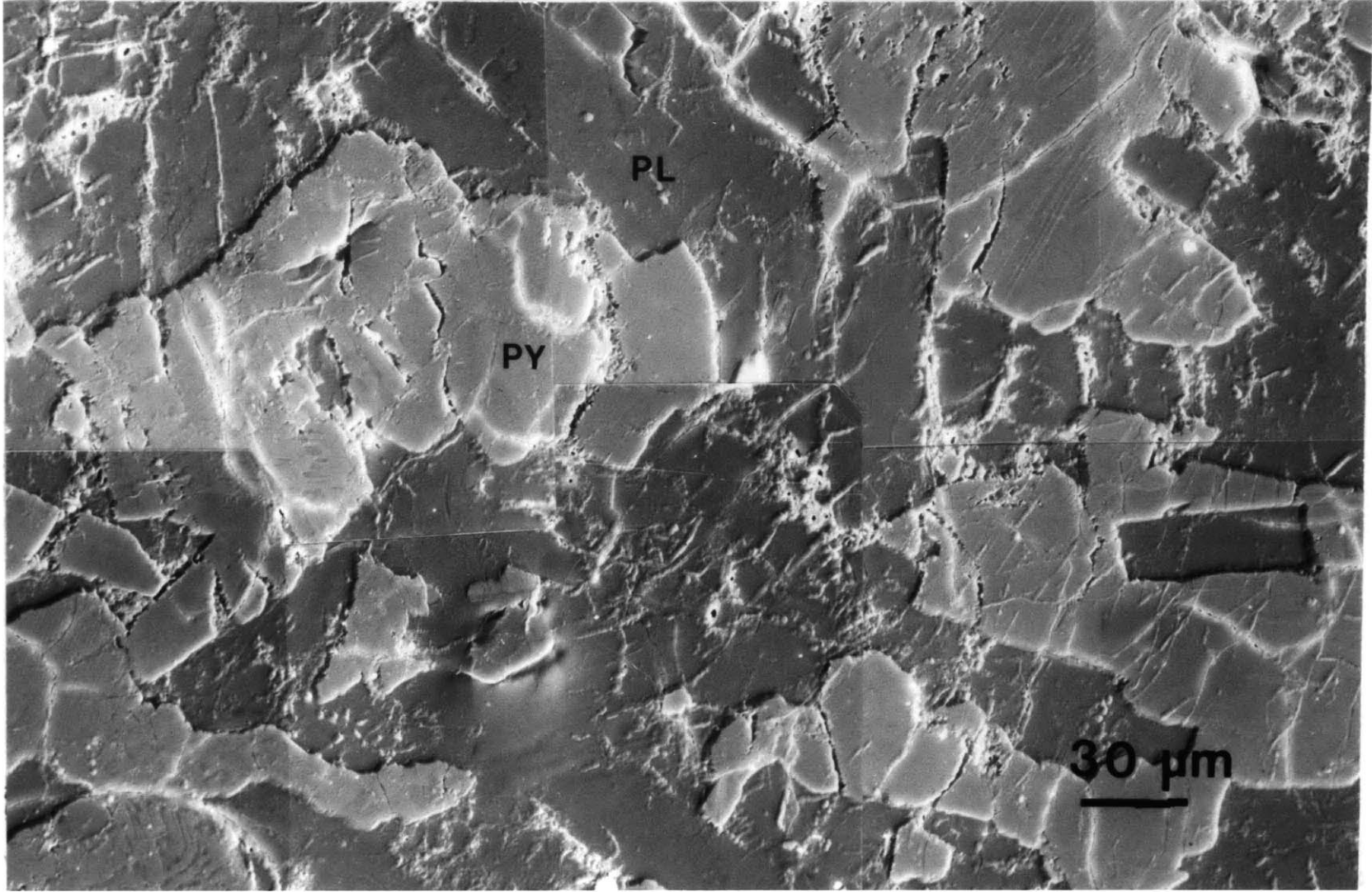
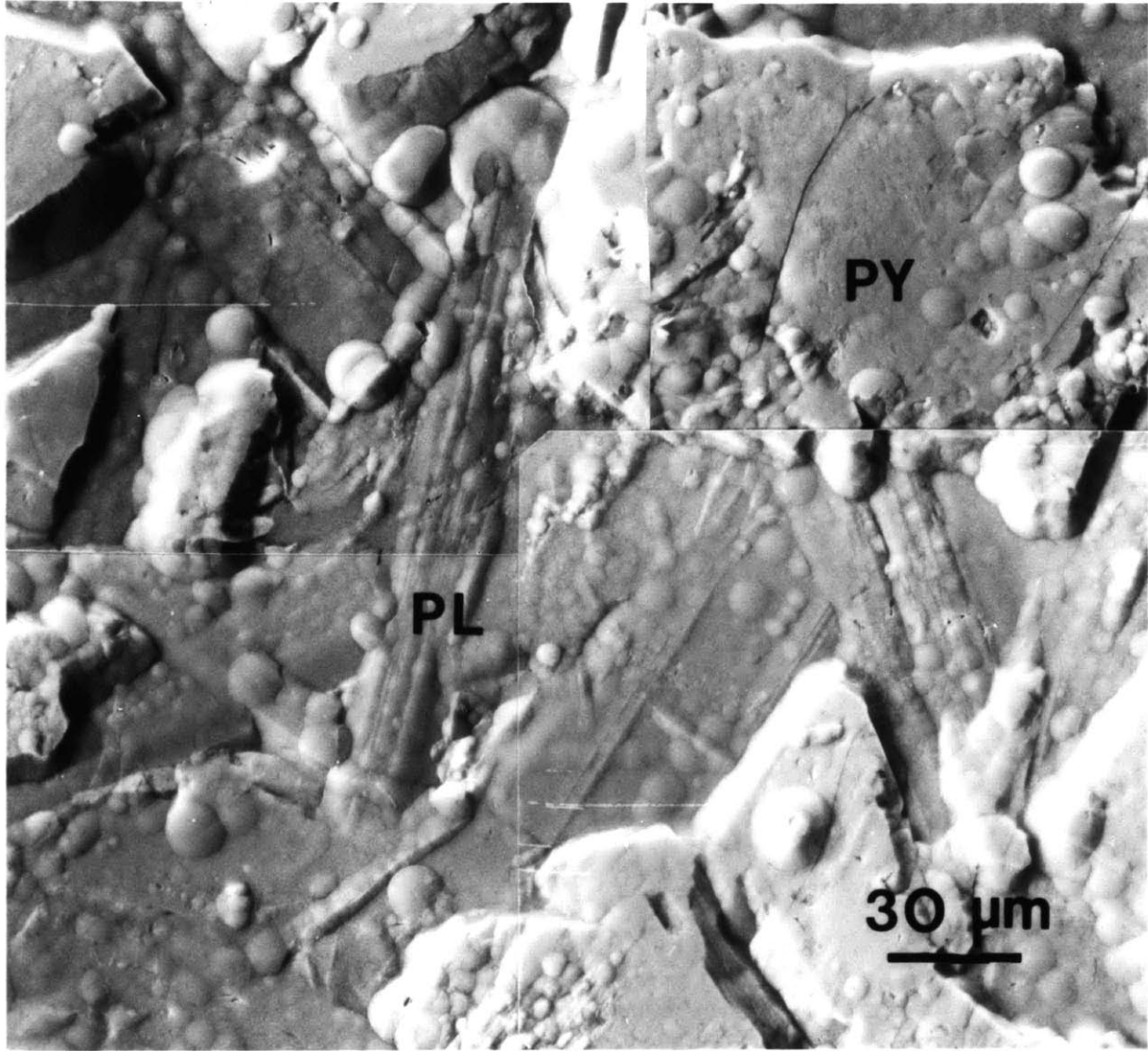


Fig. 8b. Original material: PY: pyroxene, PL: plagioclase.
Sample has been ion-milled. As a result twinning and a
few pores are clearly visible in the plagioclase.



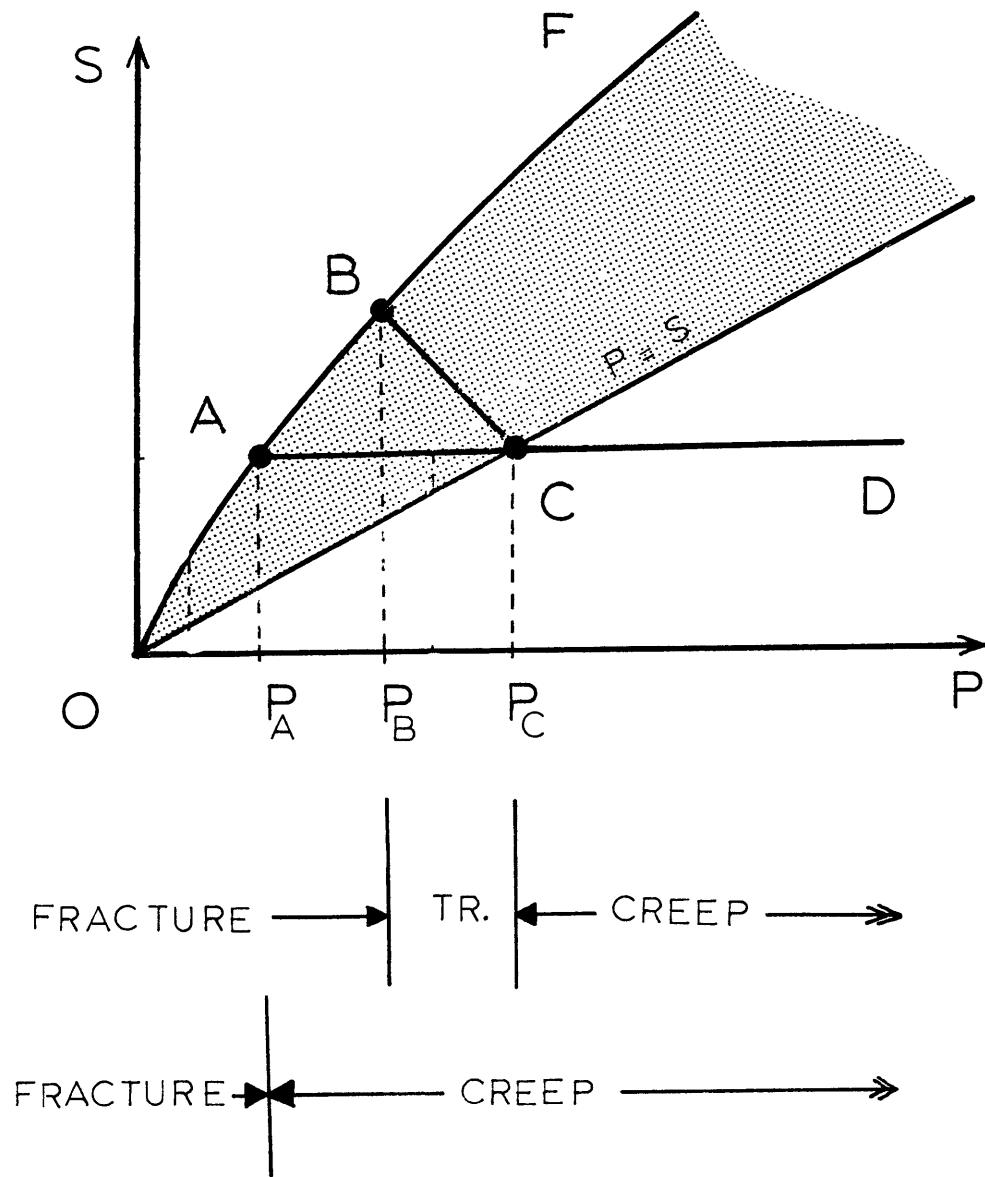


Fig. 9. Model of the transition between creep and fracture:

Paterson (1978): OACD

Our data: OBCD

No transitional regime exists in the first model. A transitional regime is identified in the second model.

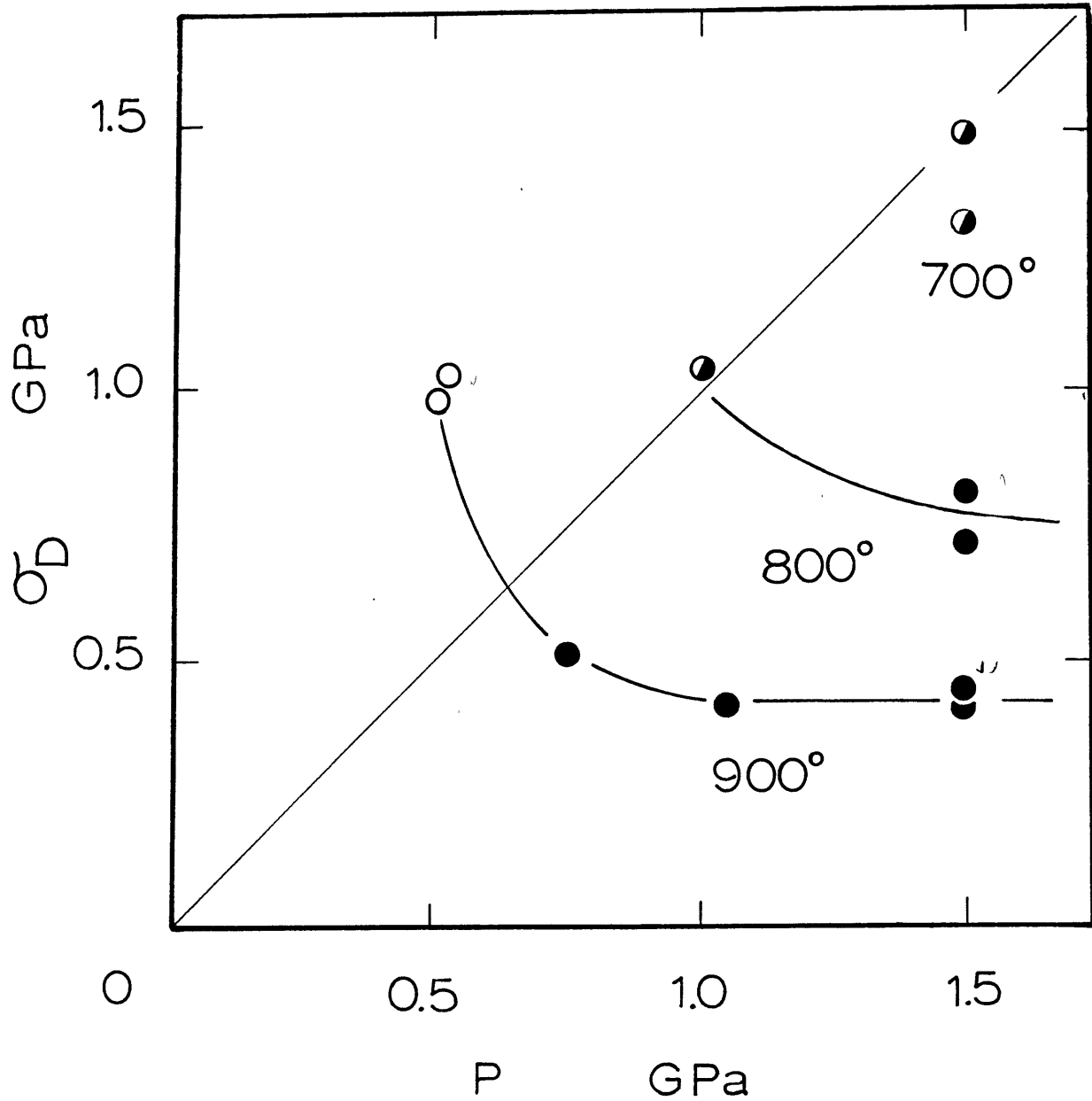


Fig. 10. Hale albite strength versus pressure (modified from Tullis et al., 1981) showing negative pressure sensitivity. The boundary between creep and transitional behavior corresponds to the same criterion as Fig. 5. For symbol convention see caption of Fig. 5.

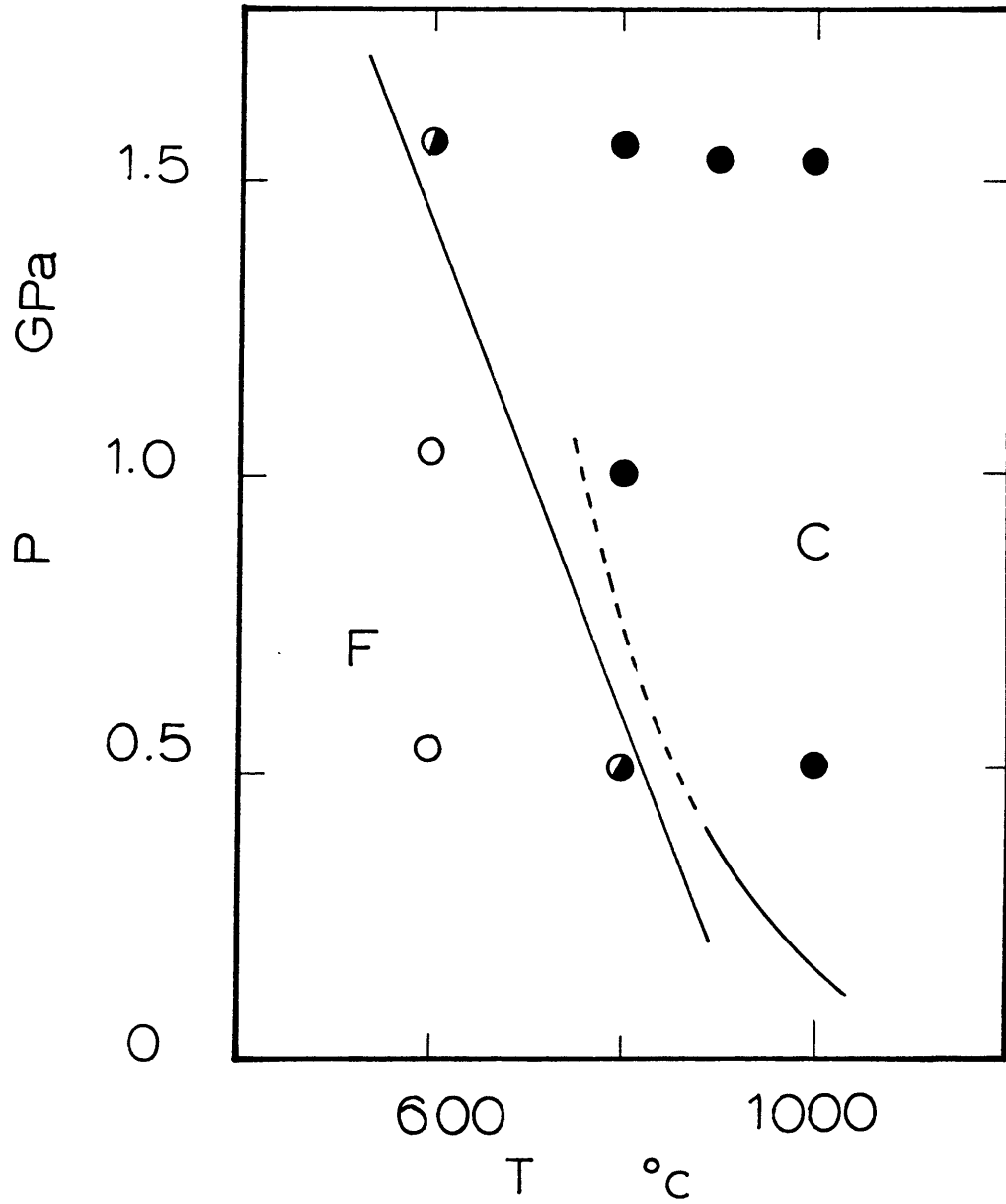


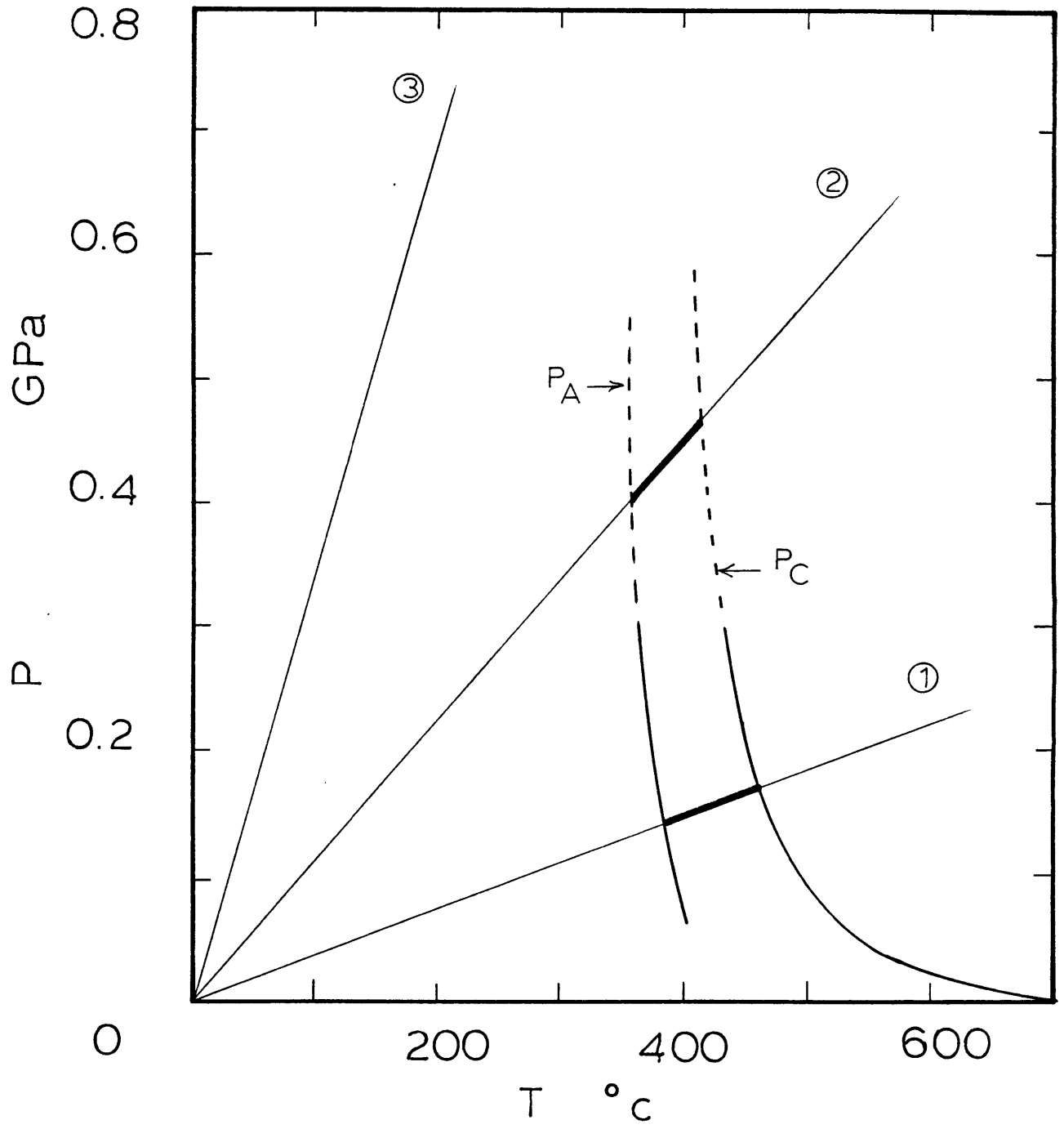
Fig. 11. Maryland diabase behavior versus pressure and temperature for a strain rate of $3 \cdot 10^{-6} \text{s}^{-1}$ (Kronenberg and Shelton, 1981). The straight line is the experimental boundary between creep and transitional behavior determined from the criterion $P = \sigma_D$ (see text) and the creep power law for Maryland diabase (Chap. I). The dashed part of that curve is the extrapolation of the power law out of its validity range.

Fig. 12. Transition from creep to fracture in a diabasic oceanic crust under geological conditions ($\dot{\epsilon} = 10^{-14} \text{ s}^{-1}$).

The straight lines correspond to (Miyashiro, 1972):

- (1) hot oceanic geotherm (ridges)
- (2) old intraplate oceanic geotherm
- (3) cold oceanic geotherm (trenches)

The two thick line segments represent the transition conditions in the old oceanic crust (350° - 400°C) and at oceanic ridges (400° - 500°). Lettering refers to Fig. 12.



CHAPTER III

DETERMINATION OF UNCERTAINTIES IN EXPERIMENTALLY
MEASURED FLOW LAW PARAMETERS

INTRODUCTION

High temperature experiments in rock mechanics are becoming more and more common. Under high-temperature conditions, most rocks behave plastically, even at laboratory strain rates, and their strength is rate dependent. Experiments are designed to measure this rate dependency as a function of temperature. Generally a small cylinder is machined out of the rock to be tested and placed between the two platens of a loading system. Temperature is then raised to the desired value and, in creep experiments, a fixed load is applied. In an ideal experiment, the sample ends would be unconstrained, the temperature would be uniform, deformation in the sample would be homogeneous, and the stress state would be the same everywhere throughout. Unfortunately all real experiments vary from those circumstances to some degree. It is the purpose of this paper to quantitatively treat the uncertainties in flow law parameters caused by some of the deviations from ideality commonly encountered in experiments.

Several experimental conditions are responsible for the uncertainties: (1) Because of end constraints and

temperature distribution the sample deformation is often not homogeneous, causing a bulged profile. Consequently, at any given position along the sample axis the stress value depends on the cross section area at that level. (2) The second measured variable, strain rate is obtained from the slope of the time displacement curve of one end of the sample. However stress and temperature are generally not uniform along the sample, causing variations in local strain rate values within the sample. We first propose a model to estimate the stress variations in the sample as a function of axial strain, and draw conclusions on the use of a homogeneous model to correct stress data. Temperature variations along the sample are then approximated by a second degree polynomial. Uncertainties in the pre-exponential constant, the activation energy and the stress exponent of the power law characterizing the sample creep properties are then estimated as a function of axial strain using these temperature and stress distribution models.

STRESS DISTRIBUTION DEPENDENCE ON AXIAL STRAIN

In order to estimate the stress distribution in a deformed sample its geometry has to be known as a function of axial strain. It is experimentally known that samples deform in a barrel shape (Rutter, 1972a). Friction tends to minimize radial strain at both ends, and temperature

profile peak to maximize radial strain at the center of the specimen. It will be assumed that the specimen shape can be approximated by a second degree polynomial, in other words that it is parabolic; deformation is thus non-homogeneous.

In the following derivations all lengths are normalized with respect to the sample initial length L_0 . From the assumptions above, the radius can be expressed as follows:

$$r = r_0 + a(x-1+\delta)x \quad (1)$$

where a is a parameter, r the current radius after an amount of deformation δ and x is the axial coordinate along the sample (Fig. 1). During plastic deformation the specimen volume does not change, although its shape is modified. After an amount of axial deformation δ the sample volume is

$$v = \int_0^{1-\delta} \pi r^2 dx = \pi [r_0^2(1-\delta) - 1/3 r_0(1-\delta)^3 a + 1/30(1-\delta)^5 a^2] \quad (2)$$

From volume conservation $v = v_0 = \pi r_0^2$

$$\text{so that: } \delta r_0^2 - 1/3(1-\delta)^3 r_0 a + 1/30(1-\delta)^5 a^2 = 0 \quad (3)$$

Solving for a :

$$a = 15 \frac{r_0}{(1-\delta)^2} (1/3 - \sqrt{\beta}) \quad (4)$$

with

$$\beta = 1/9 - 2/15 \cdot \frac{\delta}{1-\delta} \quad (5)$$

a has the dimension of L^{-1} ; it goes to zero for $\delta = 0$, and to infinity for $\delta = 1$. The maximum radius is at half length of the deformed sample, where $x = \frac{1-\delta}{2}$ so that,

according to (2) and (3)

$$\epsilon_{rM} = 15/4 (\sqrt{\beta} - 1/3) \quad (6)$$

The relevance of these results and consequently of the assumptions, can be checked by comparing to an actual sample profile of known axial deformation. Figure 2 represents such a comparison for a sample of diabase deformed at 1000°C (Chapter I). There is reasonably good agreement between the two carefully measured profiles and the profile computed with equations (1) and (4) for an axial deformation of $8.6 \cdot 10^{-2}$.

It has been assumed in the derivation of (1) that there was no radial strain at both sample ends. The stress distribution in the sample under these conditions depends on the ratio P/σ_0 where P is the confining pressure and σ_0 the applied stress at the sample ends. Brady (1971) computed the elastic stress distribution in such a sample for $P/\sigma_0 = 0.2$. The radial variation of the axial stress σ is less than 2% over 90% of the sample volume. The radial stress deviation from P is 6% at $x = 0.95$, and becomes negligible for values of x between 0.05 and 0.95. Both radial stress and axial stress variations decrease with increasing P/σ_0 . In the experimental study of polycrystalline rock plasticity confining pressures in excess of applied differential stresses are necessary to prevent a brittle behavior (Chapter II).

Therefore values of P/σ_0 greater than 0.5 will be the only values considered here. The radial variations of axial and radial stresses under these conditions are even lower than that computed by Brady for $P/\sigma_0 = 0.2$.

Furthermore, experimental observations of flow lines in plastically deformed specimens do not indicate drastic radial changes in deformation patterns (Caristan, 1981a). This suggests that the corresponding stress field has a negligible radial variation.

Consequently it will be assumed in the following study that stresses do not show substantial radial variation. The main variation in stress is axial and caused by changes in crosssectional area.

It is interesting under these conditions to compare the stress distribution in the sample under inhomogeneous deformation to the stress distribution under homogeneous deformation. In the homogeneous deformation model the decrease in length is assumed to be compensated by an increase in radius, the new radius being constant along the specimen length. Volume is conserved, so

$$v_0 = L_0 \pi r_0^2 = L \pi r^2 = L_0 (1-\delta) \pi r^2$$

so that: $(r_0/r)^2 = (1-\delta)$.

At any position of radius r along the sample axis the axial stress is given by $\sigma = \sigma_0 (r_0/r)^2$. For the homogeneous model the mean stress in the sample is given by:

$$\langle \sigma \rangle_h = \sigma_0 (1-\delta)$$

For the inhomogeneous model it is

$$\langle \sigma \rangle = \sigma_0 \frac{1}{(1-\delta)} \int_0^{1-\delta} (r_0/r)^2 dx$$

where r_0/r is given by equations (1), and (2).

$$\int_0^{1-\delta} (r_0/r)^2 dx \approx \int_0^{1-\delta} (1 - 2\Delta r/r_0) dx$$

From equations (2) and (3) it is known that

$$\int_0^{1-\delta} (r/r_0)^2 dx = 1 \approx \int_0^{1-\delta} (1 + 2\Delta r/r_0) dx$$

so that

$$\int_0^{1-\delta} (2\Delta r/r_0) dx \approx \delta$$

and

$$\langle \sigma \rangle \approx \sigma_0 (1-\delta)$$

In other words:

$$\langle \sigma \rangle \approx \langle \sigma \rangle_h = \sigma_o (1-\delta) \quad (7)$$

Consequently the mean homogeneous stress is a good approximation of the mean inhomogeneous stress for strains up to 20%. This result does not depend on the sample shape as long as volume is conserved.

In the inhomogeneous model the minimum stress in the sample is given by

$$\sigma_m/\sigma_o = (r_o/r_M)^2 = [1 + 15/4 (1/3 - \sqrt{\beta})]^{-2} \quad (8)$$

where r_M is the maximum radius, and $\sqrt{\beta}$ is given by equation (5). Both equations (7) and (8) are plotted on Figure 3. It shows that $\langle \sigma \rangle$ is closer to σ_m than to σ_o , no matter what the value of δ is.

TEMPERATURE DISTRIBUTION ALONG THE SAMPLE

High temperature experiments under confining pressure are delicate to design. Temperature gradients along the sample are due to convection in the confining medium, and volume constraints in the furnace design. Paterson (1970) designed a double coil furnace where temperature gradients can be limited to 0.5°cm^{-1} . Practically, a temperature variation of 10°C at 1000°C is excellent (Arzi, 1974,

Chapter I) considering that variations of 300°C at 1000°C have been reported in the literature (Carter and AveLallemant, 1970). Generally, in well designed experiments the highest temperature is located at the sample mid-length.

A typical temperature distribution (Chapter I) is represented on Figure 4. In the same way as the sample profile was approximated by a second degree polynomial the temperature distribution can be represented by the following equation:

$$T = T_0 + 4\Delta T_0 (x - 1/2)^2 \quad (9)$$

where T_0 is the peak temperature, ΔT_0 the temperature variation at the sample ends, and x the axial coordinate. It is assumed that the temperature profile is centered with respect to the specimen. Comparison between the measured and the computed profiles (Figure 4) shows that the approximation is a valid one.

EFFECT OF STRESS AND TEMPERATURE DISTRIBUTION ON MEASURED FLOW LAW PARAMETERS

During an actual experiment one end of the sample is fixed while the displacement δ of the other one is being monitored. Thus the recorded parameter actually represents the displacement integrated over the sample length. In practice, strain rate is obtained by measuring the slope of the displacement-time curve. If temperature and stress were constant along the sample the integrated value $\dot{\delta}$ would be equal to the local strain rate $\dot{\epsilon}$. However they both vary, and consequently so do

local strain rates. By integrating these local values it is possible to estimate the difference between the flow law parameters obtained from the recorded displacement rate, and the intrinsic flow law parameters.

It is assumed that the intrinsic rock behavior can be represented by

$$\dot{\epsilon}_x = \dot{\epsilon}_0 \sigma_D^n \exp(-Q/RT) \quad (10)$$

where $\dot{\epsilon}_x$ is the local axial strain rate, σ_D the applied differential stress, n the power law stress exponent, Q the activation energy, R the gas constant, T the temperature, $\dot{\epsilon}_0$ the preexponential constant.

Now if u is the non-normalized displacement:

$$\dot{\delta} = \dot{u} [L_0(1-\delta)]/L_0 \quad \text{and } u(0) = 0$$

where L_0 is the sample length. By definition

$$\dot{\epsilon}_x = \frac{\partial \dot{u}(X)}{\partial X} \quad \text{with } X = L_0 x$$

so that

$$\dot{\delta} = \int_0^{1-\delta} \dot{\epsilon}_x dx \quad (11)$$

where x is the axial coordinate along the sample axis. $\dot{\epsilon}_x$ depends on σ_D which in turn is equal to:

$$\sigma_D = \sigma - P = \sigma_0 (r_0/r)^2 - P \quad (12)$$

where (r_0/r) is obtained from equations (1) and (4), so that (11) can be written as

$$\dot{\delta} = \dot{\epsilon}_0 \int_0^{1-\delta} \{\sigma_0 [1 + (a/r_0)(x-1+\delta)x]^{-2-P}\}^n \exp(-Q/RT) dx \quad (13)$$

But $\dot{\delta}$ is generally represented by the following empirical relation:

$$\dot{\delta} = \dot{\epsilon}_0 \langle \sigma_D \rangle^v \exp(-\chi/RT_0) \quad (14)$$

where $\dot{\epsilon}_0$, v and χ are the experimentally determined parameters, and σ_D is given by

$$\langle \sigma_D \rangle = \langle \sigma \rangle - P = \sigma_0 (1-\delta) - P \quad (15)$$

Now, for any given stress and strain conditions in the earth, the strain rate of the deforming rock can be computed using equation (10). The uncertainty in the value obtained, $\Delta\dot{\epsilon}/\dot{\epsilon}$, comes from uncertainties in the experimental determination of the flow law parameters $\lambda_i = \dot{\epsilon}_0, n, Q$ through equation (14). It is equal to

$$\Delta\dot{\epsilon}/\dot{\epsilon} = |d\dot{\epsilon}(\lambda_i)/\dot{\epsilon}(\lambda_i)| \quad (16)$$

with

$$d\dot{\epsilon}/\dot{\epsilon} = \frac{\partial \ln \dot{\epsilon}}{\partial \lambda_i} d\lambda_i$$

Consequently, to estimate $\Delta\dot{\epsilon}/\dot{\epsilon}$ it is necessary to determine independently the uncertainty linked to each of the λ_i .

Uncertainty in the First Factor, $\dot{\epsilon}_0$

The uncertainty in $\dot{\epsilon}_0$ is obtained by comparing the measured displacement rate, equation (14), to the computed displacement rate, (13), which leads to

$$\frac{\dot{\epsilon}_0}{\dot{\epsilon}_0} = \int_0^{1-\delta} \left[\frac{(r_0/r)^2 - P/\sigma_0}{(1-\delta) - P/\sigma_0} \right]^n \cdot \frac{\exp(-Q/RT)}{\exp(-Q/RT_0)} dx \quad (17)$$

The integral depends on five independent dimensionless parameters: P/σ , $\Delta T_0/T_0$, Q/RT_0 , δ , n , and on functions of x : r_0/r , given by (1) and (4), and T , given by (9). Figures 5 to 7 represent $\dot{\epsilon}_0/\dot{\epsilon}_0$ as a function of $\Delta T_0/T_0$. $\dot{\epsilon}_0/\dot{\epsilon}_0$ has been obtained from (17) by numerical integration and parametric study.

Dependence of $\dot{\epsilon}_0/\dot{\epsilon}_0$ on axial strain, δ , and temperature variation $\Delta T_0/T_0$

Figure 5 shows the effect of axial strain, acting mainly through stress variation, and temperature distribution on $\dot{\epsilon}_0/\dot{\epsilon}_0$. The temperature effect alone is represented by

the 0% strain curve which indicates that $\Delta\dot{\epsilon}_0/\dot{\epsilon}_0 = |\dot{\epsilon}_0 - \dot{\epsilon}_0|/\dot{\epsilon}_0$ is about equal to $5 \Delta T_0/T_0$. The strain effect is represented by the intercepts of the curves with the $\dot{\epsilon}_0/\dot{\epsilon}_0$ axis. Up to about 10% axial strain the effect is not pronounced. But for higher values it becomes very important: a factor of 1.9 is obtained for 20% strain, and is due to the amplification of the stress variation by the stress exponent n . Actually, for $n = 1$, and for strains up to 20%, all curves are identical to the 0% strain curve.

From Figure 5 it appears that temperature and strain effects are working in opposite directions. These effects are due to the fact that stress decreases in the sample with increasing strain. Now, because temperatures are maximum where stress is minimum and vice versa, they will tend to compensate each other. This is apparent also on Figure 5. The temperature variation necessary to compensate for the effect of a given strain is given by the intercept of the curve corresponding to that strain value with the $\dot{\epsilon}_0/\dot{\epsilon}_0 = 1$ line; this intercept value increases with increasing strain.

Finally, as the sample strains, a particular volume of rock is actually moving with respect to the furnace and hence it changes position with respect to the temperature profile. Consequently its mean temperature increases.

This effect is covered by the strain effects for high values of δ , but it is still visible up to 15% axial strain: the curves actually cross the 0% curve, and stay below that curve for increasing $\Delta T_0/T_0$.

Effect of other parameters

Figure 6 represents the effect of Q/RT_0 on $\dot{\epsilon}_0/\dot{\epsilon}_0$ for 10% axial strain. Q/RT_0 is varied by a factor of 2. However the effect is merely to multiply the value of $\dot{\epsilon}_0/\dot{\epsilon}_0$ by a factor of 1.5. P/σ_0 does not have any significant effect on $\dot{\epsilon}_0/\dot{\epsilon}_0$ as long as its value is not too close to unity. In other words the effect of these parameters is not important but Figure 6 allows the estimation of the uncertainty in $\dot{\epsilon}_0$ for various experimental conditions.

Uncertainty in the Activation Energy, Q

The experimental activation energy χ is by definition (eqn. 14):

$$\frac{\partial \ln \dot{\delta}}{\partial (1/T_0)} = - \chi/R \quad (18)$$

χ is generally determined from differential tests, using (18) in its incremental form:

$$\frac{\ln(\dot{\delta}_1/\dot{\delta}_2)}{(1/T_2 - 1/T_1)} = - \chi/R \quad (19)$$

It is clear that (19) is a good approximation of (18) only if the testing temperatures T_1 and T_2 are not too far apart. It is strictly equal only in the limit, when $(1/T_2 - 1/T_1) \rightarrow 0$.

To determine the relation between χ and Q (18) can be used with the theoretical formulation for $\dot{\delta}$ that is given by (13):

$$\frac{\partial \ln \dot{\delta}}{\partial (1/T_0)} = - \frac{T_0^2}{\dot{\delta}} \frac{\partial \dot{\delta}}{\partial (T_0)}$$

now from (13):

$$\frac{\partial \dot{\delta}}{\partial T_0} = \dot{\epsilon}_0 \int_0^{1-\delta} \sigma_D^n \frac{\partial}{\partial T_0} [\exp(-Q/RT)] dx$$

but

$$\frac{\partial}{\partial T_0} [\exp(-Q/RT)] = \frac{Q}{RT^2} \exp(-Q/RT) \frac{\partial T}{\partial T_0}$$

From equation (9), $\frac{\partial T}{\partial T_0} = 1$

so that:

$$\frac{\partial \ln \dot{\delta}}{\partial (1/T_0)} = \frac{Q/R}{\dot{\delta}} \dot{\epsilon}_0 \int_0^{1-\delta} \sigma_D^n \exp(-Q/RT) \left(\frac{T_0}{T}\right)^2 dx \quad (19a)$$

but

$$\begin{aligned} (T_0/T)^2 &= \left[1 + \frac{4\Delta T_0}{T_0} (x-1/2)^2 \right]^{-2} \\ (T_0/T)^2 &\approx \left[1 - \frac{8\Delta T_0}{T_0} (x-1/2)^2 \right] \end{aligned} \quad (19b)$$

consequently

$$\frac{\partial \ln \dot{\delta}}{\partial (1/T_0)} = -Q/R \left[1 - \frac{8\Delta T_0}{T_0} \frac{\dot{\epsilon}_0}{\dot{\delta}} \int_0^{1-\delta} \sigma_D^n \exp(-Q/RT) (x-1/2)^2 dx \right] \quad (20)$$

Now writing

$$\chi = Q + dQ \quad (21)$$

and comparing (18) and (20) it follows that:

$$\frac{dQ}{Q} = \frac{8\Delta T_0}{T_0} \cdot \frac{\int_0^{1-\delta} \sigma_D^n \exp(-Q/RT) (x-1/2)^2 dx}{\int_0^{1-\delta} \sigma_D^n \exp(-Q/RT) dx} \quad (22)$$

The sign of dQ/Q indicates that Q is underestimated if χ is not corrected for dQ . A precise value of dQ/Q can be obtained using equations (1), (4), and (9), and numerically integrating the top and bottom integrals. However, an upper bound which does not depend on any model or strain value can be estimated by maximizing the top integral.

$$\max[(x-1/2)^2] = 1/4$$

so that

$$dQ/Q < -2(\Delta T_0/T_0) \quad (23)$$

where T_0 is the peak temperature.

Equation (23) shows that the uncertainty on activation energy is of the same order as that in temperature.

Uncertainty in the Stress Exponent n

The same type of analysis applies for the determination of the stress exponent. The stress exponent ν is generally obtained experimentally by differential tests corresponding to an equation derived from (14):

$$\nu = \frac{\partial \ln \dot{\delta}}{\partial \ln \langle \sigma_D \rangle} \quad (24)$$

The relation between n and ν can be obtained using (24) and (13):

$$\frac{\partial \ln \dot{\delta}}{\partial \ln \langle \sigma_D \rangle} = \frac{\partial}{\partial \ln \langle \sigma_D \rangle} \ln \left\{ \dot{\epsilon}_0 \int_0^{1-\delta} \sigma_D^n \exp(-Q/RT) dx \right\} \quad (25)$$

or

$$\frac{\partial \ln \dot{\delta}}{\partial \ln \langle \sigma_D \rangle} = \frac{\dot{\epsilon}_0}{\dot{\delta}} \int_0^{1-\delta} \exp(-Q/RT) \frac{\partial \sigma_D^n}{\partial \ln \langle \sigma_D \rangle} dx$$

But

$$\frac{\partial \sigma_D^n}{\partial \ln \langle \sigma_D \rangle} = n \sigma_D^{n-1} \langle \sigma_D \rangle \frac{\partial \sigma_D}{\partial \langle \sigma_D \rangle}$$

and

$$\frac{\partial \sigma_D}{\partial \langle \sigma_D \rangle} = \frac{\partial \sigma_D}{\partial \sigma_0} \frac{\partial \sigma_0}{\partial \langle \sigma_D \rangle}$$

Now from equations (12) and (15):

$$\frac{\partial \sigma_D}{\partial \sigma_0} = (r_0/r)^2 \approx (1 - \frac{2\Delta r}{r_0}) \quad \text{and} \quad \frac{\partial \sigma_0}{\partial \langle \sigma_D \rangle} = \frac{1}{1-\delta}$$

so that

$$\frac{\partial \sigma_D}{\partial \langle \sigma_D \rangle} \approx (1 - \frac{2\Delta r}{r_0} + \delta)$$

consequently

$$\frac{\partial \sigma_D^n}{\partial \ln \langle \sigma_D \rangle} = n \sigma_D^{n-1} \langle \sigma_D \rangle (1 - \frac{2\Delta r}{r_0} + \delta)$$

Now from equations (12) and (15):

$$\langle \sigma_D \rangle = \sigma_D - \sigma_0 (\delta - \frac{2\Delta r}{r_0}) \quad (25b)$$

so that, with the provision that $\sigma_D \neq 0$:

$$\frac{\partial \sigma_D}{\partial \ln \langle \sigma_D \rangle} = n \sigma_D^n [1 - \frac{\sigma_0}{\sigma_D} (\delta - \frac{2\Delta r}{r_0})] (1 - \frac{2\Delta r}{r_0} + \delta) \quad (25c)$$

Now (25) can be rewritten as

$$\frac{\partial \ln \dot{\delta}}{\partial \ln \langle \sigma_D \rangle} = n \left\{ 1 + \delta - \frac{\int_0^{1-\delta} \xi \cdot \dot{\xi}_x dx}{\int_0^{1-\delta} \dot{\xi}_x dx} \right\} \quad (26)$$

with

$$\xi(x) = \frac{2\Delta r}{r_0} + \frac{\sigma_0}{\sigma_D} (\delta - \frac{2\Delta r}{r_0}) \quad (27)$$

neglecting terms like

$$\left(\delta - \frac{2\Delta r}{r_0}\right)^2 \quad \text{in (25c)}. \quad (28)$$

Now writing

$$v = n + dn \quad \text{and} \quad \Delta n = |dn| \quad (29)$$

and comparing (26) and (24) it follows that:

$$dn = \delta - \frac{\int_0^{1-\delta} \xi \cdot \dot{\epsilon}_x dx}{\int_0^{1-\delta} \dot{\epsilon}_x dx} \quad (30)$$

Once again the integrals in (30) can be determined exactly by numerical integration, using equations (1), (4), and (9).

ξ depends then on three parameters: $\Delta T_0/T_0$, δ , and P/σ_0 .

The effect of these parameters on ξ are represented in

Figure 7, where it has been assumed that $\Delta T_0/T_0 = 0$.

For very low confining pressures:

$$\sigma_0/\sigma_D \rightarrow 1 \quad \text{while} \quad P/\sigma_0 \rightarrow 0$$

and

$$dn \rightarrow 0$$

consequently it can be seen from (29) that, at low confining pressure

$$n = \nu \quad (31)$$

For very low differential stresses, but high confining pressure:

$$\sigma_0/\sigma_D \rightarrow \infty, \text{ and } P/\sigma_0 \rightarrow 1 \quad (32a)$$

The variation of dn is represented in Figure 7 as a function of P/σ_0 . It indicates that large variations can be expected in the stress exponent for experiments conducted at high pressure, but small differential stresses. Such experiments lead to a crude underestimation of n . It should be noted that the general conclusions of this analysis are independent of the model used in describing the stress or strain distribution in the sample. The actual values of dn depend on the details of the stress distribution, but the trends shown by equation (31) and Figure 7 come from equation (25b).

$$\sigma_D - \langle \sigma_D \rangle = \sigma_0 (\delta - 2\Delta r/r_0) \quad (32b)$$

In other words under conditions of low confining pressure σ_0 is of the order of σ_D and therefore, as $(\delta - 2\Delta r/r_0)$ is generally small $\langle \sigma_D \rangle - \sigma_D$ is small. Consequently:

$$n \approx \nu$$

Under conditions of small differential stresses, σ_0 is much larger than $\langle \sigma_D \rangle$ and although $(\delta - 2\Delta r/r_0)$ is small the product $\sigma_0(\delta - 2\Delta r/r_0)$ can be as large as $\langle \sigma_D \rangle$ itself or even higher. For $P/\sigma_0 = 0.9$ and $\delta = 5\%$ the total variation in differential stress in the sample is 70% so that the representativity of $\langle \sigma_D \rangle$ becomes debatable. Consequently, although differential stresses are small, their variation in the sample can be substantial if the confining pressure is high. This is what Figure 8 indicates.

For P/σ_0 very close to unity (0.98) the model developed here is no longer adequate because the assumption that the principal stress axes are parallel and perpendicular to the sample axis is no longer correct. In this case (10) is still valid, but σ_D is no longer given by eqn. (15).

DISCUSSION

Stress Distribution in the Sample

The model developed here for stress distribution in the sample might have some bearing on experimental study of rock behavior at high confining pressures in cases where P/σ_0 is close to unity. For a given P/σ_0 ratio (constant stress test) at any given strain δ there is a critical radius r_c along the sample axis where the differential stress is zero. From equation (12) we find that: $\sigma_D = 0$ when

$$\sigma_0 (r_0/r_c)^2 = P \text{ or } r_c = r_0 \left(\frac{P}{\sigma_0}\right)^{-\frac{1}{2}}$$

Now for any position x along the sample axis such that $r(x) > r_c$, the differential stress direction is rotated 90° with respect to the σ_0 axis, and the zone affected by this reversal increases with strain. Conceivably, when enough of the sample is affected, in other words after enough strain problems of results representativity will arise.

This condition depends on the ratio P/σ_0 and on the axial strain value. $\sigma_D = 0$ at some level in the sample when $\sigma_m/\sigma_0 = P/\sigma_0$. The ratio σ_m/σ_0 is represented on Figure 3 as a function of the axial strain. In designing an experiment with P/σ_0 close to unity it is then advisable to refer to Figure 3 in order to determine the maximum axial strain value possible before some levels in the sample develop a stress field different from the expected one. This axial strain value δ_c is such that $\sigma_m/\sigma_0(\delta_c) = P/\sigma_0$. The present model does not allow a precise determination of the stress field but gives limits for the result credibility.

Activation Energy

The formula developed here (Equation 23) is valid for reasonable temperature gradients, e.g. when $\Delta T_0/T_0 \lesssim 10\%$. For gradients such that $\Delta T_0/T_0$ is greater than 10% (19a) and (19b) must be directly integrated. This is the case in Carter and AveLallemant's study of high temperature flow in dunite and peridotite (1970). In their study temperature variation of 300° are common at 1000° nominal temperature.

Equation (19b) has been numerically integrated in order to determine the uncertainty in the activation energy they report. Parameters used and results are given on Table I. For the temperature conditions specified above the uncertainty is 30%. It should be noted that their experiments were also conducted at P/σ_0 values that are close to unity. Consequently all the remarks on stress distribution and stress exponent determination under these conditions apply equally to their data.

For temperature gradients smaller than 15% the effect of temperature variation on activation energy, which is given by Equation (23), may be smaller than the effect on Q caused by the uncertainty in the temperature itself.

Stress Exponent

Few experimental data on rock creep at low differential stresses, and high confining pressures can be found in the literature. A very careful set of experiments was conducted by Schmid et al. (1977) on a fine-grained limestone. Two regimes of flow were identified. In the low differential stress regime, stress relaxation experiments described in Figure 8 were conducted to investigate the stress exponent. Fig. 8 shows that, at 3kb confining pressure and 800°C , n decreases monotonically with decreasing differential stress. This behavior can be explained in at least two different ways:

One possibility is that the stress range investigated in Figure 8 corresponds to the transition region between the low stress flow law ($n = n_1$), and the high differential stress flow law ($n = n_2$). To test this idea the stress exponent in the transitional region is computed assuming that both mechanisms are acting simultaneously, and that the total strain rate is simply a sum of the strain rates due to the individual mechanisms i.e. there are no interactive effects:

$$\dot{\epsilon} = \dot{\epsilon}_1 + \dot{\epsilon}_2 \quad (33)$$

with

$$\dot{\epsilon}_i = \dot{\epsilon}_i \sigma_D^{n_i} \exp(-Q_i/RT) \quad (i = 1, 2)$$

By definition

$$n = \frac{\partial \ln \dot{\epsilon}}{\partial \ln \sigma_D} = \frac{\sigma_D}{\dot{\epsilon}} \frac{\partial \dot{\epsilon}}{\partial \sigma_D}$$

Consequently:

$$n = n_1 / (1 + k \sigma^{n_2 - n_1}) + n_2 / (1 + k^{-1} \sigma^{n_1 - n_2}) \quad (34)$$

with

$$k = \frac{\dot{\epsilon}_2 \exp(-Q_2/RT)}{\dot{\epsilon}_1 \exp(-Q_1/RT)}$$

Equation (34) is represented by a broken line on Figure 8; the parameters used are given on Table II. The curve follows the trend of the data, but it doesn't account for the scatter and the uncertainty due to the bulging.

A second plausible explanation derives from the results obtained above (Equation 29), and are represented by the solid lines on Figure 8. These lines represent v as from Equation (29) and from interpolation of Figure 7. The n value used was 3. These curves tend to follow the data trend at least as well as the broken curve, but also provide an explanation for the scatter, and account for the effect of axial strain. Adopting this idea means that the intrinsic stress exponent, n , is equal to 3; therefore although microstructural observations indicate that some diffusional micromechanisms are active in this range the second interpretation suggests that most of the deformation could have occurred through dislocation motion, with a stress exponent of 3 and still be consistent with the data set. A few points can be made in support of this interpretation:

In the log-log plot of differential stress versus strain rate given by Schmid et al. (1977, Fig. 2) a stress exponent of 3 in a region extending from 15 MPa to 50 MPa is certainly acceptable.

Numerical integration of (30) for $n = 1$ leads to the following observations: $\frac{dn}{n}$ is smaller than 5% up to $P/\sigma_0 = 0.85$,

and for strains up to 10%. For higher P/σ_0 , dn actually increases because of changes in the differential stress orientation. In other words the trend shown on Figure 8 would be reversed.

However, it is difficult to conclude in a definite way from the available information alone. A good test would be to do stress relaxation experiments after various amount of axial strain, and to compare the results to the curve on Figures 7 and 8.

CONCLUSIONS

A parametric study has been carried out to estimate uncertainties in creep power law determination due to stress and temperature distribution during high temperature and high pressure rock testing. Five general conclusions can be drawn from this study.

1. The uncertainty in the pre-exponential constant of the power law ($\dot{\epsilon}_0$) can be as high as a factor of 2. However, because experimental as well as the geological strain rates cover orders of magnitude, this uncertainty is still tolerable.

2. The uncertainty in the activation energy Q is quite tolerable up to temperature variations of 5%. In some cases the uncertainty in Q can be substantial (Carter and AveLallemant, 1970).

3. The uncertainty in the stress exponent n is generally low, but it becomes very sensitive to the ratio of confining pressure to applied axial stress (P/σ_0) when the confining pressure is much higher than the applied differential stress. This conclusion might have some bearing on the apparent stress exponent decay observed by Schmid et al. (1977) in their study of Solnhofen Limestone.

4. Attention is drawn on the state of stress in samples. Substantial variations in the orientation of the principal stress axes can occur with increasing strain in samples tested at high confining pressure P and low differential stress. For a ratio P/σ_0 of 0.9, where σ_0 is the applied axial stress, the variation in differential stress $\Delta\sigma_D/\sigma_D$ in the sample at 5% strain is 70%.

5. Finally, this study confirms that there is incompatibility between a precise determination of creep law parameters and deformation of a rock sample to high axial strain values. Experiments where samples are highly strained (more than 10%) should be designed specifically for microstructural studies, whereas power law parameters should be determined as much as possible from low strain differential testing or from sequential testing.

References

- Arzi, A.A., 1974. Partial melting in rocks: rheology, kinetics and water diffusion, Ph.D. Thesis, Harvard University, Cambridge, Mass.
- Brady, B.T., 1971. The effect of confining pressure on the elastic stress distribution in a radially and constrained circular cylinder, *Int. J. Rock Mech. Min. Sci.*, 7, 517-526.
- Carter, N.L., and H.G. AveLallemant, 1970. High temperature flow of dunite and peridotite, *Geol. Soc. Amer. Bull.*, 81, 2181-2202.
- Paterson, M.S., 1970. A high pressure, high temperature apparatus for rock deformation, *Int. J. Rock Mech. Min. Sci.*, 7, 517-526.
- Rutter, E.H., 1972. On the creep testing of rocks at constant stress and constant force, *Int. J. Rock Mech. Min. Sci.*, 9, 191-195.
- Rutter, E.H., B.K. Atkinson, and D.H. Mainprice, 1978. On the use of stress relaxation testing method in studies of the mechanical behavior of geological materials, *Geophys. J.R. Astr. Soc.*, 55(1), 155-170.
- Schmid, S.M., J.N. Boland, and M.S. Paterson, 1977. Superplastic flow in fine-grained limestone, *Tectonophysics*, 43, 257-291.

TABLE I

	Dry Dunite	Wet Dunite
δ	6%	6%
Q/RT_0	47.4	31.6
n	4.8	2.4
χ/Q	0.706	0.717
$\Delta Q/Q$	30%	28%
$\frac{Q}{\text{kcal.mol}^{-1}}$	120 \pm 36	80 \pm 23

Parameters used in equation (19b) for estimating the uncertainty in dunite creep activation energy. Values are from Carter and AveLallemant (1970).

TABLE II

i	\dot{e}_o $\text{sec}^{-1} b^{-n}$	Q kcal/mole	n
1	$4.68 \cdot 10^{-2}$	71	4.70
2	$4.68 \cdot 10^2$	21	1.66

Parameters used in equation (34) from SCHMID et al. (1977)
(Solnhofen limestone).

Symbol List

δ	normalized axial displacement
$\dot{\delta}$	normalized axial displacement rate
δ_c	critical axial strain for stress axis reversal
ϵ_{rM}	maximum radial strain
$\dot{\epsilon}_x$	local axial strain rate
\dot{e}_0	preexponential constant
$\dot{\epsilon}_0$	experimental power law preexponential constant
L_0	sample initial length
λ_i	generic symbol for power law parameters
n	intrinsic power law stress exponent
v	experimental power law stress exponent
dn	variation in n
Δn	absolute variation in n
P	pressure
Q	intrinsic activation energy
χ	experimental activation energy
dQ	variation in activation energy
$r(x)$	sample radius at x
r_c	critical radius for stress axis reversal
r_M	maximum sample radius
r_0	initial sample radius
$\sigma(x)$	axial stress at x
$\langle \sigma \rangle$	mean axial stress
σ_0	applied axial stress at sample ends
$\langle \sigma \rangle_h$	mean homogeneous axial stress
σ_D	differential stress
$\langle \sigma_D \rangle$	mean differential stress

σ_m	minimum axial stress
$T(x)$	temperature at x
T_0	peak temperature (nominal)
ΔT_0	maximum temperature variation
u	non-normalized displacement
\dot{u}	non-normalized displacement rate
v	sample volume
v_0	sample initial volume
X	non-normalized axial coordinate
x	normalized axial coordinate

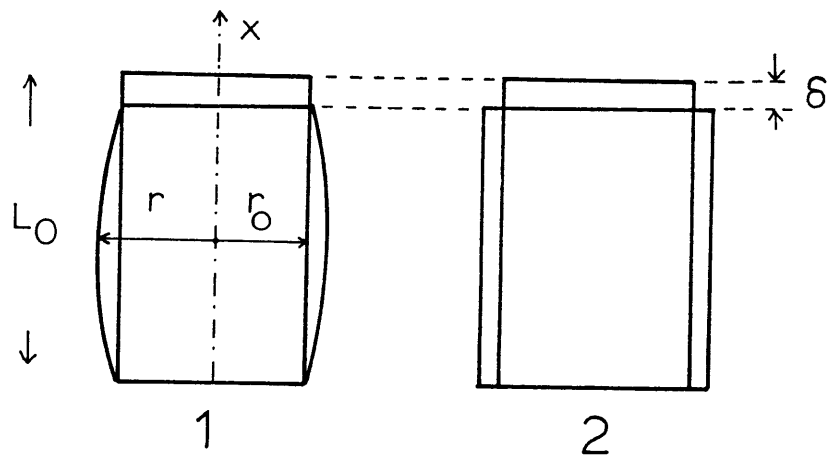
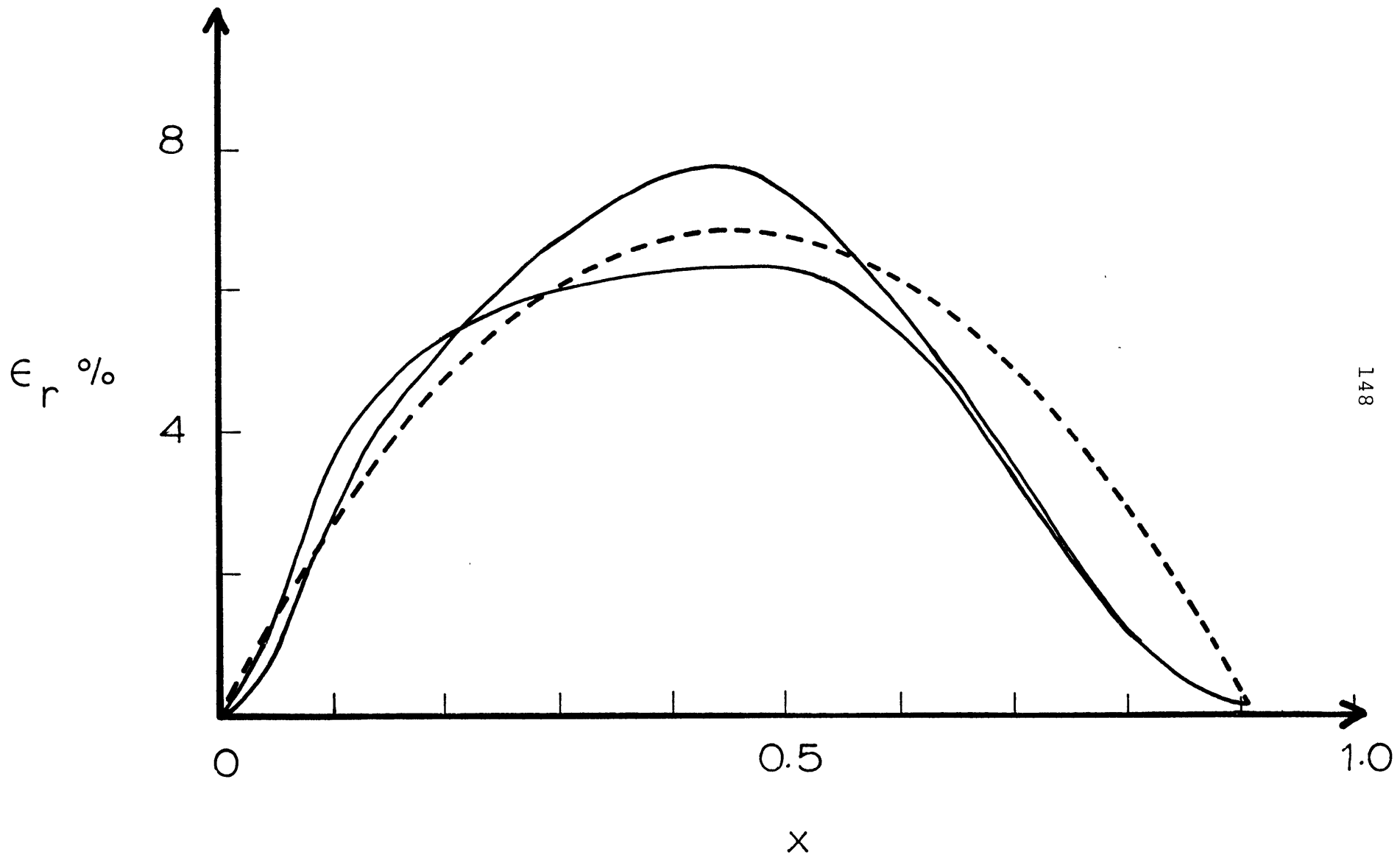


Fig. 1. Two different models of sample deformation: model 1 corresponds to inhomogeneous deformation. L_0 , the sample length, is equal to 1, δ is normalized with respect to L_0 , and the x axis origin is at the bottom of sample. Model 2 corresponds to homogeneous deformation.

Fig. 2. Measured sample profiles (solid lines) and computed sample profile (broken line) for an axial strain of $8.6 \cdot 10^{-2}$. The two solid lines represent profiles measured in two mutually perpendicular axial planes.



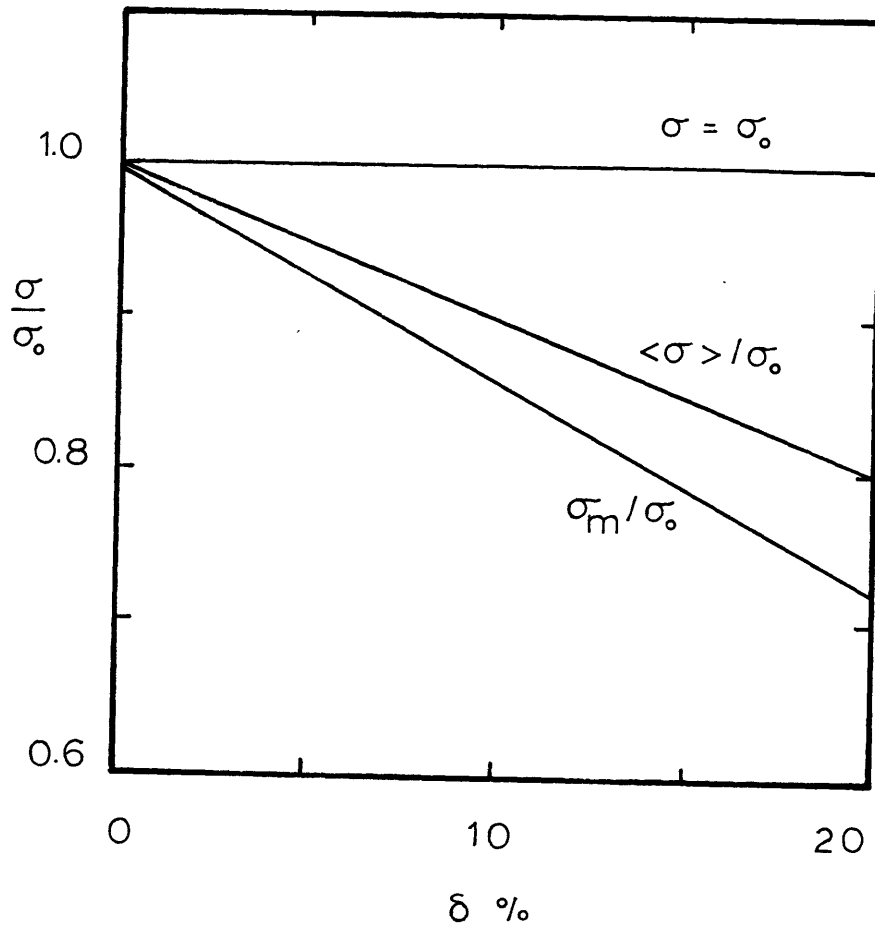


Fig. 3. Mean stress $\langle \sigma \rangle$, and minimum stress σ_m along the sample axis as a function of axial strain.

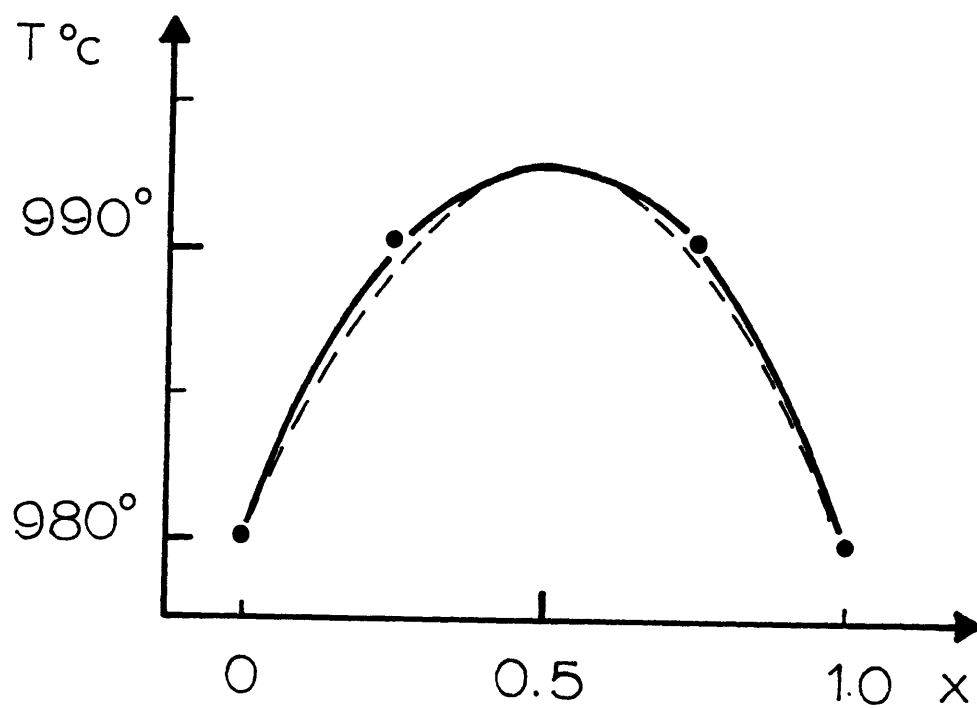


Fig. 4. Temperature distribution along the sample. The solid line is the measured distribution, the broken line is the distribution fitted with equation (9).

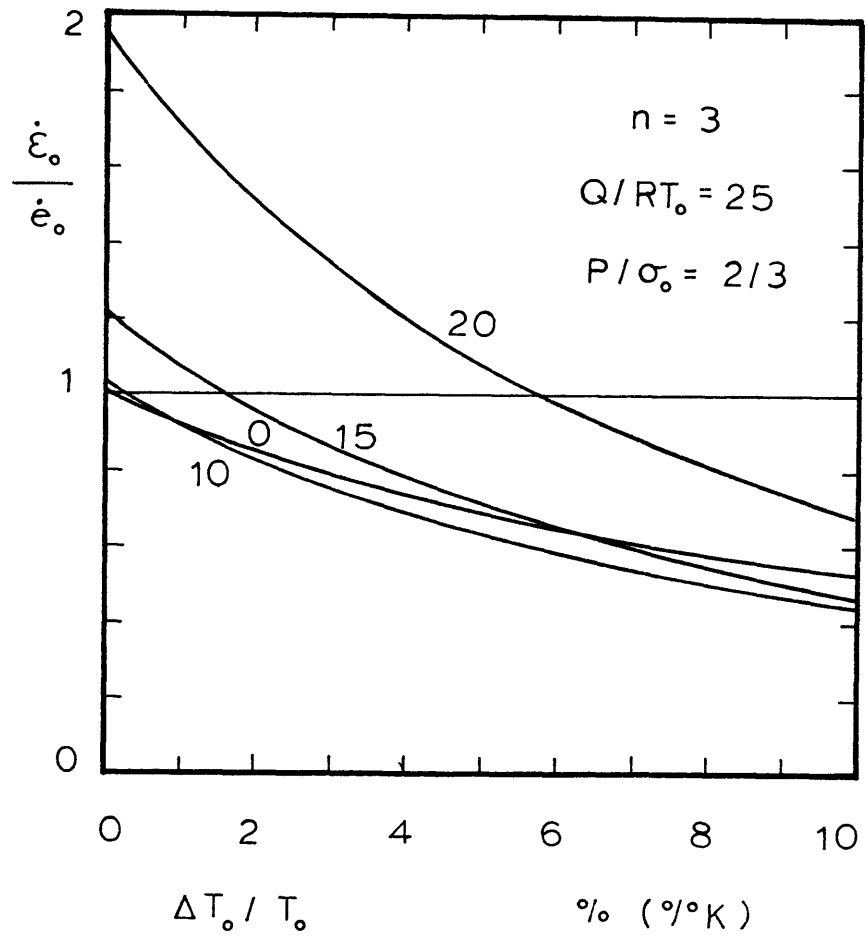


Fig. 5. Variation in $\dot{\epsilon}_0/\dot{\epsilon}_0$ as a function of temperature variation. Numbers next to the curves are axial strain values in percent.

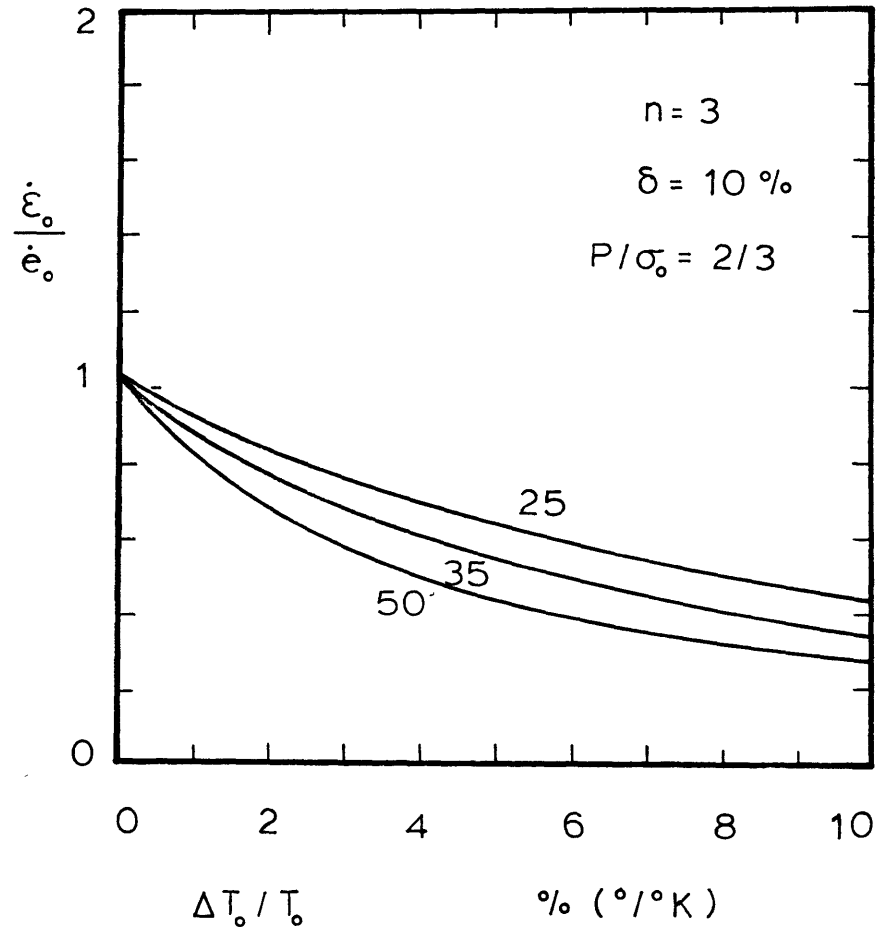


Fig. 6. Variation in the $\dot{\epsilon}_0/\dot{\epsilon}_0$ as a function of temperature variation. Numbers next to the curves represent different values of the parameter Q/RT .

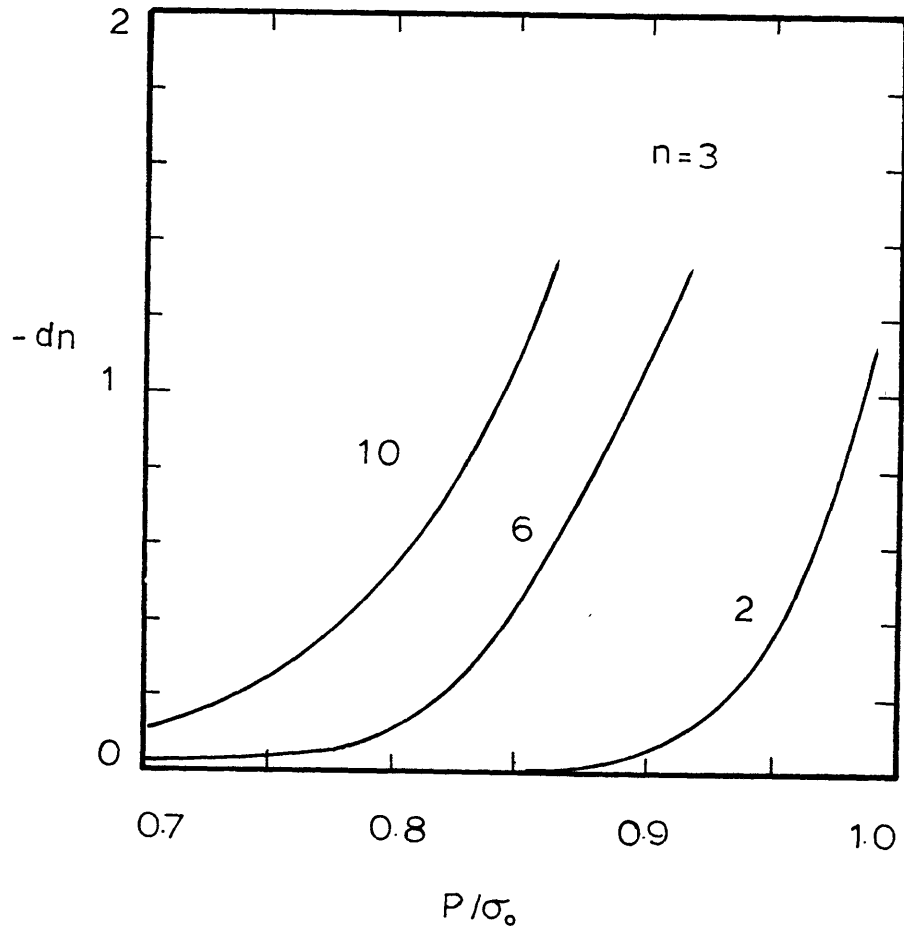


Fig. 7. Effect of pressure and applied axial stress on the stress exponent n . Numbers next to the curves represent axial strain values in percent.

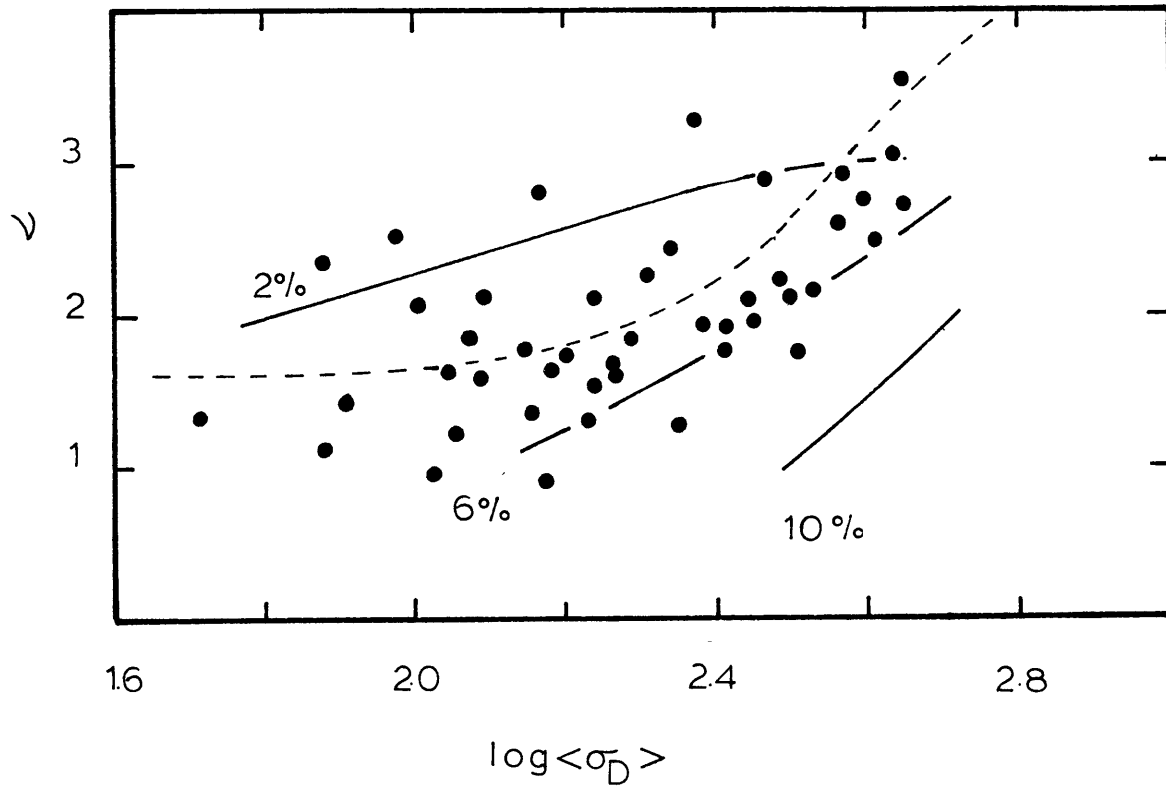


Fig. 8. Experimental data points represent the apparent stress exponent measured by Schmid et al. (1977) on Solnhofen Limestone. Solid curves are extrapolated from Figure 7 and represent ν computed with $n = 3$ for various axial strain values. Broken curve is the variation in ν to be expected in the transition zone between a high n regime and a low n regime. This broken line has been computed with equation (34) for the parametric values given on Table II.

BIOGRAPHICAL NOTE

I was born to Denise and Arcade Caristan on January 16, 1951, in Auxerre (Yonne, France), and attended primary and secondary school in various provincial cities: Auxerre, Chalons-sur-Marne and finally Nancy, where I graduated from high school in 1969. In 1971 I was accepted at the Ecole Normale Superieure, 45 rue d'Ulm, Paris, where I stayed while simultaneously attending the Université des Sciences de Paris. I obtained a Maîtrise de Sciences de la Terre from the University of Paris VII in 1973, a Diplôme d'Etude Approfondie from the same university in 1974, and a Thèse de Spécialité in Structural Geology from the University of Paris VI, in 1975. In order to complete my thesis I spent six months at MIT, during the fall of 1974 and spring 1975, learning electron microscopy under the guidance of Dr. David Kohlstedt and Professor Christopher Goetze. I subsequently applied for graduate school at MIT, where I was accepted in the fall of 1975. I worked in the Rock Mechanics Laboratory of Professor W.F. Brace under the guidance of Professor Goetze until his sudden death on November 21, 1977. I carried on the research program started under his supervision with the support of Professor Brace. I took a one-year leave of absence, from September 1978 to August 1979, for compulsory military service. In September, 1979, I resumed my research program, of which the present work is the accomplishment.